Titre: Title: Investigation on Grinding Titanium Metal Matrix Composites with Diamond Wheels

Auteur: Author: Cécile Escaich

Date: 2023

Type: Mémoire ou thèse / Dissertation or Thesis

Référence: Citation: Escaich, C. (2023). Investigation on Grinding Titanium Metal Matrix Composites with Diamond Wheels [Thèse de doctorat, Polytechnique Montréal]. PolyPublie. https://publications.polymtl.ca/53449/

Directeurs de recherche: Advisors: Marek Balazinski, Luc Baron, & Zhongde Shi

Programme: Program: Génie mécanique

POLYTECHNIQUE MONTRÉAL

affiliée à l'Université de Montréal

Investigation on Grinding Titanium Metal Matrix Composites with Diamond Wheels

CÉCILE ESCAICH

Département de génie mécanique

Thèse présentée en vue de l'obtention du diplôme de *Philosophiæ Doctor*

Génie mécanique

Avril 2023

POLYTECHNIQUE MONTRÉAL

affiliée à l'Université de Montréal

Cette these intitulée :

Investigation on Grinding Titanium Metal Matrix Composites with Diamond Wheels

présentée par **Cécile ESCAICH**

en vue de l'obtention du diplôme de *Philosophiæ Doctor*

a été dûment acceptée par le jury d'examen constitué de :

Aouni LAKIS, président

Marek BALAZINSKI, membre et directeur de recherche

Zhongde SHI, membre et codirecteur de recherche

Luc BARON, membre et codirecteur de recherche

Oguzhan TUYSUZ, membre

Wit GRZESIK, membre externe

DEDICATION

To all those who have never lost their faith,

“*The amazing thing about impossible things is that they eventually happen*.”

Jean Dutourd, Against the Disgusts of Life (1986)

A tous ceux qui n’ont jamais cessé de croire en moi,

« *Le plus étonnant dans les choses impossibles est qu'elles finissent par arriver* »

Jean Dutourd, Contre les dégoûts de la vie (1986)

ACKNOWLEDGEMENTS

My advisor, Prof. Marek Balazinski, has continuously supported me through my study and research, and I would like to express my sincere appreciation for his motivation, enthusiasm, and the trust he placed in me for the accomplishment of this project.

My special thanks go to my co-advisor, Dr. Zhongde Shi, thanks to whom the realization and the accomplishment of this project was made possible. Without his guidance and his experience, this work would not have been able to make many contributions to science. I would like to express my sincere appreciation for his patience and his availability, which he had showed me. I'm grateful to have the opportunity to have worked with one of the best researchers in his field, while I had never worked on grinding.

I appreciated the support of my co-advisor, Prof. Luc Baron as well. Thank you for accepting me as your student.

I also want to express my appreciation to the other members of my thesis committee, Prof. Aouni Lakis, Prof. Oguzhan Tuysuz and Prof. Wit Grzesik for giving me the opportunity to present the results of this doctoral project.

I want to express thanks to for the incredible people who have supported me over the past few years: Carole Fraser, secretary of the mechanical engineering department, for her kindness, her availability and her invaluable help with all the administrative work over the past seven years; Josée Laviolette, retired LAPOM technician, for her kindness and moral support; Nicola De Palma, (soon retired) NRC technician, for his help during the tests on the Makino as well as his good humor and his kindness.

Last but not least, my sincere thanks go to my mother, my little brother and my close friends for their endless love, support, patience, and encouragement.

RÉSUMÉ

Depuis leur développement dans les années 1990 en tant qu'alternative aux alliages de nickel, les composites de titane à matrice métallique sont des matériaux difficiles à usiner. De nombreux défauts subsistent sur la surface meulée, certains étant étroitement liés à la présence des particules de renforts dans ces matériaux. De manière générale, ces particules de renfort sont choisies plus dures que la matrice et présentent un comportement fragile. Dans la littérature, des études ont été menées en vue d'améliorer le fini de surface des pièces meulées, notamment la rugosité de surface. Ces études utilisent des meules conventionnelles telles que les meules en alumine blanche, alumine fondue rose, corindon microcristallin, ou encore des meules superabrasives comme la meule en nitrure de bore cubique. Or, les composites de titane à matrice métallique sont des matériaux qui présentent une sensibilité à l'augmentation de température et qui induisent une usure rapide des meules. Parmi les abrasifs répertoriés, le diamant est le matériau le plus dur répertorié à ce jour et possède une excellente conductivité thermique. Les meules en diamant s'avèreraient donc adaptées au meulage des composites de titane à matrice métallique, d'autant plus que des performances intéressantes ont été observées dans une étude récente [1].

La présente étude s'intéresse aux performances de meulage de meules en diamant galvanisées sur des composites de titane à matrice métallique renforcés de carbures de titane (TiC). L'objectif vise à étoffer les connaissances relatives au meulage des composites de titane à matrice métallique, et améliorer la compréhension du comportement de ces matériaux lors du meulage. Pour ce faire, une étude d'aptitude au meulage a été réalisée en termes de forces de meulage, consommation de puissance, rugosité de surface, énergie spécifique et analyse microstructurale. Cette étude s'est étendue à la morphologie et l'intégrité des surfaces meulées ainsi qu'au calcul des différentes composantes des forces normales et tangentielles, visant à valider les observations relatives à la morphologie et à l'intégrité de surface. Cette validation s'est faite par le biais de l'utilisation de modèles analytiques.

Les résultats des différentes études menées dans le cadre de ce projet doctoral ont permis de mettre en évidence des forces de meulage, une consommation de puissance et une rugosité de surface inférieure à celle d'un alliage de titane, et ce, pour des conditions expérimentales similaires. L'usure de la meule était également inférieure pour le composite de titane à matrice métallique que pour l'alliage de titane. Permettant de conclure quant à l'aptitude du composite de titane à matrice métallique à être meulé par une meule galvanisée en diamant. L'observations des rayures réalisées avec un seul grain abrasif ont permis d'identifier certains mécanismes relatifs à l'enlèvement de matière responsables de la morphologie et de l'intégrité de surface de la surface de travail.

Le calcul des composantes des forces normales et tangentielles relatives à ces essais a permis d'appuyer les observation des essais de rayure, notamment la prédominance de la déformation plastique de la matrice et de sa capacité à se re déposer sur la surface. La comparaison des forces calculées pour un essai de meulage avec les forces mesurées expérimentalement a permis de mettre en évidence la précision du modèle utilisé.

ABSTRACT

Titanium metal matrix composites (TiMMCs) were developed as an alternative to nickel-based alloys and are classified as difficult to machine/grind materials. The main issues encountered during the machining of the TiMMCs are related to the difference in mechanical properties between the matrix and the reinforcing particles. Studies in the literature focused on the improvement of the surface quality by comparing conventional (white alumina, pink fused alumina, microcrystalline corundum) and superabrasives (cubic boron nitride) grinding wheels. However, the TiMMCs are heat sensitive and fast cutting tool wear materials. Due to its high hardness and thermal conductivity, diamond would be the most suitable abrasive in grinding TiMMCs. In order to improve the grinding performance on heat sensitive and fast wear materials, namely the TiMMCs, the aim of this study was to provide insights and understanding of the grinding performance of TiMMC with electroplated diamond wheels. The grindability of TiMMCs with diamond wheels was studied in terms of wheel wear, power consumption, forces, surface roughness, and microstructure. The morphology and integrity of the ground surfaces were also studied through scratching tests to understand the TiMMCs behavior during the grinding. As a complement to these observations, the normal and tangential forces produced during the scratching tests were calculating using an analytical model.

The results of the study showed that the grindability of the TiMMC with an electroplated diamond wheel is better than that of a Ti alloy in the same grinding conditions. Indeed, the consumption in power, specific energy, the electroplated diamond wheel wear and the surface roughness as a function of the workspeed were lower for the TiMMC. Also, the surface roughness was found to decrease with the increase in workspeed. It could be attributed to the three-body abrasion occurring during the grinding and due to the presence of the reinforcing particles, as well as to the mixture of the ploughed matrix with the broken reinforcing particles redeposited on the ground surface. A higher material removal rate was found achievable by decreasing the depth of cut while increasing the workspeed or by increasing the grinding fluid pressure. Specific energy values ranged from 16 to 34 J/mm^3 under all the tested conditions due to the usage of high-pressure grinding fluid. The experimental study on the morphology and integrity of scratched surfaces on TiMMCs combined with the results of the analytical calculation of the components of the normal and tangential forces showed that the ploughing of the matrix was the higher force component, and so was the

predominant mechanism during the scratching tests. The comparison of the experimental and calculated grinding forces has shown the good accuracy of the model.

TABLE OF CONTENTS

DEDICATION III

ACKNOWLEDGEMENTS IV

RÉSUMÉ V

ABSTRACT VII

TABLE OF CONTENTS IX

LIST OF TABLES XII

LIST OF FIGURES XIII

LIST OF SYMBOLS AND ABBREVIATIONS XVI

LIST OF APPENDICES XVIII

CHAPTER 1 INTRODUCTION 1

1.1 Motivation and research objectives 1

1.2 Original contribution of the study 2

1.3 Thesis outline 3

CHAPTER 2 LITERATURE REVIEW 4

2.1 Titanium metal matrix composites 4

2.1.1 Introduction 4

2.1.2 TiMMCs categories 4

2.1.3 Mechanical properties 6

2.1.4 Material under study and manufacturing 11

2.2 DRTiMMCs and machining 12

2.3 Grinding of TiMMCs 14

2.3.1 Generalities about grinding Discontinuously Reinforced TiMMCs 14

2.3.2 Grinding of TiMMCs 16

2.4 Research objectives 18

2.5 Research methodology 19

CHAPTER 3 ARTICLE 1: INVESTIGATION ON WORKPIECE MICROSTRUCTURE AND WHEEL PREFORMANCE ON GRINDING TITANIUM METAL MATRIX COMPOSITES…… 21

3.1 Introduction 22

3.2 Experimental Setup and Test Conditions 23

3.3 Results and discussions 27

3.4 Conclusion 37

CHAPTER 4 ARTICLE 2: EFFECTS OF TOOL GEOMETRY AND FLUID ON THE SURFACE MORPHOLOGY AND INTEGRITY IN SCRATCHING TIMMCS 39

4.1 Introduction 39

4.2 Experimental Setup and Test Conditions 41

4.3 Results and discussions 43

4.3.1 Ground surface morphology and integrity 45

4.3.2 Scratches of tests without grinding fluid 46

4.3.3 Scratches of tests with grinding fluid 52

4.3.4 Comparison with ground surfaces 54

4.4 Conclusion 56

CHAPTER 5 ADDITIONAL RESULTS 58

5.1 Analytical forces calculation 58

5.2 Analytical model 58

5.2.1 Introduction 58

5.2.2 Methodology 59

5.2.3 Results and discussion..64

5.2.4 Conclusion...67

CHAPTER 6 GENERAL DISCUSSION...68

CHAPTER 7 CONCLUSION AND RECOMMENDATIONS...70

7.1 Conclusion..70

7.2 Recommendations..71

REFERENCES..72

APPENDICES...81

LIST OF TABLES

Table 2.1.2.1 Example of DRTiMMCs reinforcements [2] 5

Table 2.1.4.1 Chemical composition of the TiMMC used in this study [53] 11

Table 2.1.4.2 Mechanical properties of the TiMMC used in this study and produced by Dynamet technology Inc. [14] 11

Table 5.2.3.1 Experimental conditions used for analytical calculation 64

LIST OF FIGURES

Figure 2.1.1 Schematic representation of different types of reinforcements [2] 5

Figure 2.1.2 Comparative creep rate properties at 550°C[2] 8

Figure 2.1.3 Ultimate tensile strength for TiMMCs reinforced with TiB whiskers or TiC particles [2] 9

Figure 2.1.4 Schematic representation of the CHIP process [14] 11

Figure 2.5.1 Research methodology 20

Figure 3.2.1 Experimental setup 24

Figure 3.2.2 Microstructure pictures of (a) TiMMC and (b) Ti alloy 24

Figure 3.2.3 Example of power and forces measurements for the 100th passes 26

Figure 3.2.4 an example of radial wheel wear profile after 400 passes 26

Figure 3.3.1 Power, forces, surface roughness and specific energy from wheel wear tests 28

Figure 3.3.2 Workspeed effect on power and roughness 32

Figure 3.3.3 Ground surface pictures at the 20th pass for the (a) TiMMC and (b) Ti alloy with the same magnification 33

Figure 3.3.4 (a) TiMMC chip (b) enlargement of the chip 34

Figure 3.3.5 Process limits from workspeed and depth of cut combinations 34

Figure 3.3.6 Ground TiMMC surface with defects (v_w = 100 mm/s, a = 0.05 mm) 35

Figure 3.3.7 Effect of fluid pressure on the maximum depth of cut achievable 36

Figure 3.3.8 Sample cutting planes a) and microstructure after 400 passes on the b) YZ and c) XY plane 36

Figure 3.3.9 Twinning formations under the ground surface at YZ plane a) general view, b) enlarged view of a parent grain and twinning 37

Figure 4.2.1 Experimental setup with an enlarged view of the tool and sample 42

Figure 4.2.2 Optical microscopy image of the TiMMC microstructure 43

Figure 4.3.1 SEM pictures of tool tips after tests without grinding fluid a) the dressing tool, and b) the indenter 44

Figure 4.3.2 Scratch profile obtained from the broken dressing tool 44

Figure 4.3.3 Workpiece cross-section showing the microstructure under the ground surface after a) 20, b) 400, and c) 800 passes 46

Figure 4.3.4 a) Dressing tool scratch, b) indenter scratch, and c) chip re-deposition for the dressing tool, on the edge and at the bottom of the scratch 46

Figure 4.3.5 a) Broken particles pushed in the matrix in the scratching direction, b) and c) enlarged views of the square areas in a) 47

Figure 4.3.6 a) Hindering of the matrix plastic flow by the particles density increase at the bottom, b) on the edge of the scratch, and c) an enlarged view of the squared area from b) 48

Figure 4.3.7 a) Matrix waves and cupules at large scratch depth for the indenter, and b) matrix waves for the dressing tool 48

Figure 4.3.8 Chemical contrast picture showing the covering of particles by the matrix.............49

Figure 4.3.9 a) and b) Images of particles near α and $\alpha+\beta$ phases for the dressing, and c) for the indenter 50

Figure 4.3.10 Cracks at the bottom of the scratch for dressing tool from a) LEI detector, and b) LABE detector 50

Figure 4.3.11 Cupules of plastic deformation of the matrix on the edge of a particle before reaching its fracture point 51

Figure 4.3.12 a) Peeling of the matrix pieces which covered the broken particles, b) and same observation with the LABE detector 51

Figure 4.3.13 Evidence of partial particle dislodgement for the dressing tool with a) LABE detector, b) LEI detector, and for the indenter with, c) LABE detector and d) LEI detector 52

Figure 4.3.14 Evidence of partial dislodgement of broken particles. a) Holes observed with secondary electron detector, b) same observation with LABE detector 54

Figure 4.3.15 Ground surfaces after a) 20, b) 400, and c) 800 passes 55

Figure 4.3.16 a), c), e) LABE ground surfaces images, with b), d), and f) the corresponding LEI images...56

Figure 5.2.1 Calculated a), b) Normal forces, c), d) Tangential forces, e), f) Total normal and tangential forces, g) Calculated and measured forces comparison for the grinding wheel, h) Tangential forces comparison for two interfacial friction factors, and i) enlargement of the square 65

LIST OF SYMBOLS AND ABBREVIATIONS

α	Attack angle
a	Depth of cut, depth of scratch
C	Cutting grain per unit of area
CBN	Cubic Boron Nitride
CRTiMMCs	Continuously Reinforced Titanium Metal Matrix Composite
D	Indenter diameter
d_g	Grain diameter
d_s	Wheel diameter
DRTiMMCs	Discontinuously Reinforced Titanium Matrix composite
E^*	Equivalent modulus
FEM	Finite Element Modelling
H	Workpiece hardness (MPa)
HB	Brinell hardness of the workpiece
h_m	Undeformed chip thickness
L	Length between successive cuts
LAM	Laser assisted machining
l_c	Contact length
λ_s	Wheel circumference lenght
N_{gc}	Number of contacting grains
SEM	Scanning Electron Microscopy
PCD	Polycristalline diamond
PTMC	Particulate Titanium Matrix composite

r	Ratio scratch width/scratch length
R_a	Surface roughness
TEM	Transmission Electron Microscopy
TiB	Titanium Diboride
TiC	Titanium Carbide
TiMMCs	Titanium Metal Matrix Composite
UTS	Ultimate tensile strength
v_s	Grinding speed
v_w	Workspeed

LIST OF APPENDICES

Appendix A Article 3: Machining of Titanium Metal Matrix Composites.................................81

Appendix B Article 4: Performance of Electroplated Diamond Wheels in Grinding Titanium Metal Matrix Composites..99

Appendix C Conference paper award 105

CHAPTER 1 INTRODUCTION

Titanium metal matrix composites (TiMMCs) were developed as an alternative to nickel-based alloys for applications in the aerospace and automotives industries. They exhibited improved mechanical and chemical properties such as high specific strength, high specific modulus, high temperature and wear resistance [2], due to the addition of titanium carbide as reinforcing particles in a titanium alloy matrix. Despite attractive mechanical and chemical properties, the machining of the TiMMCs remained challenging owing to the higher hardness and brittle behavior of the TiC particles. The difference in mechanical properties between the matrix and the reinforcing particles caused machining issues such as premature wear of the tools, micro-cracks, broken particles and voids formation on machined surfaces [3, 4].

1.1 Motivation and research objectives

Developing an efficient machining process to obtain high surface quality was of interest in research activities on TiMMCs [5]. The surface roughness and wheel wear mechanisms were compared for different types of grinding wheels in most studies [4, 6-8]. Conventional abrasives, namely, white alumina, pink fused alumina, micro-crystal corundum as well as cubic boron nitride (CBN) superabrasives wheels, were used in these studies. Numerous defects were found on ground surfaces after grinding tests and some of them were caused by the presence of reinforcing particles. It was shown that the presence of the reinforcing particles increased the grinding force ratio under the same grinding conditions as well.

The grinding of an aluminum metal matrix composite (MMC) with diamond wheel provided more stable grinding forces and less sub-surface damage under the ground surfaces [9]. Since the use of diamond abrasives induced a few particle-related defects on the ground surfaces, they were recommended for producing high surface quality in machining MMCs [10, 11]. It was shown that the number of reinforcing particles had a noticeable effect on the surface roughness, tool wear, grinding forces as well as specific energy. For example, the specific energy obtained for diamond and CBN wheels under the same testing conditions on workpieces with different amount of particles (10% vol and 26% vol) were compared [12]. The specific energy for the diamond wheel was found to be lower than that of the CBN wheel with the decrease in particle amount, while the reverse trend was observed for the CBN wheel. The study concluded that when sharp and hard abrasives grains were used, the surface roughness is not related to the grinding parameters only. Another study compared super-abrasives (diamond or CBN) and conventional (silicon carbide and alumina) wheels [13]. It was showed that higher surface roughness and grinding forces were obtained for superabrasives wheels.

TiMMCs are heat sensitive and fast wheel wear materials. Diamond is the hardest material known so far and diamond abrasive possesses the highest thermal conductivity among all listed abrasives, which makes diamond wheels more suitable for grinding TiMMCs. A recent study [1] which reported the good performance of electroplated diamond wheels on titanium alloys motivated this thesis.

The **overall objective** of this study is to provide insights and understanding of the grinding performance of TiMMC with electroplated diamond wheels.

The specific objectives of the present research are:

- To investigate the grinding of TiMMCs with diamond wheels in terms of wheel wear, power consumption, forces, surface roughness, and microstructure.
- To enhance the knowledge of the grinding performances of TiMMCs.
- To reveal the morphology and integrity of scratched/ground surfaces on TiMMCs using single grain scratching tests.
- To use the calculation of the normal and tangential forces to improve the understanding of the morphology and integrity of scratched/ground surfaces.

1.2 Original contribution of the study

The grinding area requires further investigation on the performance on TiMMCs with diamond wheels. The grindability of TiMMCs with diamond wheels was implemented in terms of wheel wear, power consumption, forces, surface roughness, and microstructure. The present study also investigates the morphology and integrity of the ground surface to understand the effect of the removal mechanisms which took place during the grinding on the ground surface. For the first time, the morphology and integrity of the ground surface of TiMMCs which are of importance were studied in depth through scratching tests and microscopic observations and then, were related to the tool tip geometry and to the application of grinding fluid. The different aspects of the morphology and surface integrity were individually studied by single grain scratching tests. The understanding of the microscopic observation was completed by analytical modeling of the normal and tangential forces. The results made it possible to identify the aspect of the morphology and surface integrity in grinding by multi-grain abrasives.

1.3 Thesis outline

The previous section presented a general introduction on the machining/grinding of TiMMCs. Machining difficulties were addressed as well as a brief description of the objectives, and the original contribution of the study.

A comprehensive literature review on machining TiMMCs with primary emphasis on the material properties, difficulties encountered when machining Discontinuously Reinforced Titanium Matrix composites (DRTiMMCs), turning, milling, and grinding of TiMMCs was presented in Chapter 2. This literature review, which was the subject of a publication, was briefly presented and added in appendix A. Based on the literature review, the research methodology is established. The following chapters are organized by research papers. In Chapter 3, the grindability of the TiMMCs in terms of wheel wear, power consumption, forces, surface roughness, and microstructure is presented. The investigation of the morphology and the integrity of the scratched/ground surfaces on TiMMCs was addressed in Chapter 4. The analytical calculations of normal and tangential forces verifying the observations made in Chapter 4 are presented in Chapter 5.

Finally, Chapter 6 presents conclusions of the overall research as well as the recommendations.

CHAPTER 2 LITERATURE REVIEW

2.1 Titanium metal matrix composites

2.1.1 Introduction

Titanium alloys are important materials in a wide range of applications, including automotive and aerospace industries. The high specific strength, chemical stability and good biocompatibility of the materials allow various applications (structural, petrochemical, biomedical etc.). Titanium metal matrix composites have been developed to offer an alternative combining high specific strength, rigidity, and weight reduction. For example, TiMMCs based on titanium aluminides keep their strength at 760 ° C. They allow a weight reduction up to 50% compared to super nickel-based alloys while maintaining equivalent strength and stiffness. These properties are required for applications in high temperature compressors, and jet engine propulsion systems.

In the 1990s, NASA and the Titanium Matrix Composite Turbine Engine Composite Consortium (TMCTECC) made significant research efforts to increase their use in industrial applications such as large gas turbine engines. Although production costs are still high, the incredible properties of TiMMCs are a current research topic and the subject of development programs worldwide [2].

2.1.2 TiMMCs categories

The unique properties of TiMMCs are explained by the presence of non-metallic reinforcements in a titanium matrix or a titanium alloy. This combination results in the better properties of TiMMCs than a monolithic material [14]. Reinforcements are produced in different forms and allow TiMMCs to be distinguished under two main categories. The first one is the Continuously Reinforced TiMMCs (CRTiMMCs), whose reinforcing elements are continuous fibers. The second category, Discontinuously Reinforced TiMMCs (DRTiMMCs), has staple fibers or particles as reinforcements. These two categories are illustrated in Figure 2.1.1 [2].

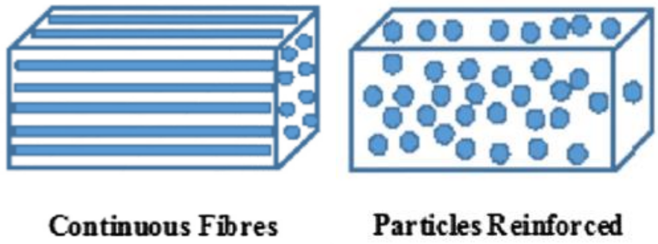

Figure 2.1.1 Schematic representation of different types of reinforcements [2]

The reinforcing particles used can be of various sizes or shapes. Most of the time, the particles are dispersed randomly, which makes it possible to give the composite isotropic properties, unlike reinforcements in the form of fibers, which have a preferential orientation. Table 2.1.2.1 present the mechanical and physical properties of common discontinuously reinforcements. The most used reinforcements are ceramics [2, 14, 15].

Table 2.1.2.1 Example of DRTiMMCs reinforcements [2]

Reinforcements	**Melting point (°C)**	**Density (g/cm ^{3})**	**Elastic modulus (GPa)**	**Coefficient of thermal expansion (x10 $^{-6}$K $^{-1}$)**
TiB	2200	4.50	425-480	8.60
TiC	3160	4.99	440	6.52-7.15 (25-500°C)
TiN	3290	3.97	420	8.30
SiC	2697	3.19	430	4.63 (25-500°C)
TiB_2	2980	4.52	500	4.60-8.10
Graphene	~3852	2.00	~1000	-
CNTs	~3379	1.70-2.00	~1000	-
B4C	2447	2.51	445	4.78 (25-500°C)
La_2O_3	2217	6.51	-	5.8-12.1 (100-1000°C)

Discontinuously Reinforced Titanium Composites (DRTCs) were developed in recent years. The craze is due to the less difficult and cheapest manufacturing than CRTiMMCs. The particles can be mixed with the matrix more efficiently and in greater proportion while avoiding rupture or delamination of the reinforcements [14, 16]. Many particles such as Al_2O_3, SiC, TiN, ZrC can be used, and carbon nanotubes. TiB and TiC are the most used [2, 17-21]. Some particles studied in the literature are classified as unstable like Si_3N_4, which react at high temperature to form titanium silicide [2, 22]. Thermal stability is an essential criterion for the design of TiMMCs which will be exposed to high temperatures in aeronautical applications.

2.1.3 Mechanical properties

The mechanical properties of TiMMCs are related to the reinforcement used. The properties of titanium or titanium alloy used for manufacturing as bulk material are widely known. The addition of reinforcements will change these properties by their state (fiber, particle, whiskers), their chemical composition and affinity with the matrix. Shypitsa and al [23] argued that the mechanical properties depend on the hardness and the mode of rupture of the reinforcement particles and, are defined by the interactions between the particles and the matrix.

2.1.3.1 Fatigue behavior

The primary objective of the emergence of TiMMCs was to develop a material with a good fatigue resistance under high stresses and high temperatures, such as rotating components of jet engine compressors [2, 24]. Fatigue resistance is linked to stiffness. This is why ceramics with high stiffness are chosen to produce TiMMCs.

The fatigue behavior of TiMMCs is however quite difficult to assess and interpret because the rupture mechanisms are different from those presented by isotropic materials such as metals. Indeed, different from metals, the accumulation of damage for a TiMMCs is not done by the propagation of a single macroscopic crack, but by the accumulation of general damage within the composite. The different types of damage commonly encountered for DRTiMMCs are cracking matrix or particles matrix debonding. The difficulty in interpreting the mechanisms lies mainly in the interactions between these different mechanisms and their own speed propagation. Especially since the mechanisms can be different in different orientations, in particular for TiMMCs with fiber reinforcements [25] or clusters of reinforcement particles for DRTiMMCs. It is well known that the proportion of reinforcements, the homogeneous distribution or not have a significant impact on the fatigue strength of the composites. Numerous studies have shown that the inhomogeneous distribution of reinforcements affected considerably the fatigue service life [26]. The clusters of particles will promote the formation of microcracks and lead to the propagation of premature cracks. As with metals, surface roughness has been shown to play an important role in the initiation of fatigue cracks and their propagation. In addition to the distribution of reinforcements, the manufacture approach of the composite plays a predominant role in its resistance to fatigue, for the propagation of cracks in the matrix and the interfacial adhesion between the matrix and the reinforcement [27, 28].

The parameters affecting the fatigue life of TiMMCs are crucial for the interpretation of the fatigue life of composites. Indeed, even if certain facts are well known, there are no American Society for Testing and Materials (ASTM) standards allowing to regulate and normalize the fatigue behavior of TiMMCs composites. This is why it is common to see that the fatigue strength of DRTMMCS is assessed in an equivalent way to that of bulks materials [2, 29, 30]. Although the results can be consistent for DRTiMMCs, this is not the case of TiMMCs reinforced with fibers. The fatigue strength of DRTiMMCs is dependent on the proportion of particles contained in the composite [18, 31]. The studies of Premkumar, Hashimoto, Ritchie et al. [32-34] showed that the higher the proportion of particles, the higher the stress-number of cycles (S-N) curve shifts to higher stress amplitude curve, to the detriment of ductility and toughness fracture [18].

The effects of particles on the fatigue life of DRTiMMCs are discussed in the literature. In fact, the improvement in fatigue life has not been observed by all the authors. Some highlighted the dependence on the shape and size of the particles [35]. Others rely on improvement in high cycle fatigue as well as on significant deterioration in fatigue performance cycle [36]. Others like Soboyejo et al. [37] argued that TiB whiskers lead to premature fatigue cracking despite improved general mechanical properties. Whiskers, unlike particles, do not seem to bring any noticeable improvement in the fatigue properties of TiMMCs.

2.1.3.2 Creep properties

TiMMCs designed to be used in high temperature environments, their creep properties are essential. A large proportion of TiMMCs present three stages of creep: the initial (primary), secondary (steady state), and tertiary (matrix creep and unnoticeably creep of particles, fibers, or whiskers). The second stage is the most important because that is when the creep strain (deformation) occurs. Generally, this stage is interesting for aeronautical applications because the reduction of the creep rate provides a better creep resistance.

As with fatigue resistance, improving the creep resistance of DRTiMMCs is questionable. Hayat et al. [2] showed that reinforcing particles do not necessarily improve the creep properties. Figure 2.1.2 from their study shows a significant improvement in creep properties when the particles are added in pure titanium, but also a reduction in creep properties when added in Ti-6Al-4V. In addition, Ti-6AL-4V has better creep properties without reinforcements [38].

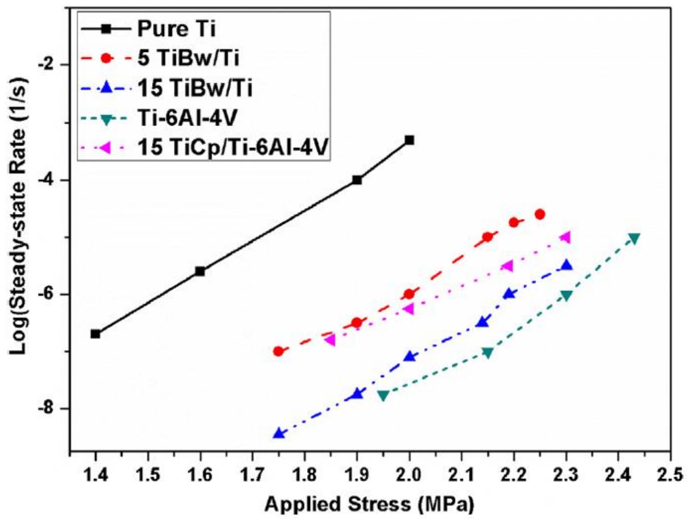

Figure 2.1.2 Comparative creep rate properties at 550°C[2]

Zhu et al. [39] and Tsang et al. [38] proposed the following three phenomena operating in TiMMCs reinforced by particles in order to improve the resistance of composites based on pure titanium: as for TiMMCs reinforced with continuous fibers, there is transfer of charge towards the reinforcements which are stiffer, which allows a higher modulus; interactions between reinforcements and dislocations which introduce a threshold stress and finally the former mechanism. The creep resistance of Ti-6Al-4V composites can be explained according to the authors, by the grain size, the morphology of the α and β phases, and the proportion of these phases, which constitute a considerable obstacle to the displacement of dislocations.

Finally, other authors like Wang et al. [40] have shown that the use of whiskers in Ti_6Al_4V could slow the creep rate. Their work showed that the distribution and use of a suitable volume of reinforcements made it possible to slow the deformation of the matrix and thus considerably improve the creep resistance. Thus, the break occurs only once the debonding between the whiskers and the matrix occurs and that the cracks are sufficiently large.

2.1.3.3 Charpy impact behavior

Although impact resistance is not one of the main requirements of TiMMCs, it is imperative that they have enough impact strength. Indeed, for applications in aeronautics, it is possible that the parts used are subject to impact damages as bird strikes. Impact behavior for DRTiMMCs has not been widely studied in the literature. The study available in the literature compare the impact strength of Ti alloys and fiber reinforced TiMMCs [41]. The results showed that impact resistance is less good than for TiMMCs, due to the deleterious effect of the reinforcing fibers. The fibers break during impact which leads to interfacial cracking and finally to the propagation of cracks leading to rupture.

2.1.3.4 Static properties

For DRTiMMCs, although the improvement in UTS (Ultimate Tensile Strength) is not as important as when using reinforcing fibers, improvement is prominent at high temperature. The presence of reinforcing particles or whiskers does not allow a considerable increase in UTS as in the case of fibers. These reinforcements make it possible to improve the UTS by being an obstacle to the movement of dislocations [2]. Figure 2.1.3 compares DRTiMMCs with monolithic alloys at different temperatures.

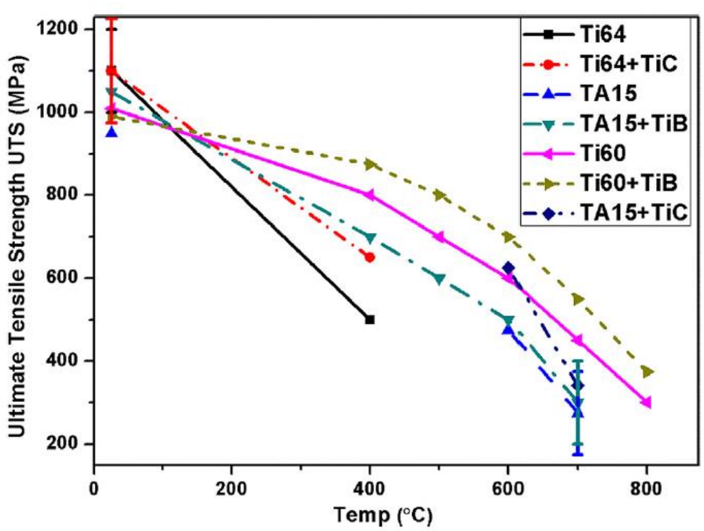

Figure 2.1.3 Ultimate tensile strength for TiMMCs reinforced with TiB whiskers or TiC particles [2]

The literature [17, 18] showed that the most effective reinforcements for improving the UTS of DRTiMMCs are TiB whisker and TiC particles. Their effectiveness is based on their chemical compatibility with titanium, high modulus, and hardness, but also, a coefficient of thermal expansion and a density close to those of titanium. In most cases, TiMMCs mechanical properties are limited by the temperature resistance of the matrix. Thus, increasing the proportion of reinforcements in DRTiMMCs would increase their high temperature strength at the expense of ductility and oxidation-resistance. The solutions in the literature have therefore been developed in order to obtain better mechanical properties at high temperature without damaging other aspects. Some authors [42-44] recommended the use of particles of different natures to combine the advantages of each type of particle. Others [45] have shown that tailoring reinforcement distribution is a solution for improving the ductility, deformability and high temperature strength of DRTiMMCs. Finally, Liu et al. [46] meanwhile, proposed a solution combining the two previous improvements. They used TiC particles and Ti_5Si_3 ultrafine needles as reinforcements. Their results showed an improvement in the properties which they explain by the hybrid strengthening effect, the tailored network structure, and the solid solution strengthening effect.

2.1.3.5 Wear and tribology

The low hardness of titanium and titanium alloys does not make it a favorite material for wear resistant applications. However, the addition of particles increases their hardness. And as for the mechanical properties seen previously, the hardness of TiMMCs is proportional to the volume percentage of ceramic reinforcements. The tribological and wear properties of DRTiMMCs are widely reported in the literature [43, 47-51]. Kim et al. [43] highlighted the effects of the content of reinforcing particles on the wear properties. They have shown that a high content of reinforcing particles makes it possible to reduce the wear resistance and thus improve the friction characteristics. As for Chaudhari et al [42] and An et al. [52], they focused on DRTiMMCs with a controlled microstructure. The two studies showed that the wear mechanisms depend on the size of the network formed by the reinforcement particles, and that the control of these microstructures makes it possible to expect the ideal properties for applications where resistance to wear is important.

2.1.4 Material under study and manufacturing

The material used in this study is a titanium metal matrix composite manufactured by Dynamet Technologie Inc. It is the well-known titanium alloy Ti_6Al_4V reinforced with TiC particles of irregular shape and 10-20 µm size. These particles are present from 10-12% by volume fraction. The chemical composition is presented in %mass in Table 2.1.4.1.

Table 2.1.4.1 Chemical composition of the TiMMC used in this study [53]

	Aluminium	Vanadium	Carbon	Oxygen	Fer	Nitrogen	Hydrogen
%mass	5.55	3.84	0.97	0.26	0.004	0.21	< 0.003

The mechanical properties are presented in Table 2.1.4.2 below. The material is the same as used in the study conducted by Maryam Aramesh [14] and Kamalizadeh et al [53].

Table 2.1.4.2 Mechanical properties of the TiMMC used in this study and produced by Dynamet technology Inc. [14]

Yield strength (MPa)	Tensile strength (MPa)	Elastic modulus (GPa)	Shear modulus (MPa)	Thermal conductivity (W/mK)	Specific heat (J/kgK)	Density (kg/m^3)
1014	1082	135	51.7	5.8	610	4500

The manufacturing process used is the CHIP process (Cold and Hot Isostatic Pressing) which provides parts near "net shape" [14]. Figure 2.1.4 illustrates the different stages of this process.

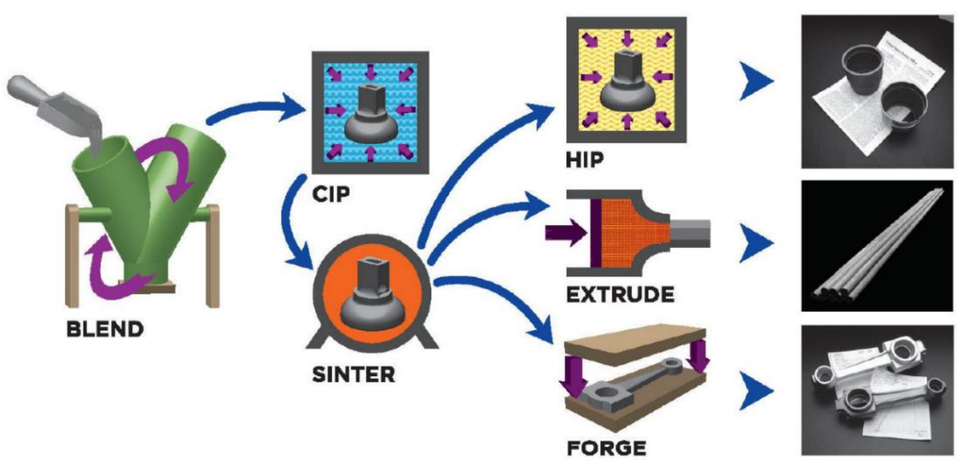

Figure 2.1.4 Schematic representation of the CHIP process [14]

First, the powders of the base materials are mixed and compacted at room temperature by high hydrostatic pressure. This is the CIP (Cold Isostatic Pressing). The cold pressed mixture is then heated under vacuum at high temperature below the melting point. At this stage the material is densified by the diffusion of the powder until the formation of the alloy or the MMC. The last manufacturing step is the HIP (Hot Isostatic Pressing). It consists in applying a medium temperature and hot argon gas pressure. This will reduce the residual porosity and improve the mechanical properties of the product. Finally, as illustrated in Figure 7 other processes can be used at the end of the process to obtain the final shape of the product [14].

2.2 DRTiMMCs and machining

The section below is based on the paper in appendix A1.

The nature of DRTiMMCs makes them difficult to cut. The difference in mechanical properties between the reinforcing particles and the matrix significantly affects the surface quality, material removal rates, and tool life. As shown in the paper, the literature review is not very exhaustive on the machining of TiMMCs. The purpose of this section is to provide an overview of the difficulties encountered in processes other than grinding. The other processes presented in the literature for the machining of TiMMCs are mainly milling and turning.

The papers on milling of TiMMCs are mainly concerned with tool wear, surface roughness, and chip morphology. Studies on tool wear [53, 54] have shown that a combination of optimum parameters makes it possible to minimize it. However, different wear mechanisms have been observed depending on the nature of the tool. Carbide tools showed adhesion as the main wear mechanism while PCD tools showed edge chipping, abrasion, and peeling. Even if studies talk about an acceptable tool wear, TiMMCs remain very poor thermal conductors. The high temperature close to the cutting-edge during milling results in high tool wear. This increase in temperature induces phenomena such as the chemical wear mechanism due to the chemical affinity between the tool material and the TiMMCs, or even oxidation. The chemical wear mechanisms are mainly chemical reactions, diffusion, and adhesion of the cutting tool [55]. The chip formation does not allow the evacuation of all the heat generated [56] and the scraped melted materials adhere to the tool [57]. These mechanisms, associated with the presence of abrasive particles and the high resistance to plastic deformation of a TiMMC, are the main ones responsible for the rapid wear of cutting tools regardless of their composition (PCD, CBN, etc.). Surface roughness also appears to be dependent on the type of tool used. Asgari et al. [53, 54] showed in their study that when using a carbide tool, the feed rate is the cutting parameter that has the most impact on roughness. Whereas, with a PCD tool, roughness depends on a set of parameters, not a particular cutting parameter. TiMMCs reinforced with carbon nanotubes, for their part, showed that the surface roughness was dependent on the cutting speed. However, the study does not specify the nature of the cutting tools and does not allow comparison [58]. The comparison of the mechanisms which operate during milling involves the study of chip morphology. The literature has shown that serrated chips are characteristic of the machining of TiMMCs. Kamalizadeh et al. [53] observed that the serration level increases with milling time, as do the cutting forces, friction force, and temperature. When turning TiMMCs, serrated chips are also obtained, and the serration level is dependent on the cutting speed [53, 59, 60].

Studies on the turning of TiMMCs are also mainly concerned with tool wear, surface roughness, chip morphology, but also the mechanisms of the first moments of cutting, unconventional techniques such as Laser Assisted Machining (LAM), or even dust emission. In most cases, studies on tool wear [54, 61] have shown a high wear rate for carbide and PCD tools, tool chipping as well as tool failure. However, these studies have also shown that increasing cutting speed helps reduce tool abrasion and thus tool wear. At higher cutting speed fewer particles are broken, and the simple displacement of particles results in less abrasion wear of the tool. Beyond 180 m / min, the mechanisms change and the increase in cutting speed no longer makes it possible to limit tool wear. LAM has also been shown to be effective in reducing tool wear, although this leads to other wear mechanisms such as diffusion, or adhesion of the tool to the machined part [62]. In the study conducted by Duong et al. [63], adhesion and diffusion during the first moments of cutting are effective in increasing the life of the tool thanks to the formation of a "wear shield" on the surface of the tool. This "wear shield" will act as a wear protection until it is itself consumed by wear and thus increase the tool life. In addition to limiting tool wear, increasing cutting speed results in a better surface roughness with lower roughness [60]. This can be explained by the decrease in particle breakage. Indeed, at low machining speed, a lot of particles are broken and therefore leave many pieces of particles on the surface, explaining the increase in surface roughness. While at high speed, if the particles are less broken and displaced in the matrix, fewer pieces of particles will remain on the surface and therefore reduce the roughness. No particle debonding was observed whatever the turning conditions. Cutting speed also plays an important role in chip formation [64]. The breakage or no breakage of the particles causes differences in the formation mechanisms of the chips in addition to the increase of the segmentation of the chips with the increase of the cutting speed.

Dust emission is of major interest for compliance with health and safety standards at work. Turning of the TiMMCs showed the emission of fine and fine particles under different conditions of the grinding fluid. The lowest particle emission would be at greater grinding fluid rate, at the expense of the surface roughness.

2.3 Grinding of TiMMCs

Since DRTiMMCs are difficult to cut materials due to the mechanical properties difference between the matrix and the reinforcing particles, grinding machinability has been studied in recent years as an alternative to conventional or heavy machining operations. Although the literature is not exhaustive on the grinding of TiMMCs, the main subjects seem to have been studied. The following paragraphs present the subjects discussed in the literature for DRTiMMCs in general and then for Ti_6Al_4V/T_iCp (Ti_6Al_4V reinforced with particles of titanium carbides) more particularly.

2.3.1 Generalities about grinding Discontinuously Reinforced TiMMCs

The material under study in this thesis is a titanium-based metal matrix (Ti_6Al_4V) composite reinforced with TiC particles. This paragraph briefly describes what has been studied for composites which do not have a titanium base matrix, or which have types of reinforcement other than TiC particles. Studies in the literature range from experimental observations to the development of numerical models to describe removal behavior.

Since grinding is a machining method used to improve surface integrity [11], studies in the literature are particularly interested in surface roughness. Despite the grinding difficulties linked to the difference in behavior between the reinforcement particles and the matrix, some authors [65] argued that Al/SiC composites have better results in grinding than aluminum alloys without reinforcements. Their observations revealed a better surface roughness and a lower tendency to clog the wheel. Soft materials like aluminum are known to have poor grindability. During grinding, the clogging of the wheel is caused by chip adhesion [12, 66]. The efficiency of the different types of wheels for grinding aluminum matrix composites was therefore of interest. The study conducted by Di Ilio et al. [13] on an Al / SiC composite revealed that the use of conventional wheels showed better performance than super abrasives: including a better surface roughness, lower grinding forces, and lower wheel clogging. Experimental observations have shown that the lower tendency to wheel clogging is mainly due on the one hand to a most open structure among the employed wheel, and on the other hand to the higher notch effect associated with the grinded composite. The authors suggest that if the wheel selection criteria is the minimum tendency for clogging, then the choice would be a conventional abrasive wheel. The cutting data tendency such as grinding forces or grinding temperature are of greatest importance, in terms of tool life or quality of the surface roughness. Thiagarajan et al. [67] studied the influence of particle volume on grinding forces, grinding temperature, and surface roughness for an Al / SiC metal matrix composite. They observed that an increase in the particle content led to an increase in grinding forces, temperature, and surface roughness. Their study showed that a high wheel and workpiece velocities induced a low grinding force and made it possible to obtain an improvement in surface roughness and a damage-free surface (without microcrack). The presence of micro-cracks on the ground surface has been studied in the literature, in particular in creep-feed grinding of a titanium alloy with an abrasive SiC wheel [68]. The study showed that optimum grinding parameters allow cracking-free surfaces. Hood et al. [69] obtained similar results in a different study with a single-layer electroplated diamond wheel. Either the absence of cracks or fractures in surface area and subsurface of the workpiece in creep-feed grinding. Creep-feed grinding is recognized for significantly enhance the removal rate or the surface quality, which are benefits for applications in aerospace [68, 70].

The study of the chip formation mechanism was carried out for an Al / SiC metal matrix composite [71]. The authors saw that the formation of the chip depended on the nature of the machined phase: matrix or reinforcing particle. Indeed, the aluminum matrix has a ductile behavior while the SiC particles are fragile. Four kinds of motion traces of grit were observed, resulting in four different types of chips: Al-matrix chips, SiC particle chips, and Al-SiC mixed chips: chunky chips or saw-tooth chips. Other authors have also studied the SiC / Al composite chip formation. Some authors [72] were interested in the shape of the chips without looking at the formation mechanisms, while others like Joshi et al [73] also investigated the formation mechanisms of the chips and in particular the impact of cutting parameters such as cutting depth. An analytical model was used to study the surface roughness on a GT35 (steel matrix based) with TiC reinforced particles [74]. Four stages of material removal were revealed by the results: ductile removal of the matrix, ductile removal of the particles, brittle fracture, and pull-out of the particles. According to the authors, plowing striations and fracture zones occurred at the same time. They were also able to determine the critical undeformed chip thickness for the transition from ductile to brittle behavior of the particles. Their experimental results have confirmed the importance of this critical value. Indeed, at small, undeformed chip thickness the particles present the ductile removal mode. Beyond this value, the brittle fracture of the particles occurs and considerably increases the surface roughness. The results of the model and experimental results are consistent. They helped to highlight the dependence of the surface roughness the feed rate and grinding depth.

The studies presented in the literature deal with different subjects such as chip formation or the influence of the different cutting parameters on the surface roughness, the grinding forces or temperature. These parameters have significant effects on the surface roughness.

2.3.2 Grinding of TiMMCs

The section below is based on the paper in appendix A.

The aim is to present the different aspects of Ti6Al4V / TiCp or Ti6Al4V / TiCp + TiBw (TiMMCs) grinding which have been discussed in the literature. This information is subject to publication, a summary of the importance of each grinding parameter, material removal mechanism, or experimental observation will be presented to highlight the gaps in the literature.

Grinding could be used for finishing or heavy machining operations. Mastery of a single process would limit the costs associated with subsequent machining operations such as milling or turning [13, 75]. The surface roughness is therefore a recurrent parameter when grinding TiMMCs and is often discussed in the literature. Microcracks, pile up, grinding scratches, or cavities [7] were observed on the ground surface after grinding. These surface defects significantly affect the surface roughness. Li et al [7] showed that the state of the grinding forces, as well as the size of the undeformed chip thickness, influence the ground surface morphology, in particular the presence of microcracks. Some surface defects affecting surface roughness are related to the presence of particulate reinforcements. Increasing the reinforcing particle content decreases surface roughness, according to the work of Blau et al [76]. As for the cutting parameters that influence the cutting force, these are mainly the depth of cut and the cutting speed. A comparison of the cutting forces between a cut at 120 m/s and 20 m/s showed that an increase in cutting speed led to lower cutting forces [7, 77]. This decrease in cutting forces is due, according to the authors, to a lower friction coefficient. Although increasing the cutting speed will reduce cutting forces, this does not only bring benefits for the grinding of TiMMCs. Indeed, the increase in cutting speed also increases the action of grinding grains in the contact zone per unit of time as well as a drop efficiency of the coolant, increasing temperature. A grinding temperature too high [6, 78, 79] affects the microstructural or mechanical integrity and can cause the creation of surface microcracks [4]. The main changes observed following a too high grinding temperature are a microstructural change under the surface of the cutting part and a change in the microhardness values [6, 8]. Studies on cutting parameters altering microstructural and mechanical integrity [6, 8] on the part have shown that the depth of cut is the parameter that induces a higher microstructure variation. The undeformed chip thickness is a grinding parameter that influences many parameters such as the grinding force, grinding temperature, surface roughness, and material removal mechanism [4, 7, 80]. Observations in the literature show that an increase in undeformed chip thickness will produce deep and wide cavities on the ground surface, but also lateral cracks. These dependencies increased surface roughness [7, 8]. Studies on chip morphology have shown that the material removal behavior is divided into three main stages [8, 80]. The first and last stages correspond to a ductile regime removal of the matrix with serrated chip formation. The second stage corresponds to the brittle regime removal, for which the brittle fracture, crack initiation, and crack propagation take place. Ding et al [80] also showed that the chip morphology is dependent on the cutting speed. An increase in cutting speed led to finer and discontinuous chips. Finite element (FE) analysis studies [7, 8] on material removal mechanisms have shown that particle crushing depth is affected by undeformed chip thickness, especially in high-speed grinding.

The grinding wheel performance is one of the main concerns when addressing the grinding of TiMMCs. The presence of TiC particles causes premature wear of tools by abrasion. The various studies in the literature [4, 6, 81] were interested in the grinding wheel performance in terms of force, temperature, and energy, but also of ground surface roughness. Theses research aim to find the most suitable tool, which has the longest life according to precise cutting conditions and produce a low surface roughness. These studies compare the effectiveness of conventional grinding wheels (white alumina (WA), pink fused alumina (PA), and micro-crystal corundum (SG)) [6], with super abrasive wheels in CBN (Cubic Boron Nitride) [4, 81]. In high-speed grinding, the brazed CBN wheels are those with the largest removal rate, the lowest cutting force and cutting temperatures, and which minimize the presence of surface defects. For grinding at conventional speed, the SG wheel is the one that minimizes surface defects (grooves and voids).

2.4 Research objectives

Based on the literature review on the grinding of TiMMCs, the research plan is intended to address the following objectives:

Objective 1:

- Investigate the grinding of TiMMCs with diamond wheels in terms of wheel wear, power consumption, forces, surface roughness, and microstructure (*Objective 1.a*)
- Enhance the knowledge of the grinding performances of TiMMCs (*Objective 1.b*)
    - To investigate the wear of the wheel and the effects on the grinding performance.
    - To explore the effect of workspeed on power and surface roughness.
    - To investigate the limits of the process by varying the depth of cut and the workspeed to obtain the higher material removal rate while maintaining a good surface quality.
    - To find out the maximum depth of cut achievable by varying the grinding fluid pressure without ground surface defects.
    - To compare the grindability of the TiMMC and a Ti (titanium) alloy.

These goals under Objective 1 were accomplished in Chapter 3.

Objective 2:

- Reveal the morphology and integrity of scratched surfaces on TiMMCs using scratching tests (single abrasive grain)
    - To investigate the effect of tool tip shape and use of grinding fluid on the scratched surfaces morphology and integrity.
    - To identify the surface morphology and integrity of the scratched surfaces, and by comparison, identify the surface morphology and integrity of the ground surfaces.
    - To reveal the effect of wheel wear on the surface morphology and integrity in grinding TiMMCs.

These goals under Objective 2 were accomplished in Chapter 4.

Objective 3:

- Improve the understanding of the morphology and integrity of scratched/ground surfaces on TiMMCs
    - To predict the normal and tangential forces related to the scratching tests using an analytical model.
    - Perform the calculation for the scratching tests.
    - To reveal the similarity between the calculated forces and the morphology and integrity of scratched/ground surfaces on TiMMCs.
    - Verify the accuracy of the model with experimental grinding forces from Chapter 3.

These goals under Objective 3 were accomplished in Chapter 5.

2.5 Research methodology

The objectives mentioned above incorporate mainly experimental investigations. The different phases and steps of investigation to conduct this research are presented in Figure 2.5.1. The entire research was split into three phases. Phase 1 included the experimental part which led to the achievement of the objective 1, the grindability study of the TiMMC with a diamond wheel. The results were examined in terms of grinding force, temperature, tool wear, surface roughness and microstructure to evaluate the efficiency of the grinding performance. Phase 2 was the scratching tests, and the evaluation of the morphology and integrity of the scratched surfaces. The SEM observations led to the identification of the surfaces particularities and were an input for the identification of the particularities of the ground surfaces from phase 1. Tool tip shape and grinding fluid use has been considered for the identification of the morphology and integrity of the scratched and ground surfaces. The results obtained completed the Objective 2.

Finally, Phase 3 used the experimental parameter from phase 1 and 2 to calculate the normal and tangential forces of scratching tests. The results which included the sliding, ploughing and cutting components of normal and tangential forces, completed the understanding of the morphology and integrity of the scratched surfaces identified in Phase 2. Then, the normal and tangential forces of the grinding tests from phase 1 were also calculated to compare them with the experimental results to determine the accuracy of the model used. These results led to the achievement of the objective 3.

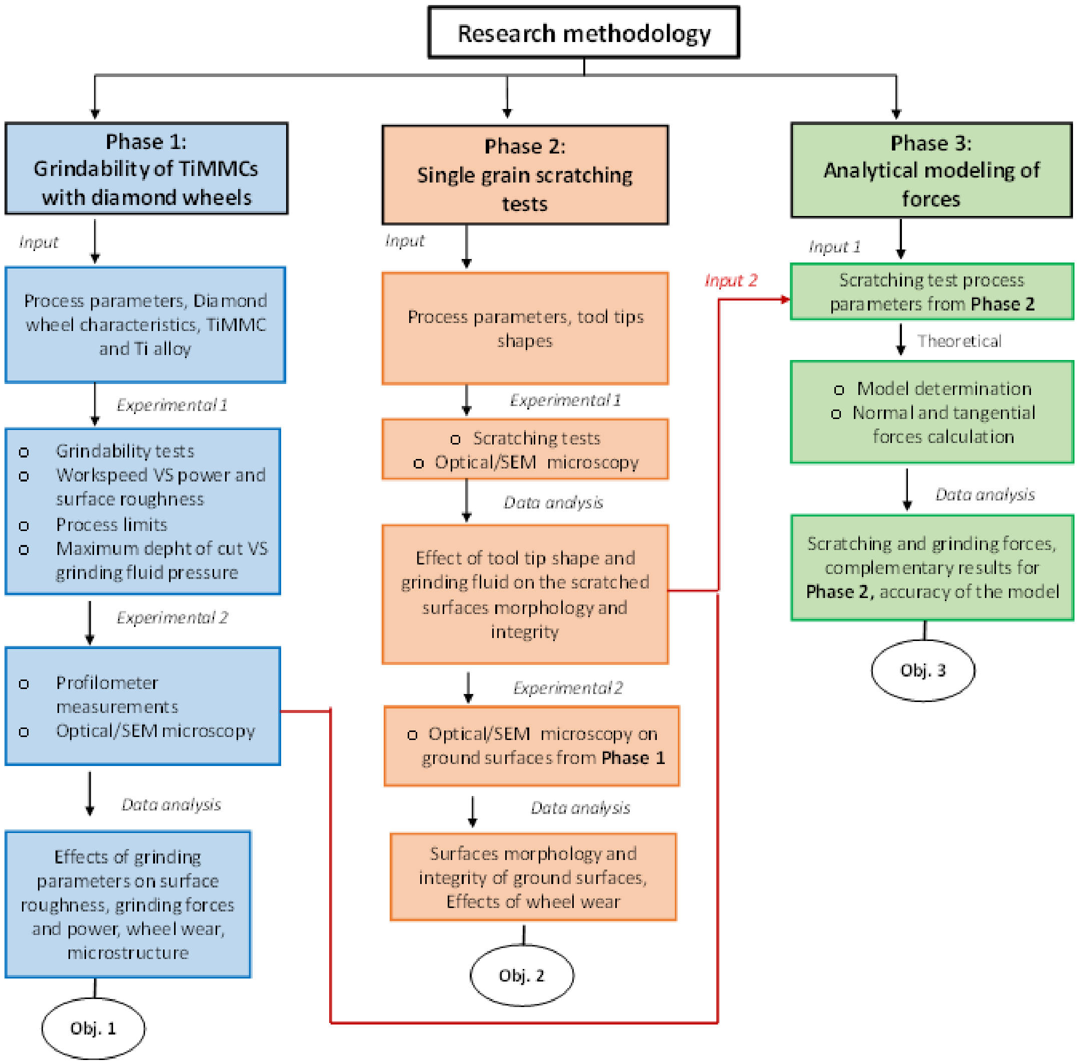

Figure 2.5.1 Research methodology

CHAPTER 3 ARTICLE 1: INVESTIGATION ON WORKPIECE MICROSTRUCTURE AND WHEEL PREFORMANCE ON GRINDING TITANIUM METAL MATRIX COMPOSITES

Coauthors: Zhongde Shi, Luc Baron, and Marek Balazinski

Submitted on October 28, 2022, and accepted for publication on January 13, 2023.

International Journal of Abrasive Technology

Abstract

An experimental study is reported on the grinding of a titanium metal matrix composite (TiMMC) using electroplated diamond wheels. Flat surface grinding experiments were performed at a fixed wheel speed v_s = 20 m/s, various depths of cut a = 0.03 - 0.08 mm, and workspeeds v_w = 10 - 100 mm/s. Additional tests were also conducted on titanium alloy (Ti alloy) for comparisons. The wheel wear and its effects on grinding forces, power, surface roughness, and workpiece microstructures are presented. The process limits were also investigated. It was revealed that steady state wheel wear on TiMMC was slightly slower than on Ti alloy. Low specific energy ranging from 16 – 34 J/mm^3 was obtained for both materials. It was found that surface roughness decreases for TiMMC, but increases for Ti alloy, with increasing workspeeds. Plastic deformation leads to microstructural change in the form of twinning below ground surfaces.

Keywords: Grinding, titanium metal matrix composite, electroplated diamond wheel, wheel wear, surface integrity

This paper is a revised and expanded version of a paper entitled *Performance of Electroplated Diamond Wheels in Grinding Titanium Metal Matrix Composites*, presented at the 23rd International Symposium on Advances in Abrasive Technology, 30 Nov. - 3 Dec. 2021, Hokkaido.

An excellent paper award was obtained for this paper (appendix B).

3.1 Introduction

Titanium metal matrix composites (TiMMCs) are an alternative to Ti alloys for use in the automotive and aerospace industries as they exhibit excellent mechanical and chemical properties such as high specific strength, high specific modulus, high temperature and wear resistance [2, 82]. However, machining TiMMCs is challenging due to the difference in properties between the matrix and the reinforcing particles. The difference leads to ductile removal of the matrix material and brittle removal of the particles. The issues encountered during machining of TiMMCs include mainly premature wear of cutting tools, voids, pileups, not to mention micro-cracks, broken particles, and microstructural changes [3, 4, 6, 8]. Research on machining TiMMCs was focused on developing efficient machining processes to get high surface quality [5]. Several studies [4, 6-8] compared the performance of different types of grinding wheels in terms of surface roughness and wheel wear mechanisms. The studies were carried out with either superabrasive wheels, in particular cubic boron nitride (CBN) wheels, or conventional abrasive wheels such as white alumina, pink fused alumina, or micro-crystal corundum. Numerous defects were found on ground surfaces with all the tested wheels. Some of these defects were caused by the presence of TiC or TiB reinforcing particles. It was shown that their presence increased the ratio of normal to tangential grinding forces compared to Ti_6Al_4V for similar grinding parameters. Studies on grinding metal matrix composites (MMCs), including TiMMCs, were reported. But none of them was concerned with the radial wheel wear, which is of importance for estimating wheel life.

Grinding aluminum MMC with diamond wheels was found to provide lower and more stable forces in both fine (220-grit) and ultra-fine (3000-grit) grinding [9]. It was showed that lower grinding forces led to less sub-surface damage to the ground samples. A few particle-related defects were present in the ultra-fine grinding. But particle debonding from the matrix was not found. Hence the use of diamond abrasives was recommended for obtaining an ultra-smooth surface roughness in grinding MMCs [10]. The specific energy was compared under an identical removal rate ($Q_w' = 2.5$ mm^2/s) and conditions on grinding aluminum MMC with diamond and CBN wheels. The specific energy (25 J/mm^3) for the diamond wheels was higher than that of the CBN wheel (15 J/mm^3) on the material with a 26% vol of reinforcement. The trend is reversed when the percentage was reduced to 10%. It was revealed that the surface roughness was not strongly dependent on the grinding parameters when sufficiently hard and sharp abrasive grains were used [12]. It was showed that lower grinding forces, surface roughness, and percentage of wear flat area were obtained with conventional wheels (SiC and Al_2O_3) than with superabrasives wheels (diamond or CBN) [13]. Another study recommended using SiC wheels to conduct initial rough grinding and fine-grained diamond wheels for finishing operations [11] in order to obtain both high material removal rate and good surface roughness.

Diamond is the hardest material known so far and possesses the highest thermal conductivity among all abrasives. Such properties of diamond make diamond wheels more suitable for grinding heat sensitive and fast wheel wear materials. TiMMCs are among this type of materials. It was recently showed that electroplated diamond wheels performed very well on grinding Ti alloys [1], which motivated this study. The present paper is concerned mainly with the grinding performance in terms of forces, power consumption, wheel wear of TiMMCs with a diamond wheel, as well as the workpiece microstructure. The objective is to investigate the grinding of TiMMCs with diamond wheels and to enhance the knowledge of the grinding performance of TiMMCs. The grinding of a Ti alloy and TiMMC under identical conditions are compared throughout the paper.

3.2 Experimental Setup and Test Conditions

Straight flat surface up-grinding tests were performed on a Makino A88E high-speed and high-power machining center. The wheel was a 120-grit electroplated diamond wheel of diameter d_s = 50.8 mm and width b_s = 38 mm. Figure 3.2.1 shows the experimental setup. A water-based grinding fluid of 7% soluble oil was applied at a flow rate of 140 L/min and a pressure of 2.8 MPa (400 PSI) through a rectangular nozzle with an opening width of 15 mm and a height of 2.5 mm. The workpieces were rectangular blocks of TiMMC with a length of 76.2 mm (3 inches) along the grinding direction and a width of 12.7 mm (0.5 inches). The TiMMC is composed of Ti_6Al_4V matrix reinforced with 10 - 12% vol of TiC particles. The average size of the TiC reinforcing particles is 10 - 20 µm. Figure 3.2.2 (a) shows the bimodal microstructure of the material. The globular α phase is surrounded by Widmanstätten platelets. Widmanstätten structure (α+β) is composed of retained β phase lying between the α platelets. The TiC reinforcing particles are distributed in the matrix. Tests were also conducted on Ti_6Al_4V (hereinafter referred to as the Ti alloy). Figure 3.2.2 (b) shows the Ti alloy microstructure. The microstructure of the Ti alloy has the same phases as the matrix of the TiMMC.

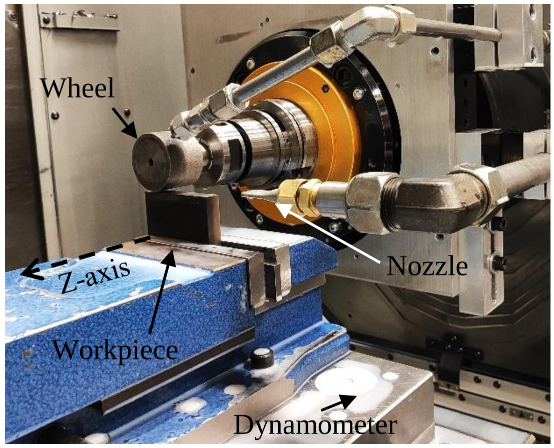

Figure 3.2.1 Experimental setup

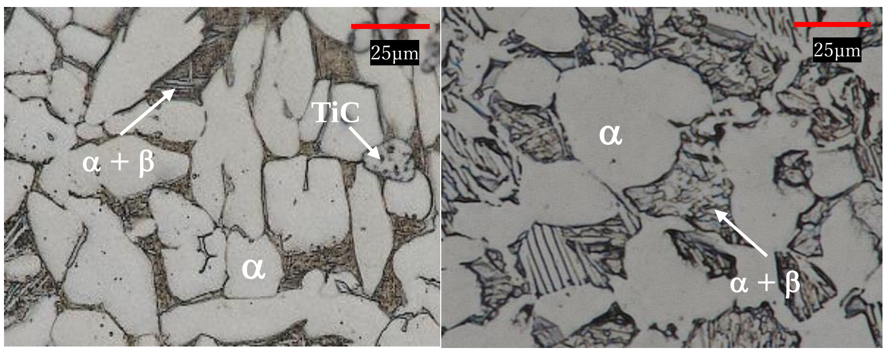

(a) (b)

Figure 3.2.2 Microstructure pictures of (a) TiMMC and (b) Ti alloy

Four sets of tests were performed at a fixed wheel speed v_s= 20 m/s. The first set of experiments was to investigate the wear and its effect on the grinding performance of the wheel. The workspeed was fixed at v_w= 50 mm/s and the depth of cut at a = 0.05 mm. The second set of experiments was to explore the effects of workspeed. The workspeed was varied from v_w = 10 to 100 mm/s corresponding to a specific material removal rate of Q_w' = 0.5 - 5 mm^2/s. The third set of experiments was to investigate the limits of the process by varying the depth of cut and the workspeed to obtain the combinations of the parameters allowing higher material removal rates while maintaining a good ground surface quality. The last set of tests was to find out the maximum depth of cut achievable by varying the grinding fluid pressure. For these tests, the workspeed was fixed at v_w = 50 mm/s. Additional tests were conducted on the Ti alloy with the conditions of the first and the second sets of tests to compare the grindability of TiMMCs and the Ti alloy. The Ti alloy workpieces were selected to have the same shape and size as those of the TiMMC workpieces. A different width section of the same wheel used for grinding the TiMMC was utilized to grind the Ti alloy. Conducting the tests on both materials using the same wheel, instead of two nominally identical wheels, was helpful for eliminating the effects of the inevitable variations of nominally identical wheels.

Grinding Power, forces, surface roughness, and radial wheel wear were measured. A universal power cell was used to measure the electrical power of the spindle motor, and a Kistler 9255B dynamometer for the forces. The forces and power measured in this way included net components for material removal, and non-grinding components due to the impact of grinding fluid and various frictions. The net components, which are of the interest for the data analysis, were extracted following a previous approach [83]. An example showing the total components of forces and power, the non-grinding components, and the net components for the 100th pass in the first set of tests on TiMMC is presented in Figure 3.2.3. The average net horizontal and vertical forces were F_h = 36 N and F_v = 89 N, respectively. The average net power was P = 0.56 kW corresponding to a specific energy of u = 17.6 J/mm^3. The large non-grinding forces were apparently due to the impact of high-pressure fluid jet. Radial wheel wear was measured by grinding a graphite specimen wider than the workpieces. The section of the wheel width not used for grinding the workpieces provided a reference surface to measure the wear. The wear depth was obtained by making a stylus trace across the grinding track of the specimen using a Taylor-Hobson profiler [84]. An example of the radial wheel wear profile is presented in the Figure 3.2.4. This profile was measured after 400 wear passes and showed a wear depth of about 20 µm. Three measurements of roughness for each test were conducted with a portable Taylor-Hobson Surtronic 3+ surface roughness checker. The microstructural observations and evaluations of surface integrity were done with an optical microscope Keyence VHX-7000, after mirror polishing and chemical attack with Kroll's reagent.

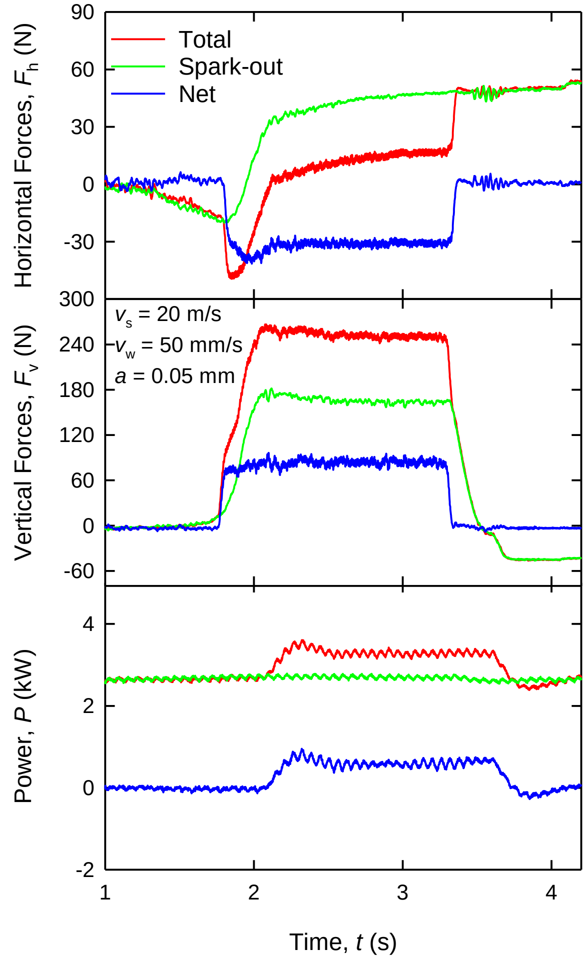

Figure 3.2.3 Example of power and forces measurements for the 100th passes

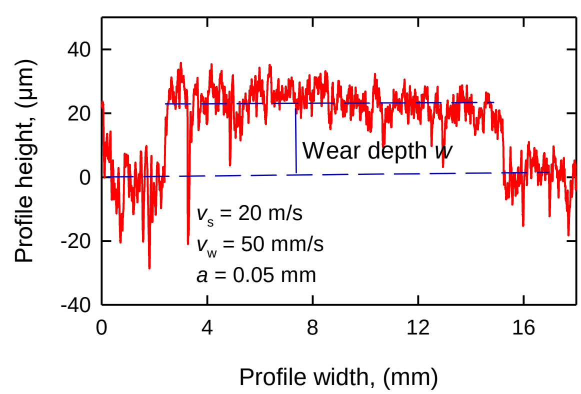

Figure 3.2.4 an example of radial wheel wear profile after 400 passes

3.3 Results and discussions

A total of 800 passes were conducted in the wheel wear tests. It should be noted that the wheel was still in its good condition at the end of the tests and could grind more passes. But the wear tests were stopped following the completion of the 800th pass to save the workpiece material. The results for the vertical force F_v, horizontal force F_h, power P, surface roughness R_a, and radial wear depth w in the wear tests are summarized in Figure 3.3.1. The initial radial wheel wear after the first pass was about w = 16 µm for the TiMMC and 5 µm for the Ti alloy. The radial wear exhibited a clear transient run-in from the start up to the 50th pass for the Ti alloy and increased throughout the tests. Small increases were also observed at the 200th and 600th pass. For the TiMMC, only small increases are observed at the 100th, 400th, and 800th pass. A weak steady state was reached by the end of the 800th passes for Ti alloy and the TiMMC. In a previous study [85] on Ti alloy, the initial radial wheel wear was around 10 µm. Initial wear is affected by the initial wheel conditions and grinding forces. It is due to the pull-outs of weakly bound diamond grains. A larger grinding force and/or a wheel with more weakly bonded grains lead to more grain pull-outs and hence a higher initial wear value. This might explain the initial wear values reported in this study. The higher initial wheel wear value obtained for the TiMMC was consistent with the higher grinding forces measured. At the end of the tests, the wear depth reached w = 28 µm for TiMMC and 27 µm for Ti alloy, respectively.

Power, forces, and surface roughness changed progressively due to the continuing radial wheel wear. In the case of the TiMMC, the vertical and horizontal forces stabilized after the end of the initial transient run-in at the 100th pass. The vertical force varied between F_v = 76 and 92 N at the beginning and then increased gradually up to F_v = 98 N at the 800th pass. The horizontal force followed a similar trend with its value varying between F_h = 33 and 40 N, and then gradually increased to F_h = 40 N. The forces for the Ti alloy were more stable and its trend did not coincide with that of transient radial wheel wear. The vertical force was F_v = 73 N at the first pass, then increased to F_v = 82 N at the 5th pass and gradually reached F_v = 85 N at the 800th pass. The horizontal force followed the same trend, the values ranged from F_h = 32 to 37 N. The horizontal and vertical forces obtained for the TiMMC were of the same order of magnitude but slightly higher than the corresponding forces of the Ti alloy. For example, the vertical forces with the TiMMC were 3 N at the 100th pass and 18 N at the 800th pass higher than the corresponding forces of the Ti alloy.

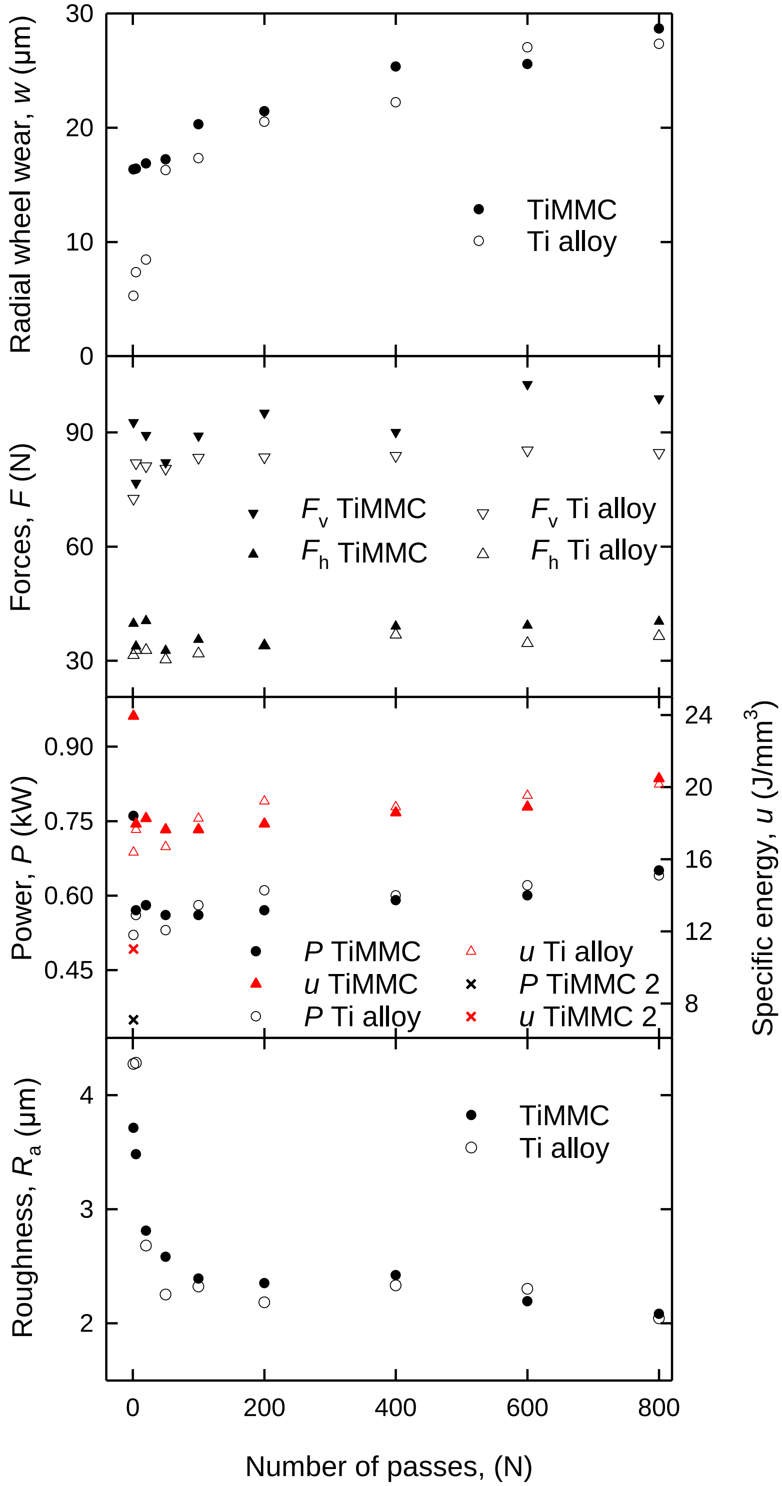

Figure 3.3.1 Power, forces, surface roughness and specific energy from wheel wear tests

The power values for both materials were quite close. The power for the TiMMC was just slightly higher than that for the Ti alloy from the 5th to the 50th pass, and in the 800th pass. They presented a maximum difference of 6.5% except in the first pass, for which a difference of 32.7% was observed between the values. The power for the TiMMC reached P = 0.76 kW in the first pass and then decreased down to P = 0.57 kW in the 100th pass. After that, it increased progressively to P = 0.65 kW at the 800th pass. The power trend here was different from the general power trend with electroplated superabrasive wheels, in which the power increases progressively with continued grinding or wheel wear. The power signal in the first pass was analyzed again to investigate the violation of the general trend. It was found that the pass was conducted with a workspeed of v_w = 65 mm/s, instead of the planned v_w = 50 mm/s. The measurement of the initial power for the workspeed v_w = 50 mm/s was repeated with a new wheel. The initial power was about P = 0.35 kW and presented as "TiMMC 2" in the Figure 3.3.1. The repeated measurement followed the general power trend. It should be noted that the original result was previously published [86] for the workspeed v_w = 50 mm/s. The abnormal power trend was not clear in that publication, and it was mentioned that further investigation would be needed.

In the case of the Ti alloy, the value was P = 0.52 kW in the first pass and gradually increased reaching P = 0.64 kW in the 800th pass. It is worth mentioning that the power values in the present study are of the same magnitude of the power obtained in a previous study on the grinding of the same Ti alloy with a nominally identical diamond wheel [1]. The power values for the first and the 800th passes from the previous study were P = 0.60 kW and P = 0.95 kW, respectively, which were slightly higher than obtained in the present study, which were P = 0.52 kW and P = 0.64 kW. As mentioned above, the tests were carried out with two nominally identical grinding wheels. The slight difference between the power values can be attributed to the difference of the initial wheel conditions.

The surface roughness for the TiMMC decreased quickly from its initial value R_a = 3.71 down to 2.39 µm in the 100th pass and then decreased slowly reaching R_a = 2.08 µm at the end of the wear tests. The surface roughness for the Ti alloy followed a trend similar to that of the TiMMC. However, it decreased faster from its initial value R_a = 4.27 µm down to 2.25 µm in the 50th pass and reached R_a = 2.04 µm at the end of the tests as shown in Figure 3.3.1. It is well known that surface roughness in grinding with electroplated superabrasives wheels is closely related to radial wheel wear. A large radial wheel wear leads to a smoother wheel surface and hence lower ground workpiece surface roughness. The surface roughness and radial wheel wear obtained in this study agreed well with the above-mentioned relationship. The initial surface roughness for the TiMMC was lower than that for the Ti alloy, which was consistent with the radial wheel wear of w = 16 µm for the TiMMC and w = 5 µm for the Ti alloy. The almost equal radial wheel wear of w = 28 µm for the TiMMC and w = 27 µm for the Ti alloy, at the end of the wear tests resulted in almost equal surface roughness values, R_a = 2.08 µm for the TiMMC, and R_a = 2.04 µm for the Ti alloy.

The measured radial wheel wear in Figure 3.3.1 was used to calculate the G-ratio, which is the volumetric ratio of the material removal and wheel wear. A higher G-ratio value indicates a higher wheel wear resistance. The G-ratios calculated from the total wear depths were 680 and 710 for the TiMMC and Ti alloy, respectively. It should be emphasized that the above G-ratios were calculated from the total wear depth, which included the initial wear depths and were affected by the initial wheel conditions. To exclude the effect of the initial wheel wear, the G-ratios were further calculated using the wear depths from the 50th to the 800th passes, which is more suitable for comparing the G-ratios from different materials. The G-ratio values reached 1648 and 1026 for the TiMMC and Ti alloy, respectively. In a previous study on grinding the same Ti alloy under identical conditions [1], the total and the 50th to 800th passes G-ratios were respectively 944 and 1884. They are slightly higher compared with the present study. The difference can be attributed to the wheel conditions.

As mentioned in the previous section, the present tests were conducted with different width sections of the same wheel. Therefore, differences in the G-ratios for the two materials can be considered from the materials only. The G-ratio for the TiMMC from the 50th to the 800th passes was higher than that of the Ti alloy, which might be attributed to the three-body abrasion phenomenon found in grinding of superalloys and ceramic [87, 88] and turning of MMCs [89-92]. Three-body abrasion is a sub-category of abrasion wear and is defined as the wear caused by a free particle at the interface between a solid body and a counter-body [93]. Dislodgments and/or breakages of the reinforcing TiC particles in MMCs have different effects during grinding. The particles help the removal of workpiece material through three-body abrasion on one hand. On the other hand, they cause wheel wear. The abrasion resistance of a cutting tool depends on the relative hardness of the materials [89]. Diamond, being much harder than TiC (Knoop microhardness: 54 – 84 GPa for diamond and 20 – 30 GPa for TiC), was much less subject to the additional abrasion wear than MMC matrix, which is softer than the TiC particles. The combined abrasion effects to the wheel and the workpiece eventually led to a higher G-ratio with the TiMMC.

Specific energies are also shown in Figure 3.3.1. As mentioned earlier, the measurement for the initial pass on the TiMMC was repeated in order to obtain the power for the planned workspeed v_w = 50 mm/s. The specific energy calculated from the repeated measurement was about u = 11.0 J/mm^3. It increased progressively to 20.5 J/mm^3 at the end of the tests. The initial value for the Ti alloy was u = 16.4 J/mm^3 and gradually increased to u = 20.2 J/mm^3. Similar to the power, the specific energy for the TiMMC was slightly lower than that for the Ti alloy. This was expected since the tests for both materials were conducted under an identical material removal rate. The specific energy values reported in literatures were generally higher than those in the present study. Specific energies between 88 and 288 J/mm^3, i.e. 4 to 14 times more than obtained in the present study, were reported in a study on the grinding of a TiMMC with a conventional wheel [6]. The specific energy values in the present study were also lower than those of other metal materials such as hardened steel and nickel alloys ground with various types of wheels and conditions [94]. The low specific energy values in the present study can be attributed to the usage of high-pressure grinding fluid and the wheel surface cleaning by the high the pressure fluid spray. The combined effect of the high-pressure fluid and wheel surface cleaning avoided the wheel surface loading with sticky chips, which were mainly responsible for the high specific energy with titanium-based materials in other studies.

The results of power and surface roughness for the effects of workspeed in the second set of experiments are shown in Figure 3.3.2 for both materials. For each of the tested condition, two grinding passes were conducted. No variations were observed in power between the two passes. The power values at the workspeed v_w = 10 mm/s were P = 0.22 kW for the TiMMC and 0.17 kW for the Ti alloy. The power increased with increasing workspeed and reached P = 1.37 kW and 1.93 kW, respectively, at the maximum tested workpseed v_w = 100 mm/s. It can be seen that the power for the TiMMC was lower than that for the Ti alloy, except at the workspeed v_w = 10 mm/s.

6 Workspeed effect on power and roughness

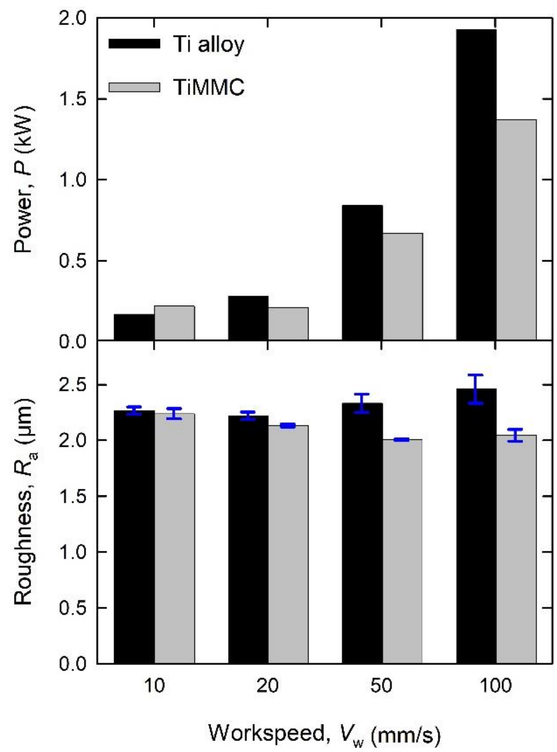

Figure 3.3.2 Workspeed effect on power and roughness

As mentioned in the previous section, the second set of tests were conducted following the wheel wear tests where the wheel reached its steady wear stage. The wheel wear by the very limited number of grinding passes in the second set of tests can be neglected, which provided the basis to precisely compare the effects of materials in the tests. The power for the 800th pass in the first set of tests on the TiMMC was compared with the power at the workspeed v_w = 50 mm/s in the second set of tests. The power was P = 0.64 kW for the 800th pass, and 0.67 kW in the second set of tests. The power values were almost equal, which confirmed that the wheel wear caused by the second set of tests can be neglected.

The roughness was R_a = 2.24 µm for the TiMMC at the workspeed v_w = 10 mm/s and 2.05 µm at 100 mm/s. The corresponding values for the Ti alloy were R_a = 2.27 µm and 2.46 µm, which is higher than the values of the TiMMC. Different trends were clearly observed. The roughness increased with increasing workspeed for the Ti alloy, which was consistent with the general findings of the roughness and workspeed relationship. For the TiMMC, the roughness, however, decreased with the increase in workspeed. To confirm the trends, SEM observations were made on the ground surfaces. As an example, the SEM pictures of the surfaces ground in the 20th passes for both materials are shown in Figure 3.3.3 with the same magnification. The surface of the TiMMC exhibited grooves, pileups, and defects, especially embedded particles. Similar grooves and pileups were also observed on the surface of the Ti alloy, but at much large scales. This led to the higher surface roughness with the Ti alloy.

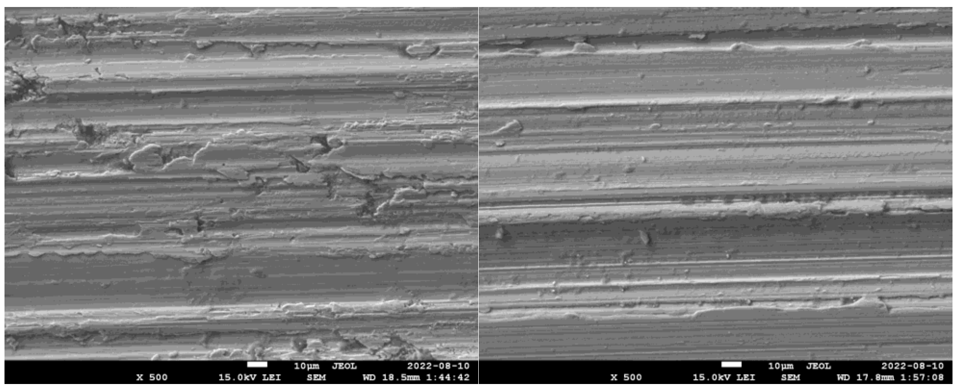

(a) (b)

Figure 3.3.3 Ground surface pictures at the 20th pass for the (a) TiMMC and (b) Ti alloy with the same magnification

As mentioned above, broken, and dislodged TiC particles trapped between the grinding wheel and the workpiece participated in the grinding of the TiMMC through three body abrasion. Similar to the abrasive grains in lapping operations, the particles, which were much smaller than the diamond grains, led to a smoothening effect on the grooves, ridges, and pileups and eventually the reduced surface roughness. The surface roughness trend for the TiMMC can be explained with the dependence of chip size on the workspeed. It is well known that increasing workspeeds leads to a larger size of chips without changing the total chip number. A larger chip for sure has a larger surface area than a smaller one and hence shed more TiC particles during grinding. This results in more particles trapped in the grinding zone, which increased effect of the three-body abrasion and produced smoother ground surfaces with a higher workspeed.

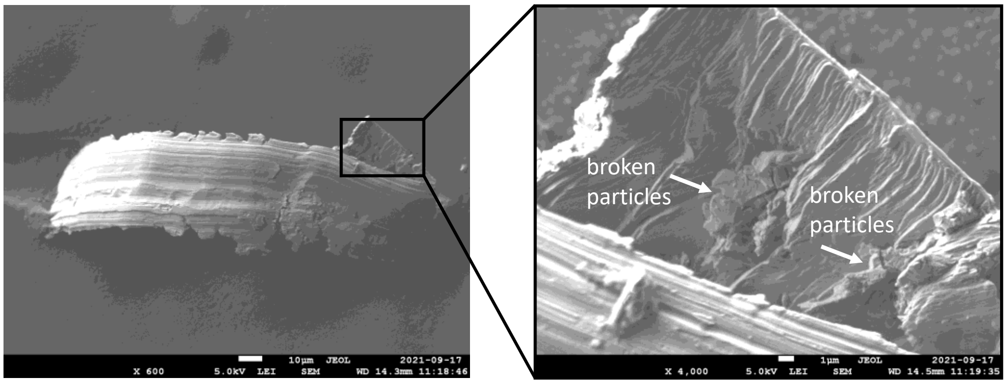

(a) (b)

Figure 3.3.4 (a) TiMMC chip (b) enlargement of the chip

To confirm the existence of broken particles, SEM observations were made on chips. SEM pictures of a TiMMC chip is shown in Figure 3.3.4. The chip morphology revealed characteristic of the low thermal conductivity of titanium alloy, which led to adiabatic shear and the formation of segmented chips [60]. The close-up picture revealed the presence of broken TiC particles. This observation is similar to what was found in turning or milling on the same material [61].

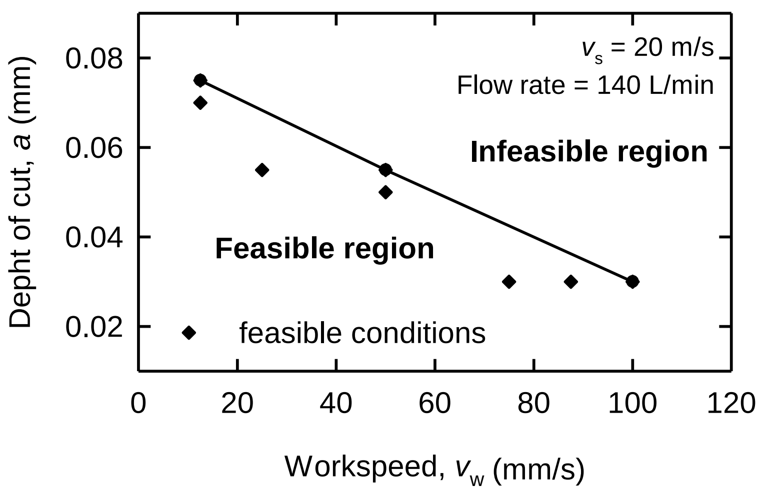

Figure 3.3.5 Process limits from workspeed and depth of cut combinations

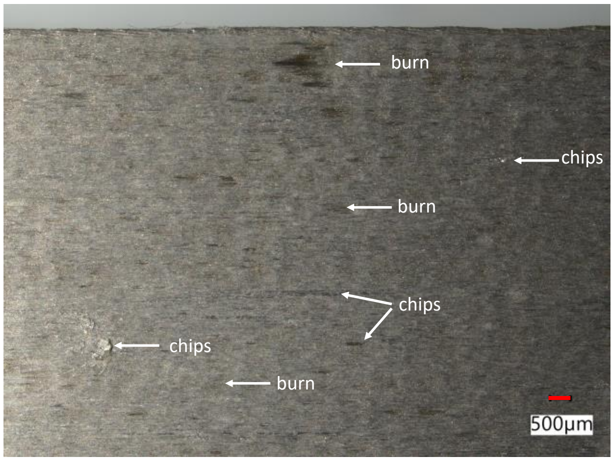

Figure 3.3.6 Ground TiMMC surface with defects (v_w = 100 mm/s, a = 0.05 mm)

The process limits for grinding the TiMMC are given in Figure 3.3.5 showing the depth of cut and workspeed combinations dividing feasible and infeasible regions. The tested conditions leading to good ground surfaces are also included in the figure. A feasible region is formed by all the combinations producing ground surfaces without defects. As an example, a picture of a ground surface with defects produced by a combination in the infeasible region is presented in Figure 3.3.6. Searching for the limits was started with the workspeed v_w = 50 mm/s and depth of cut a = 0.05 mm. The depth of cut was first increased by intervals of 0.005 mm up to signs of high grinding temperature or surface quality degradation. Sticking chips were found on the ground surface at the depth of cut a = 0.06 mm. The workspeed was then reduced to find the maximum one without defects while fixed the depth of cut at 0.06 mm. Eventually, surfaces without sticking chips were produced at the workspeed v_w = 12.5 mm/s. The process limits were found by repeating this procedure.

The results for the effects of grinding fluid pressure on the maximum depth of cut achieved without ground surface defects in the last set of tests on the TiMMC are summarized in Figure 3.3.7. It should be noted that the tests were conducted with the same nozzle. This means that increasing the fluid pressure led to increases of fluid flow rate too. The flow rate corresponding to the lowest tested pressure 1.38 MPa (200 psi) was 95 L/min (25 GPM). This flow rate was more than needed for the tested removal rates. Therefore, the effect of the increases in flow rate can be neglected. At the lowest pressure of 1.38 MPa, the maximum depth cut without ground surface defects was a = 0.04 mm. As expected, the maximum depth of cut increased with increasing fluid pressure and reached 0.08 mm at the highest tested pressure of 5.52 MPa (800 psi). The improvement in depth of cut was apparently due to the deeper penetration of the fluid into the grinding zone at higher pressures. It should be emphasized that all the other tests in this study were conducted at the pressure 2.8 MPa (400 psi), which were much higher than normally used in other studies in literatures. This was one of the reasons for the lower specific energy achieved in this study.

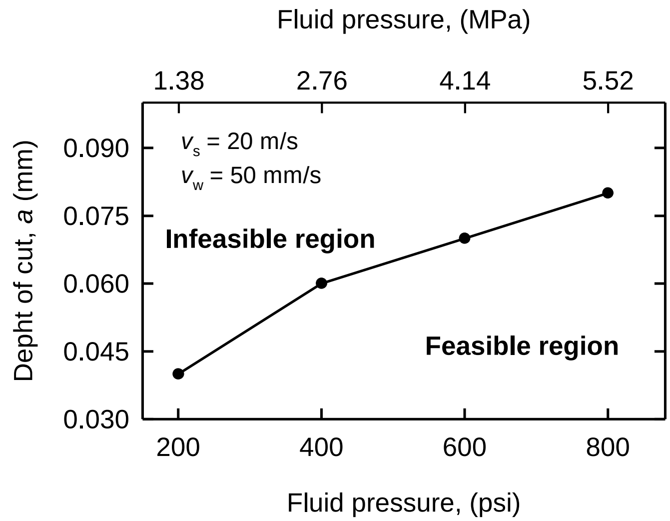

Figure 3.3.7 Effect of fluid pressure on the maximum depth of cut achievable

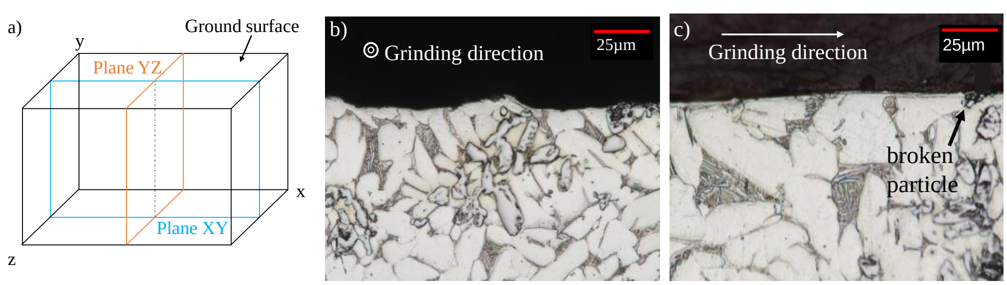

Figure 3.3.8 Sample cutting planes a) and microstructure after 400 passes on the b) YZ and c) XY plane

To study the microstructure, TiMMC samples for the 400th pass were cut using EDM perpendicular (YZ plane) and parallel (XY plane) to the direction of the workspeed, as shown in Figure 3.3.8. Only minor changes in the sub-surface microstructure were observed. As an example, pictures of the microstructure are presented in Figure 3.3.8 (b) and (c). Plastic deformation of the globular structure of the α phase and the Widmanstätten platelets occurred either in the ZY and XY planes from the ground surface up to 3 μm in depth. Twinning, which is a mechanism of plastic deformation leading to atomic rearrangements in a parent gain, also took place under the ground surface as shown in Figure 3.3.9. For the Ti alloy, the plastic deformation happened from the ground surface up to 5 μm in depth. Different from the TiMMC, twinning was not observed in spite of the deeper plastic deformation with the Ti alloy. Diamond is an excellent thermal conductor, it helps conduct the heat away from the grinding zone and lower grinding temperatures, which might be responsible for the minor changes of microstructure.

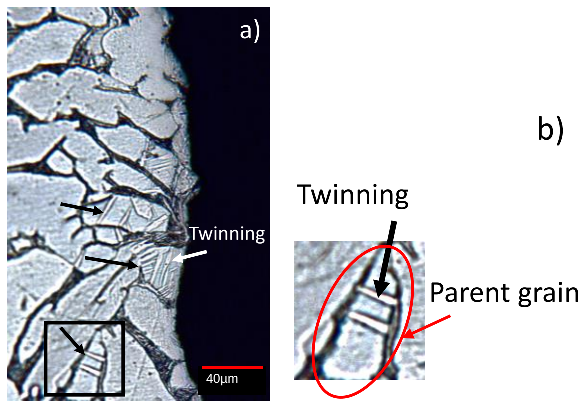

Figure 3.3.9 Twinning formations under the ground surface at YZ plane a) general view, b) enlarged view of a parent grain and twinning

3.4 Conclusion

An experimental study on the grinding of a TiMMCs and a Ti alloy with an electroplated diamond wheel was carried out. The following can be drawn:

- Electroplated diamond wheels wear slower on TiMMCs than on Ti alloys. Under the tested condition, steady state G-ratios of 1,648 and 1,026 were obtained for the TiMMC and the Ti alloy, respectively.
- Grinding the TiMMCs consumes less power and specific energy than grinding the Ti alloy under identical grinding and wheel wear conditions. Lower specific energy ranging from 16 to 34 J/mm^3 was obtained under all the tested conditions in this study for both tested materials, which can be attributed to the usage of high-pressure grinding fluid.
- Surface roughness decreases with increasing workspeed for the TiMMCs. But, it increases with the workspeed for the Ti alloy. The roughness values for the TiMMCs under different

workspeeds were lower than the corresponding values of the Ti alloy. The differences are due to the effect of three body abrasion with the TiMMC.

- Decreasing the depth of cut while increasing the workspeed is in favour of achieving higher material removal rates. Material removal rate can also be improved by increasing grinding fluid pressure.
- Broken particles were found on both chip and ground surfaces. Twinning due to plastic deformation was observed under the ground surface for the TiMMC.

CHAPTER 4 ARTICLE 2: EFFECTS OF TOOL GEOMETRY AND FLUID ON THE SURFACE MORPHOLOGY AND INTEGRITY IN SCRATCHING TIMMCS

Coauthors: Zhongde Shi, Luc Baron, and Marek Balazinski

Submitted on December 15, 2022.

International Journal of Abrasive Technology

Keywords: Grinding, scratching, titanium metal matrix composite, surface morphology, surface integrity

Abstract. An experimental study is reported on the surface morphology and integrity in scratching of TiMMCs. Experiments were performed at a fixed scratching speed vs= 20 m/s, and given depths of scratching ranging from 0.004 to 0.024 mm. Scratching tools with round and conical tips were selected for the tests with and without grinding fluid. Microscopic observations of the tool tips and the scratches were conducted. It was revealed that ploughing of the matrix and the re-deposition of the matrix on the scratched surface led to the mixing of the matrix with broken TiC particles. The use of grinding fluid influenced the TiC removal mechanisms in terms of "comet tail" phenomenon and different severities of the particle breakage. The depth of scratch had a greater effect on the cupules formation. Comparison of the bottom of the scratches and the ground surfaces showed that the wheel wear had significant effects on the ground surface morphology and integrity. No evidence of whole particle dislodgements was observed.

4.1 Introduction

Titanium metal matrix composites (TiMMCs) were developed in the early 1990s as an alternative to Ti-based alloys for the aerospace and automotive industries. Despite possessing excellent mechanical and chemical properties such as high specific strength, light weight, high wear and chemical resistance, and high thermal stability [2], machining of the material remained challenging. The main issues encountered during machining were premature wear of the tools, broken particles, and void formations on machined surfaces [3, 4] due to the difference in mechanical properties between the matrix and the reinforcing particles.

A few studies have addressed the fundamental understanding of the material removal behavior. Publications on the grinding of TiMMCs with cubic boron nitride (CBN) wheels [7, 8, 80], suggested that the removal mechanism of TiMMCs included the ductile removal of the matrix and the brittle removal of the reinforcing particles in two stages that were sequentially repeated along workpiece surfaces. The first stage corresponded to the ductile removal of the matrix dominated by the serrated chip formation. The second stage was led by crack initiation and propagation, characteristic of the brittle removal of reinforcing particles. These removal mechanisms were also predicted by finite element modelling (FEM) and experimentally validated.

Another study [95] modeled the simultaneous actions of two abrasive grains on a CBN wheel during the grinding of a TiMMC. In this model, if the reinforcing particle had a residual crack, the results showed that the second pass of an abrasive grain propagated the crack up to the tensile failure of the particle and led to its breaking off from the matrix. If a reinforcing particle did not have a residual crack, the second pass would not induce the tensile failure of the particle, instead brittle removal occurred. The presence of a residual crack affected the maximum Von mises strain in the second pass. This maximum stress caused the tensile failure of the particle during the passage of the second grain.

Other studies on grinding TiMMCs with CBN grinding wheels were focused on the experimental understanding of the material removal behavior. The results showed that the material removal behavior is closely related to the undeformed chip thickness [4, 7, 8, 80]. A small undeformed chip thickness caused a tiny fracture of the reinforcing particle and thus, a shallow cavity on the ground surface. On the other hand, a large undeformed chip thickness led to a larger fracture, inducing a deeper and wider cavity on the ground surface, and therefore a higher surface roughness. According to Li et al. (2016), the undeformed chip thickness led to lateral crack formation resulting in micro-cracks on ground surfaces. A larger undeformed chip thickness induced deeper lateral cracks which interacted each other and emerged on the ground surface resulting in higher surface roughness. The presence of micro-cracks on ground surfaces were also attributed to severe residual stresses on the ground surfaces [7].

Surface morphology and integrity are of importance in grinding TiMMCs. Studies in this aspect, however, are very limited. Previous studies on material removal mechanisms/behaviors on grinding TiMMCs were somewhat related to ground surface morphology and integrity. But, these studies were not sufficient enough to reveal the surface morphology and integrity in depth. As part of an investigation on grinding TiMMCs with electroplated diamond wheels, the present paper is concerned with the surface morphology and integrity of scratches on TiMMCs with focus on the effect of scratching tool tip geometry and the application of grinding fluid. The results from the scratching tests were also compared with what were obtained in grinding (removal by multiple abrasive grains).

4.2 Experimental Setup and Test Conditions

Single grain up-scratching tests were performed on a Makino A88E high-speed and high-power machining center. A rotating disk mounted with single grain tools, instead of a grinding wheel of multiple abrasive grains, was used in the tests. The tools were single point diamond dressing sticks and diamond indenter. Each dressing stick had a single diamond grain with a tip included angle of 75°. The indenter had a 50 μm radius ball tip. The dressing tools were selected to simulate the pointed and sharp grains in new wheels while the indenter to simulate grains in worn wheels. These tools were mounted on a round disk of 225.4 mm (8.86 inches) diameter, with a counterweight installed on the opposite end of the diameter to avoid unbalance. The tool tip protruded 14.30 mm above the disk peripheral surface leading to a tool tip rotating diameter of 254.0 mm. Figure 4.2.1 shows the experimental setup. For the tests with fluid, a film of water-based grinding fluid of 7% soluble oil was applied on the sample surfaces prior to the tests.

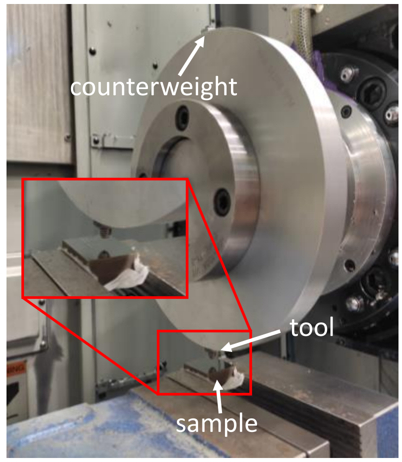

Figure 4.2.1 Experimental setup with an enlarged view of the tool and sample

The experiments were conducted at a fixed tool tip speed of vs= 20 m/s and workspeed of vw= 175 mm/s. The workspeed was selected to obtain two to five distinct scratches in each scratching pass depending on the given depths of scratch. A total of six scratching passes were conducted on each sample. The depth of scratch was set to 0.004 mm for the first pass and increased by 0.004 mm for each subsequent pass. A total of four sets of tests were carried out to investigate the effect of tip shapes (spherical and pointed) and grinding fluid on the scratched surface morphology and integrity. The tests were first performed with the dressing tool with grinding fluid for six passes. Then, a new tool was used to run the same conditions but with grinding fluid in the second set of tests. After that, the third and the fourth sets of tests were conducted with diamond indenters using the conditions of the first and the second sets of tests, respectively.

The test samples were rectangular blocks of TiMMC with a length of 30 mm (1.2 inches) along the workspeed direction and a width of 25.4 mm (1.0 inch). The sample surfaces were mirror polished before the tests to eliminate the effects of the presences of pre-test scratches. The TiMMC used in this study was composed of Ti6Al4V matrix reinforced with 10 - 12% vol of TiC particles. The size of the TiC reinforcing particles was between 10 and 20 µm. Figure 4.2.2 shows the matrix of the material composed of the globular α phase (the lightest feature) surrounded by Widmanstätten platelets. Widmanstätten structure (α+β) consisted of retained β phase (brown) distributing between the α platelets (white). The TiC reinforcing particles were randomly distributed in the matrix.

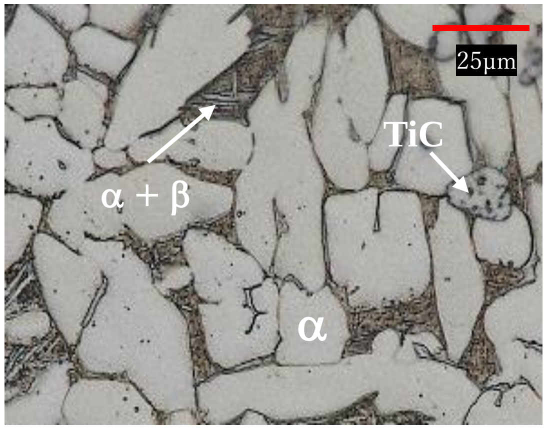

Figure 4.2.2 Optical microscopy image of the TiMMC microstructure

Samples from a previous study in grinding TiMMC with an electroplated diamond wheel [86] were also used for comparison and identification of the surface morphology and integrity in multi-grain grinding. The workpiece surfaces of these samples after 20, 400 and 800 wheel wear grinding passes were observed to reveal the effects of wheel wear. Also, a section view parallel to the grinding direction was used to evaluate the aforementioned mechanisms that cannot be studied from the top view of the scratched surfaces. The depths of the scratches were measured by 3D scanning with an optical Keyence VHX-7000 microscope. The scratches and chips were observed with optical and scanning electron microscopy (SEM) (Hitachi TM3030). The SEM observations were performed with the lower secondary electron detector (LEI) and the low angle backscattered electron detector (LABE). The former focused on the topographic contrasts and the latter on the chemical contrast and helped differentiate the TiC particles from the matrix while.

4.3 Results and discussions

A total of 80 scratches were obtained to determine the surface morphology and integrity of the TiMMC under single scratch tests. The actual depth of the scratches ranged from 7 to 20 μm for the dressing tools, and 6 to 44 μm for the indenters. It should be noted that the tips of the tools, most notably the dressing tools, deteriorated after 6 - 8 passes in tests with and without the grinding fluid.

SEM images were taken to show the worn tips of the tools (Figure 4.3.1). For the dressing tool (Figure 4.3.1 a)), the tip was broken, and chip accumulation was seen on the tip. The darker circular area around the tip showed the worn part of the tip. For the indenter (Figure 4.3.1 b)) the worn part was also seen (darker part) with chips sticking on it (lighter part on the worn surface). Unlike the dressing tool, only a small piece of the tip was broken off. It is important to note that more chip accumulation was observed on the sharper dressing tool tip than on the round indenter.

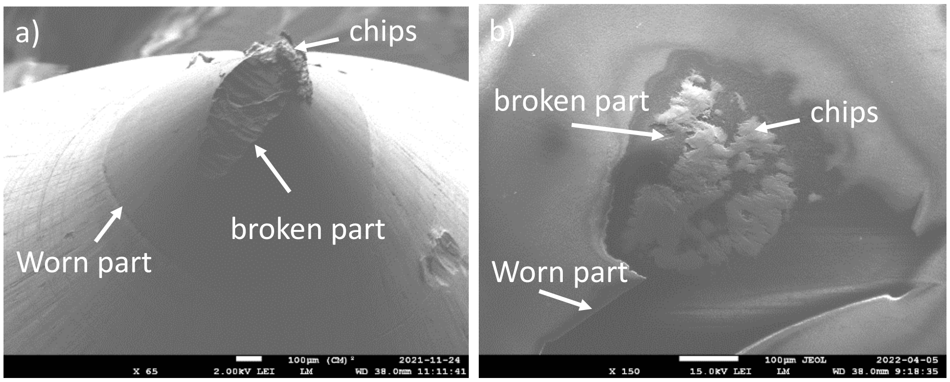

Figure 4.3.1 SEM pictures of tool tips after tests without grinding fluid a) the dressing tool, and b) the indenter

An example of a scratch profile across the scratching pass corresponding to the broken dressing tool is presented in Figure 4.3.2. This profile was used to analyze the effect of tip breakage on the scratch profile. The profile confirmed an irregular tip with a step corresponding to the edge created by its breakage. Pile-ups were also observed on each side of the scratch, which were due to the plastic flow of the material on the side of the tool.

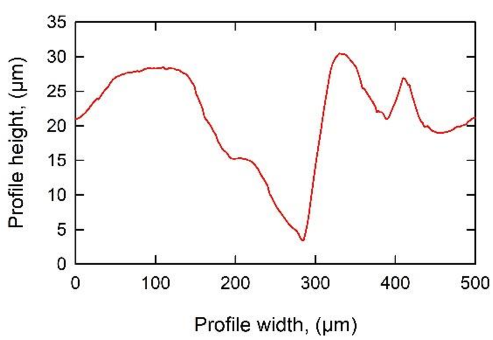

Figure 4.3.2 Scratch profile obtained from the broken dressing tool

Abrasive grains on wheel surfaces are not necessarily pointed, but have sharper edges or random profiles, such as those seen in the broken tool tips. The results obtained with the broken dressing tools were used in the present study and they were considered to be more representative of service conditions than a brand-new pointed tool.

The following sections present observations and discussions of the morphology and integrity of surfaces in singe grain scratching of TiMMC with and without grinding fluid as well as a comparison with multigrain grinding.

4.3.1 Ground surface morphology and integrity

As mentioned in the previous section, ground samples from a previous study [86] were observed for the surface morphology and integrity, which cannot be studied from the top view of the scratched surfaces. Observations of these samples are helpful for investigating the scratched surface morphology and integrity in single grain testing.

The images from the section view parallel to the grinding direction under the ground surfaces after 20, 400 and 800 passes are shown in Figure 4.3.3. The particles contained in the matrix appeared darker, and the matrix brighter. It is well known that the matrix is subject to plastic deformation forming grooves on the ground surface due to grinding actions. Breakages of TiC particles below the ground surfaces were observed in the images (Figure 4.3.3). This observation contradicted to what was reported in literatures [80, 95] which concluded that the contact between the tool and the TiC particle was the precursor of the brittle fracture of the latter. Figure 4.3.3 of the workpiece cross-sections showed that particles were cracked and broken up to 40 μm in depth below the ground surfaces. These broken particles were ground leading to the mixing of the pieces of the broken particles with the plastically deformed matrix. Then, the mixture is either ploughed forward and re-deposited on the surface or removed by forming a chip. It is well accepted in the literature that the material removal behavior of the TiMMC matrix is dominated by serrated chip formation [53].

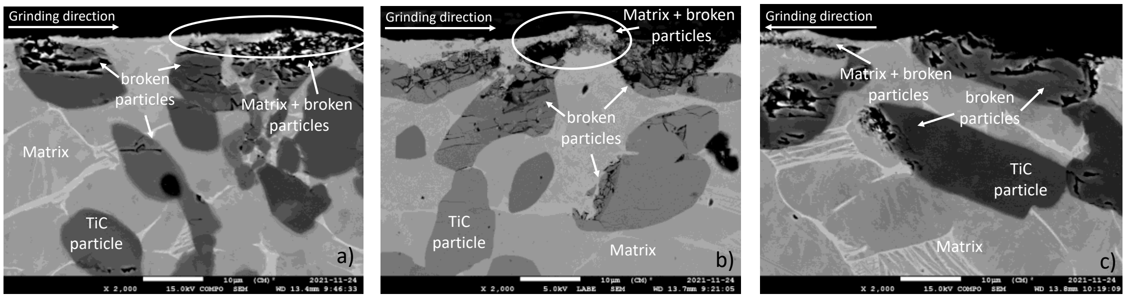

Figure 4.3.3 Workpiece cross-section showing the microstructure under the ground surface after a) 20, b) 400, and c) 800 passes

The aforementioned SEM observations revealed the ploughing of the matrix related to its plastic deformation, and re-deposition of the matrix on the scratched surface. The ploughing and re-deposition of the matrix induced its mixing with broken TiC particles, which is of importance and constitutes the basis for understanding the results and discussion in the following sections for scratch testing with and without grinding fluid.

4.3.2 Scratches of tests without grinding fluid

The scratch morphologies for the dressing tool and the indenter without grinding fluid are presented in Figure 4.3.4 a) and b), respectively. The typical scratch obtained for the dressing tool has grooves at the bottom of the scratch, which were due to the irregular shape of the broken tip. Significant pileups were observed on the most pointed side of the tip. The typical scratch obtained from the indenter was much more regular and had a smoother appearance, as well as smaller pileups on each side of the scratch.

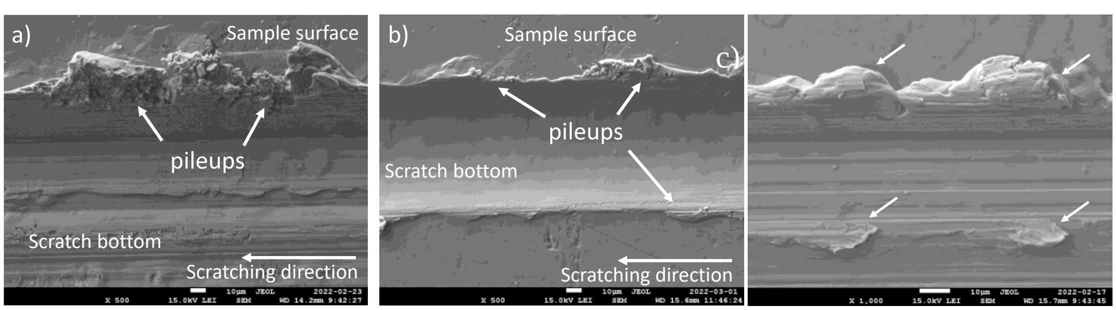

Figure 4.3.4 a) Dressing tool scratch, b) indenter scratch, and c) chip re-deposition for the dressing tool, on the edge and at the bottom of the scratch

Chip re-deposition was observed at different scratch depths. For the dressing tool, chip re-deposition took place at both the bottom and on the edges of the scratches, while for the indenter it took place only on the edges of the scratches, as indicated by the arrows in Figure 4.3.4 b) and c), respectively. An increase in depth of scratch resulted in the re-deposition of the chips on the pileups, for the dressing tool.

As mentioned in the previous section, the matrix was subject to plastic deformation during the tool passes which push broken particles resulting in a mixture of the matrix and the broken particles. The pushing of the broken particles by the matrix at the bottom of the scratch is presented in Figure 4.3.5. At small scratch depths (<10µm), the broken particles were visible close to the particle from which they originated from. They were pushed and embedded in the neighboring matrix in the direction of scratching, especially for the dressing tool. This shape was similar to the "comet tails" observed in sample polishing. For the indenter, the broken particles were observed close to the particle they came from without forming "comet tails".

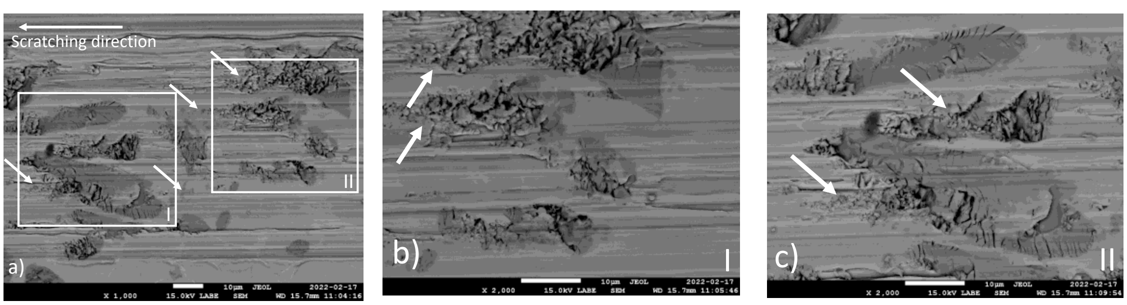

Figure 4.3.5 a) Broken particles pushed in the matrix in the scratching direction, b) and c) enlarged views of the square areas in a)

On the edge of the scratches, the pileups formed from the plastic flow of the material on the side of the tool led to an accumulation of the plastically deformed matrix and the mixture (matrix with pieces of broken particles) on the pileups. The matrix was no longer able to act as a binder (leading to the breakage of the pileup), or the re-deposited chip stuck on the pileup, which indicated that the density of broken particles was too high comparatively to the amount of matrix. In other words, the plastic flow of the matrix was hindered by the increase of particles or the density of broken particles. This phenomenon was also observed at the bottom of the scratches, generating surface defects due to high density of broken particles. Examples of this phenomenon at the bottom of the scratch and on the pileups are presented in Figure 4.3.6.

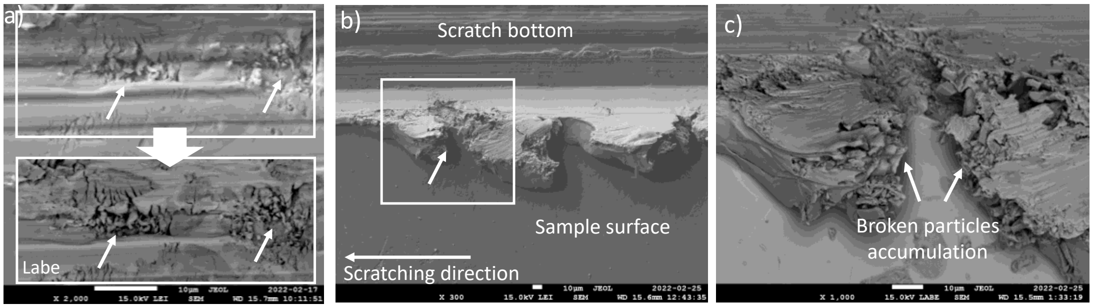

Figure 4.3.6 a) Hindering of the matrix plastic flow by the particles density increase at the bottom, b) on the edge of the scratch, and c) an enlarged view of the squared area from b)

At larger depths of scratches (>10 µm), a larger amount of material was pushed by the tool resulting in larger pileups and greater chip production. This is supported by a previous study on grinding MMCs [80]. In the present study, the pileup size was greater than 26 µm for both tools. Beyond 10 µm depth of scratch, the quantity of chips produced, and the size of the pileups remained constant (between 10 and 15 µm). The quantity of sticky chips on the tools and deposited on the edges of the scratches did not increase at larger depths of scratch either. Observations at the bottom of the scratches revealed that the layer of the plastic flow of the matrix was thicker.

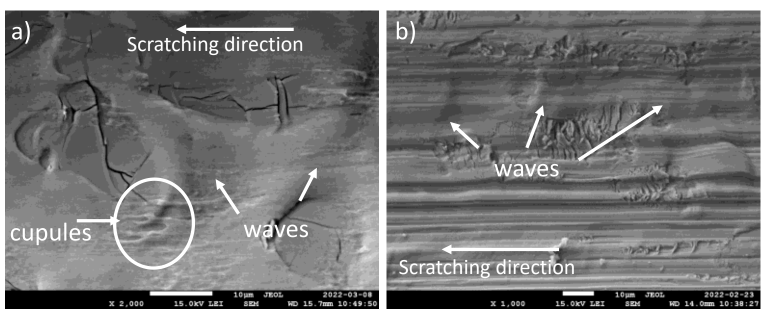

Figure 4.3.7 a) Matrix waves and cupules at large scratch depth for the indenter, and b) matrix waves for the dressing tool

Cupules, characteristic of the plastic deformation, as well as matrix “waves” were observed for the scratches obtained with each of the tools. Matrix waves around the particles might be due to the action of lateral force during the test from the tool or due to the re-deposition of a large quantity of the mixture of matrix and particles at the bottom of the scratches. The exact causes of the matrix waves are unclear at this stage of the study and require further investigation. Figure 4.3.7 show matrix waves at scratch depth greater than 26 µm for the dressing tool and the indenter. The accentuated presence of these ductility markers at the bottom of the scratches indicated that a greater quantity of matrix was deformed. Observations carried out on the particles also revealed the presence of a larger matrix thickness. As explained in the experimental section of this paper, the LABE detector of the SEM highlighted the atomic contrasts of the alloy on the surfaces. This chemical contrast showed a clear difference between the particles and the matrix (Figure 4.3.8). When the plastic flow of the matrix is thicker it covered the particle resulting in weaker contrast.

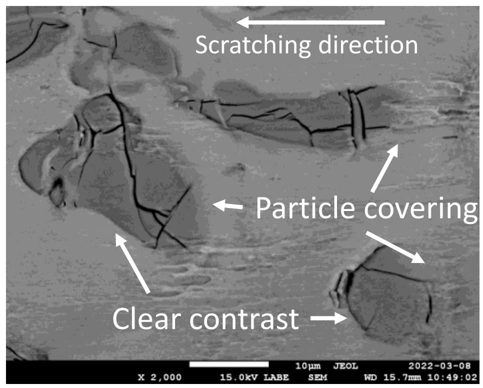

Figure 4.3.8 Chemical contrast picture showing the covering of particles by the matrix

The LABE detector was used for several depths of cut to observe particles. Figure 4.3.9 a) and b) show the observations of the dressing tool and Figure 4.3.9 c) of the indenter using the Labe detector. For the dressing tool, below 10 µm, the depth of the scratch had no influence on the severity of particle breaking, the particles were only cracked or broken into pieces. The severity of particle breakage might depend on the size of the particle itself and the surrounding matrix phase. For example, if a large TiC particle (>10 µm) or $\alpha+\beta$ phase was near a small particle, the small particle cracked and broke into pieces but retained its integrity. While a small particle or α phase near the particle induced the breakage of this particle which did not keep its integrity as shown in Figure 4.3.9 a) and b). This behavior might be due to the nature of the neighboring phases. The alpha phase has a lower hardness than the $\alpha+\beta$ phase and tends to deform plastically during the process. The $\alpha+\beta$ phase is harder due to the alternation of the phases and hence blocks the dislocations, which led to reduced plastic deformation of the matrix and allowed the particles to maintain their integrity [96]. For the indenter, below 10 µm of scratch depth, the small and big particles were mainly cracked, and rarely broken into many small pieces (Figure 4.3.9 c)).

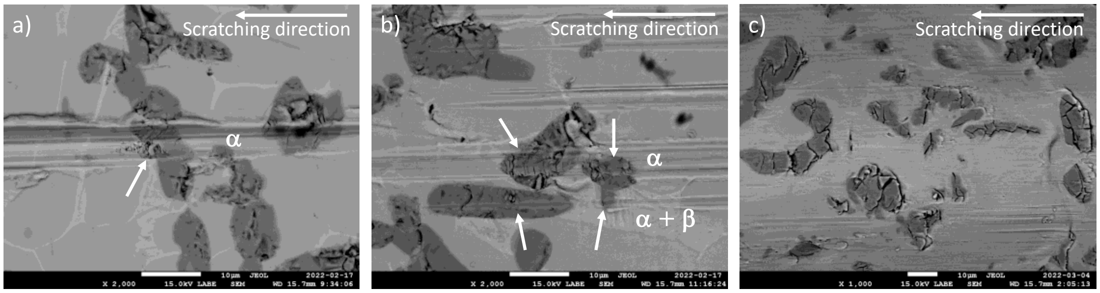

Figure 4.3.9 a) and b) Images of particles near α and α+β phases for the dressing, and c) for the indenter

SEM images taken from both detectors on the same location of a scratch bottom are presented in Figure 4.3.10. Cracks were seen on the image taken by the LEI detector (Figure 4.3.10 a)). These cracks were further confirmed to be from broken particles as shown in the image taken by the LABE detector (Figure 4.3.10 b)). As mentioned previously, the matrix flows plastically during the action of the tools. The level of plastic flow of the matrix, as well as the depth of the layer of plastic flow at the bottom of the scratch, depended on the depth of the scratch. The broken particles at the bottom of the scratch were covered by the plastic flow of the matrix. It is well known that materials have a fracture point. When passing the tool through the particles, the pieces of broken particles were unstable and there was a lack of matrix supply to maintain the continuity of the plastic flow of the matrix. The combination of the instability of the particles and the previous plastic flow of the matrix caused the matrix to reach its fracture point resulting in residual cracks on the surface.

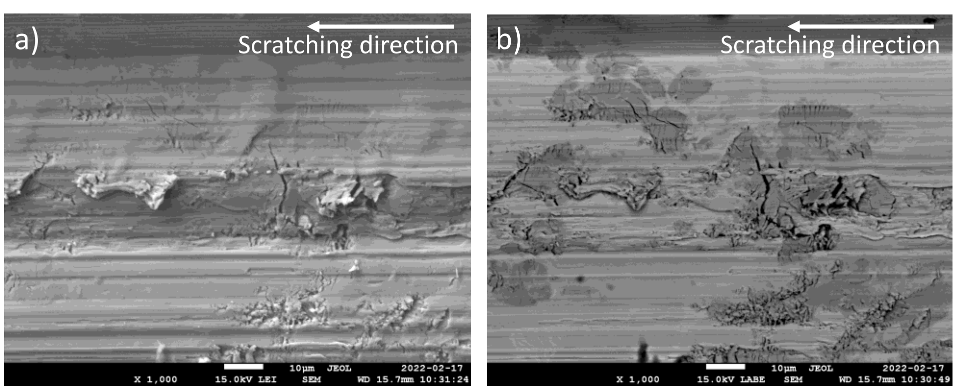

Figure 4.3.10 Cracks at the bottom of the scratch for dressing tool from a) LEI detector, and b) LABE detector

Figure 4.3.11 shows cupules of plastic deformation of the matrix on the edge of a particle before reaching its fracture point. Previous studies on TiMMCs with CBN grinding wheels attributed the presence of “micro-cracks” to the large residual stresses on the ground surface [4, 80]. However, the observation of the present study closely correlated the presence of these “micro-cracks” to the fracture point of the matrix. Areas with a lot of broken particles showed a higher density of surface cracks (Figure 4.3.10). Peeling of the matrix pieces was also observed in some areas (Figure 4.3.12). This might be attributed to various factors such as the instability of the broken particles on which the matrix was ploughed, or even a spring-back of the matrix.

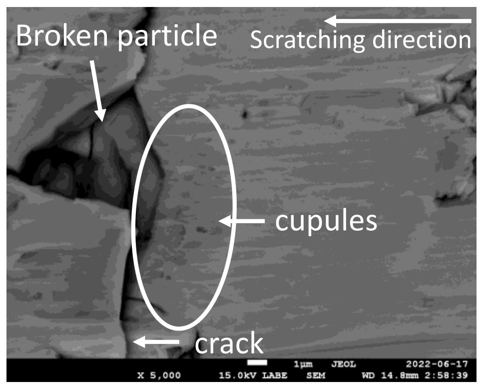

Figure 4.3.11 Cupules of plastic deformation of the matrix on the edge of a particle before reaching its fracture point

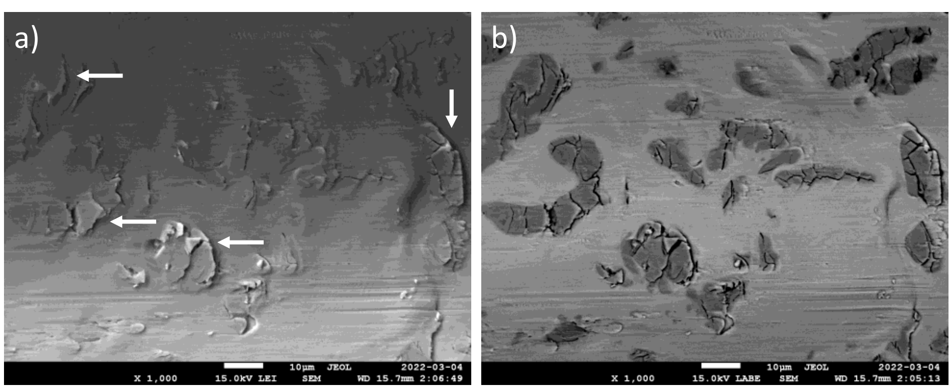

Figure 4.3.12 a) Peeling of the matrix pieces which covered the broken particles, b) and same observation with the LABE detector

There was no evidence of whole particle dislodgements as it was reported in turning TiMMCs [60]. Only partial particle dislodgement was observed. This partial particle dislodgment corresponded to the broken parts of the particle that was carried away by the tool and/ or the flow of the matrix plastic deformation. Figure 4.3.13 shows the evidence of partial particle dislodgment with the LABE and LEI SEM detectors.

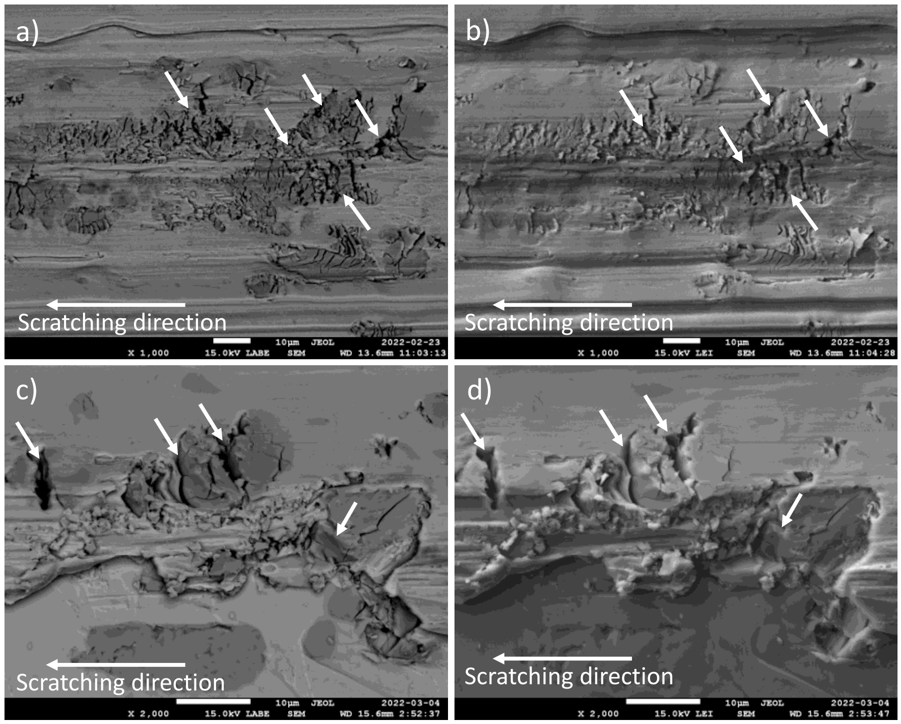

Figure 4.3.13 Evidence of partial particle dislodgement for the dressing tool with a) LABE detector, b) LEI detector, and for the indenter with, c) LABE detector and d) LEI detector

The aforementioned observations of morphology and integrity of surfaces were done for surfaces of scratch tests without grinding fluid. The next section presents the mechanisms for testing with grinding fluid.

4.3.3 Scratches of tests with grinding fluid

Tests performed with grinding fluid gave similar results to those without the grinding fluid. But, a few differences were observed. For the dressing tool, grooves were observed at the bottom of the scratches whereas smoother surfaces were observed for scratches with the indenter. For both types of tools, re-deposited chips and pileups on the edges of the scratches were observed. Chip re-deposition at the bottom of the scratches for the dressing tool with grinding fluid was not present. The grinding fluid prevented chip sticking to the tools.

The behavior of the particles with the dressing tool and grinding fluid was comparable to that observed with the indenter without grinding fluid. The broken particles were not embedded in the neighboring matrix in the scratching direction at either a small (<10 µm) or big (>10 µm) scratch depth. The "comet tails" phenomenon was not observed. The broken particles are pushed with the matrix inducing a reduced number of particles at the bottom of the scratch for the dressing tool. On a larger scale, the reduced number of broken particles might be a significant factor for the reduction of surface roughness.

Regardless of the size of the particle or the depth of the scratch, the particles at the bottom of the scratches are broken and maintain their integrity for the dressing tool with grinding fluid. They were broken, but did not break into a multitude of broken pieces, thus explaining the absence of comet tails. Different from observed with grinding fluid, the severity of the particle breakage did not depend on the neighboring phase or the size of the particle itself. The presence of grinding fluid cooled the matrix at the bottom of the scratch, reducing the plasticity of the matrix. The limited plastic flow of the matrix led to particle breakage, but to a lesser extent.

The accumulation of the matrix and broken particles mixture still occurred with grinding fluid creating pileups at the scratch edges. The presence of grinding fluid for the dressing tool might facilitate the flow of the material towards the edges of the scratches. The pileups were larger. The approximate height of a pileup for the dressing tool was around 4 µm without grinding fluid, and minimum 10 µm with grinding fluid. In the case of the indenter, the pileups were smaller (7 µm) than those without grinding fluid (around 10 µm) regardless of the depths of scratch. The decrease in the number of the chips and pileups for the indenter implied that the matrix flow took place at the bottom of the scratch. An increase in the depth of scratch led to a higher covering of the particles by the matrix plastic flow. Also, a reduced number of cracks at the bottom of the scratches were observed for the indenter. Cupules of plastic deformation and matrix waves were formed at the bottom of the scratch, even at low scratch depth (<10 µm) for the dressing tool, but only at higher scratch depth for the indenter (>10 µm).

An increased number of broken particles in the pileups was observed. Unlike the scratches performed without grinding fluid, the broken particle pieces were not partly embedded in the matrix (comet tail) and were part of the mixture of matrix and broken particle pieces. This might justify the increased density of broken particles in the pileups. The holes indicated in Figure 4.3.14 were evidence of partial particle dislodgement observed with grinding fluid. The images obtained with the LEI and LABE detectors were compared to highlight the missing particle pieces.

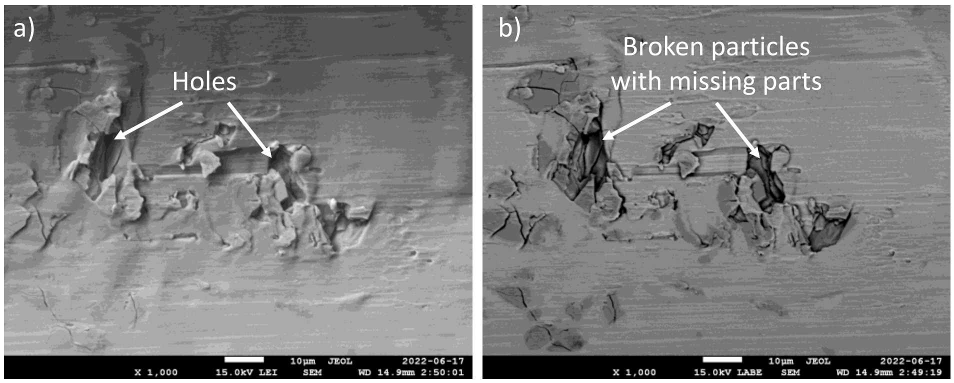

Figure 4.3.14 Evidence of partial dislodgement of broken particles. a) Holes observed with secondary electron detector, b) same observation with LABE detector

The results and discussions for the single grain tests have been highlighted in the previous sections by SEM image analysis. A comparison between the images of the single grain test for the dressing tool and the indenter, with the images of the ground surfaces of the previous paper is presented in the next section. The goal was to identify the morphology and integrity of surfaces for multigrain testing (conventional grinding with a wheel).

4.3.4 Comparison with ground surfaces

The ground surface images from the previous study [86] were compared with the images obtained from the scratching test. The ground surfaces for the 20, 400, and 800th passes for the same TiMMC are presented in Figure 4.3.15 and Figure 4.3.16 and compared with Figure 4.3.4 a) and b) from the previous section, which showed the bottom of the scratches obtained from the dressing tool and the indenter.

The comparison showed that the grooves on the ground surface after the maximum 800 passes were smoother and had morphology similar to that of the scratches from the indenter. While after 20 and 400 passes, the ground surface exhibited a large number of small grooves similar to the grooves in the scratches produced by the dressing tools. The general view of the ground surfaces in Figure 4.3.15 also showed the presence of pieces of particles at 20 and 400 passes (appear as small asperities) compared to 800 passes.

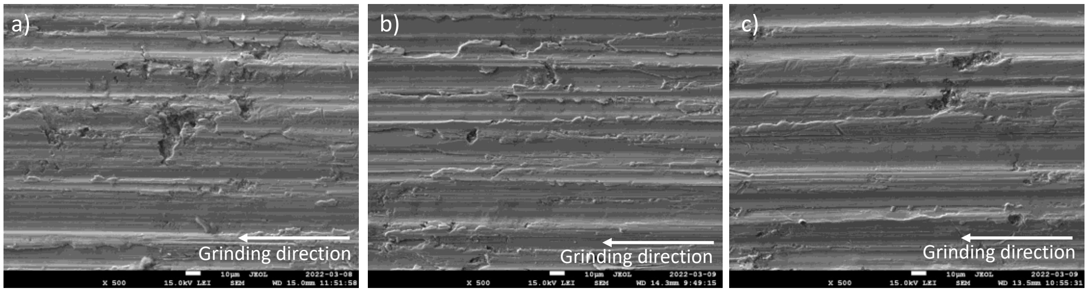

Figure 4.3.15 Ground surfaces after a) 20, b) 400, and c) 800 passes

The observations in Figure 4.3.16 revealed that the matrix plastic flow and the behavior of the particles were the same as that observed at the bottom of the scratch. The comparison of the ground surfaces at 20, 400 and 800th passes showed that an increase in the number of passes, or more wheel wear, induced a particle behavior closer to that observed with the indenter. Whereas at a low number of passes (20 and 400 passes) the behavior of the particles was closer to what observed with the dressing tool. Namely, the particle pieces pushed and embedded in the matrix and the presence of comet tails. There was also chip re-deposition at the bottom of the scratches and, marked pileups due to an important matrix flow and containing broken particles. The particles at the bottom of the scratches were, however, covered with matrix plastic flow, as can be seen by comparing the images obtained with the different SEM detectors. Characteristic cracks of broken particles covered by matrix flow were rare.

At a large number of passes (800 passes), side plastic flow of the matrix was reduced. It might indicate that the flow of the matrix occurred at the bottom of the scratches as observed for the indenter with grinding fluid. Less chip re-deposition and cracks were also observed. There was no evidence of partial dislodgement or comet tail phenomenon.

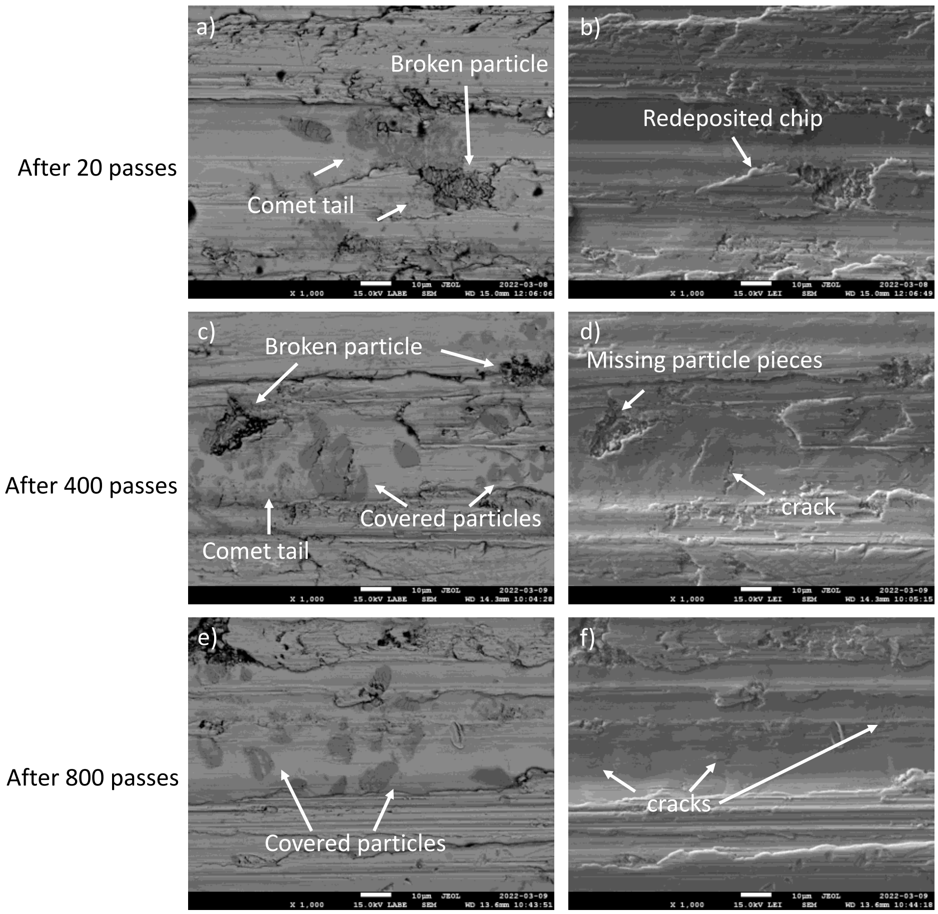

Figure 4.3.16 a), c), e) LABE ground surfaces images, with b), d), and f) the corresponding LEI images

4.4 Conclusion

An experimental study on the morphology and integrity of scratched surfaces on TiMMCs was carried out with scratching tools of different tool tip geometries (round and conical) and tests conditions (with and without grinding fluid). The scratches were observed using SEM microscopy and the results were compared with those of the ground surfaces from a previous study. It was found that the morphology at the bottom of the scratches was affected by the geometry of the tool tips. Smooth scratches were obtained with tools of round tips. Irregular grooves were generated with tools of sharp tips. Ploughing of the matrix, related to its plastic deformation, and re-deposition on the scratched surface were found led to the matrix mixing with broken TiC particles. The surface morphology and integrity were affected by the application of grinding fluid. Without the grinding fluid, “comet tail” phenomenon and different severity of the particle breakage were observed. The severity of the particle breakage depended on the neighboring phase or the size of the particle itself. Cupules, matrix waves, and cracks related to the plastic deformation of the matrix and the depth of scratch were also observed. The comparison of the morphology at the bottom of the scratches and on the ground surfaces showed that the morphology and integrity of surfaces were dependent on the wear of the grinding wheel.

CHAPTER 5 ADDITIONAL RESULTS

This section presents additional results that have not been published in the paper presented in a previous chapter (Chapter 4).

5.1 Analytical forces calculation

An analytical force study was conducted to determine the forces during scratching and grinding tests. The main objective of this study was to determine the normal and tangential forces on an abrasive grain during scratching tests and then, find the experimental value of the grinding wheel forces measured during grinding tests in paper 1 (Chapter 3) by calculation.

5.2 Analytical model

5.2.1 Introduction

Grinding is a machining process widely used in the manufacturing industry. During the grinding, complex interactions are involved, such as grinding wheel, workpiece, and machining parameters. Since grinding forces are dependent on the grinding parameters, they are substantial to evaluate grinding performance, the wheel wear of the grinding wheel, grinding specific energy, workpiece surface quality, etc. Complex mechanical interactions take place between the wheel wear and the workpiece. These latter are difficult to define due to the random nature of the grinding wheel, including grain size, grain shape and the random grain distribution on the grinding wheel. As a result, grinding force modeling is needed to understand the evolution of mechanical behavior of the abrasive material removal process. Modelling has been studied extensively and can be divided into several categories, namely, empirical, semi-empirical and analytical models. Analytical models are based on the physical understanding of the model and previous models to describe the mechanism. While empirical models do not consider the cutting mechanism [97] and are determined from the information obtained from the grinding process. They are dependent on the specific research conditions. Most of studies on the grinding forces are empirical, due to the random nature of the grinding wheel.

The first empirical studies on grinding forces model were regression function between the grinding forces and process parameters such as depth of cut, wheel speed, workspeed, wheel diameter, and grain density initially proposed by Werner et al [98]. Malkin et al [99] first argued that grinding forces are composed of different components, namely chip formation and sliding forces. While Li et al [100] proposed an improvement of the Werner's model by considering grinding forces as cutting and frictional forces. Later, grinding forces empirical models based on multivariate regression analysis were also proposed by Liu et al [101] and Guo et al [102]. It is well known that forces in abrasive machining are related to three separate mechanisms: sliding, ploughing, and chip formation. Sliding of the abrasive grain (or tool) on the workpiece surface results in wear due to the rubbing of the tool without penetration into the workpiece material. Ploughing is related to the penetration of the abrasive grain in the workpiece surface, which plows the surface. It generates wedge formation with or without removing the material. While chip formation corresponds to a deep cut into the workpiece and result in chip carving out [103]. Younis et al [104] as well as Durgumahanti et al [105] proposed a model for the grinding forces considering theses three mechanisms. In this model the focus was on the ploughing effect through a variable friction coefficient. Grinding force modelling was also investigated from different perspective as the undeformed chip thickness [106-108], grinding hardening effect [109], grinding energy [110, 111], etc. Mathematical models were also proposed. For example, Tang et al [112] proposed a mathematical model which focus on the calculation of chip formation force and allows to classify the chip formation forces into static or dynamic forces, based on Malkin's theory and the material cutting theory.

As a part of this project, studying the different components of the grinding forces with an empirical model can provide additional information to the observations made in paper 2 (Chapter 4) and improve the understanding of the morphology and integrity of the workpiece surface after abrasive machining (grinding or scratching tests).

5.2.2 Methodology

The different steps used to determine the normal and tangential forces were as follows:

1- Calculation of the undeformed chip thickness for each tool depending on the shape of the tool and on the depth of cut.
2- Calculation of critical penetration depths based on the material properties and tool tip diameter.

3- Determination of the contact mechanism for each tested condition.
4- Determination of the normal and tangential forces related to the previous steps, and the resultant forces.

The tool references and parameters used for the calculation were those of the tools presented in paper 1 (Chapter 3) and paper 2 (Chapter 4). Tool wear was assumed to be negligible for the calculations.

5.2.2.1 Determination of input values for calculating the forces

5.2.2.1.1 The tool topography

Several tools were used as references for the calculation of the forces: single point diamond dressing stick (conical), diamond indenter (sphero-conical), and an electroplated diamond wheel.

For the dressing stick, the average grain diameter d_g was determine using the equations related to a cone, and was dependent to the depth of scratch a:

$$d_g = \frac{a}{\tan \alpha} \tag{1}$$

The attack angle α was calculated equal to 52.5° from the tool tip angle geometry (trigonometry).

For the indenter, the average grain diameter d_g and the attack angle α were calculated with the equations related to a sphere. As for the dressing stick, the average grain diameter varies with the depth of scratch. It should be noted that the attack angle was also determined as a function of the depth of scratch for the depth of scratch values below one-third of the sphere diameter D (sphero-conical intender). Beyond one-third of the sphere diameter, the attack angle α was considered equal to 30° since the tool tip angle is 120° (conical part).

$$d_g = 2\sqrt{\left(2.\frac{D}{d} - a\right)a} \tag{2}$$

Where D is the sphere diameter.

For the grinding wheel, the average grain diameter d_g was calculated with the well-known formula [75]:

$$d_g = \frac{15.2}{M} \tag{3}$$

Where M is the grit number of the wheel, or 120 in the present study.

As the grinding wheel is a multigrain abrasive tool, the number of contacting grains N_{cg} was obtained with:

$$N_{cg} = C^{0.5}.l_c \tag{4}$$

Where C is the cutting grain per unit area and l_c the contact arc.

5.2.2.1.2 Undeformed chip thickness and grinding wheel attack angle

For the dressing stick and the indenter, the chip thickness h_m formula was determined by [113]:

$$h_{m-L} = 2.L\frac{v_w}{v_s}\sqrt{\frac{a}{d_s}} \quad \text{with} \quad L = \frac{v_s}{v_w}.l_c \tag{5}$$

Where v_w is the workspeed, v_s is the wheel speed or scratching speed, and d_s is the diameter of the wheel.

For the grinding wheel, the undeformed chip thickness h_m was calculated as follow [75]:

$$h_{m-IS} = \left[\frac{4}{C.r}\frac{v_w}{v_s}\left(\frac{a}{d_s}\right)^{0.5}\right]^{0.5} \tag{6}$$

Where C and r are respectively the number of grains per unit area and the scratch width on height ratio.

The attack angle α for the grinding wheel was calculated according to the geometry of the grain movement [103]:

$$\alpha = \tan^{-1}\left(\frac{\sqrt{h_m(d_g - h_m)}}{\frac{d_g}{2} - h_,}\right) \tag{7}$$

5.2.2.1.3 Contact mechanism

The contact mechanism was determined by calculating the critical penetration depths for the elastic, elasto-plastic and plastic deformation [103]. The comparison of the undeformed chip thickness h_m with these critical penetration depths allows to determine the contact mechanism and thus to select suitable formula to calculate the normal force of sliding in the next section.

$$h_{el} = \left(\frac{3\pi}{4}\right)^2 \left(\frac{P}{E^*}\right)^2 \left(\frac{d_g}{2}\right) \tag{8}$$

$$h_{el-pl} = \left(\frac{3\pi}{4}\right)^2 \left(\frac{39H}{100E^*}\right)^2 \left(\frac{d_g}{2}\right) \tag{9}$$

$$h_{pl} = \left(\frac{3\pi}{4}\right)^2 \left(\frac{H}{E^*}\right)^2 \left(\frac{d_g}{2}\right) \tag{10}$$

Where P, E^* and H are respectively the critical pressure defined by $P = 0.39H$, the equivalent elastic modulus and the workpiece hardness (MPa).

5.2.2.2 Calculation of normal and tangential forces

The resultant of the normal and tangential forces was determined by adding the forces of sliding, ploughing, and chip formation respectively. The calculation of the normal and tangential forces was the result of a combination of several models from the literature due to the experimental conditions which were beyond the limits of some models, making them inapplicable.

5.2.2.2.1 Normal forces

The normal forces were determined by calculation based on the Hertz Theory and previous work from the literature [114-116]. The models used are based on the local description of the asperities of the abrasive tools which are approximated to hard spherical indenters and consider the different modes of deformation of the workpiece. The normal sliding force was calculated according to the contact mechanism determined in the previous section. In the case of this study, the purely plastic deformation was obtained. The following equation give the corresponding normal sliding force [115]:

$$F_{N-Sp} = \pi . d_g . H . h_m \tag{11}$$

Where H is the workpiece hardness (MPa).

The normal ploughing force induced by an abrasive grain can be obtained with:

$$F_{N-P} = \frac{2\Delta_\gamma E^*}{H} \sqrt{d_g . h_m} \tag{12}$$

Where Δ_γ is the specific adhesion energy, taken equal to 1.88 J/m² (diamond/titanium) in this study.

The normal force induced by an abrasive grain in the chip formation stage can be expressed [116]:

$$F_{N-C} = \frac{\sqrt{28}}{3}[h_m]^2 . HB \tag{13}$$

Where HB is the Brinell hardness of the workpiece.

5.2.2.2.2 Tangential forces

The tangential forces are calculated by multiplying the normal forces by the friction coefficient. The friction coefficient of sliding was determined with the model from Bowden [117] based on the material properties, as follow:

$$\mu_S = \frac{\tau}{H} \tag{14}$$

So, the tangential sliding force is given by:

$$F_{T-S} = F_{N-Sp} . \mu_S \tag{15}$$

Where τ is the shear stress of the workpiece.

The ploughing coefficient calculation was based on the attack angle α of the tool [118]. The ploughing coefficient is given by:

$$\mu_P = \frac{\tan \alpha}{\pi} \tag{16}$$

Therefore, the tangential ploughing force will be:

$$F_{T-P} = F_{N-P} . \mu_P \tag{17}$$

The chip formation coefficient can be determined by using the asperity model deformation [119]. The particularity of this model is that it agrees with the two basic laws of friction: the proportionality of the tangential force to the normal force, and the independence of the coefficient of friction with respect to the area of the surfaces in contact. The calculation of the chip formation coefficient is based on the attack angle α of the tool and the interfacial friction factor f.

$$\mu_C = \tan\left(\alpha - \frac{1}{4}\pi + \frac{1}{2}\cos^{-1} f\right) \tag{18}$$

The value of the interfacial friction factor is between 0 and 1. Previous study [120] showed that using grinding fluid decreases the value of this factor during grinding. In another study [121], it was showed that for dry grinding the value of the interfacial friction factor is in the range of 0.7 to 0.9. While for grinding with grinding fluid the range of the value of the interfacial friction factor is from 0.4 to 0.7. In this study, the values of the interfacial friction factor selected for the calculation with and without grinding fluid were respectively 0.4 and 0.7.

So, the tangential chip formation force is reported as:

$$F_{T-C} = F_{N-C}.\mu_C \quad (19)$$

The calculation of the normal and tangential forces for the grinding wheel were obtained following the same methodology and by multiplying each resultant force by the number of contacting grains N_{cg} determined in the previous section.

The resultant calculation of the normal and tangential forces for the dressing stick, the indenter and the grinding wheel can be obtained as:

$$F_R = \sqrt{(F_{N-tot})^2 + (F_{T-tot})^2} \quad (20)$$

5.2.3 Results and discussion

The proposed model was applied for different experimental conditions listed in

Table 5.2.3.1. The normal and tangential forces for the dressing stick, the indenter and the grinding wheel are presented in Figure 5.2.1.

Table 5.2.3.1 Experimental conditions used for analytical calculation

	Dressing stick	Indenter	Grinding wheel
v_s (m/s)	20	20	20
v_w (mm/s)	175	175	50
a (mm)	0.005, 0.01, 0.02, 0.05	0.005, 0.01, 0.02, 0.05	0.05
Grinding fluid	With and without	With and without	With

The normal, tangential, and resultant forces changed as a function of the scratching depth in Figure 5.2.1 a) to f), h) and i) for the dressing stick and the indenter. An increase in scratching depth induced larger scratches and thus a larger quantity of the mixture of matrix and broken particles ploughed, re-deposited and/or chip forming. The three force components, namely sliding, ploughing and chip formation, increased as well as the calculated resultant forces. The calculated scratching forces as a function of the depth of cut presented a trend similar to those calculated in grinding for an AISI 1060 steel in grinding in the literature [103].

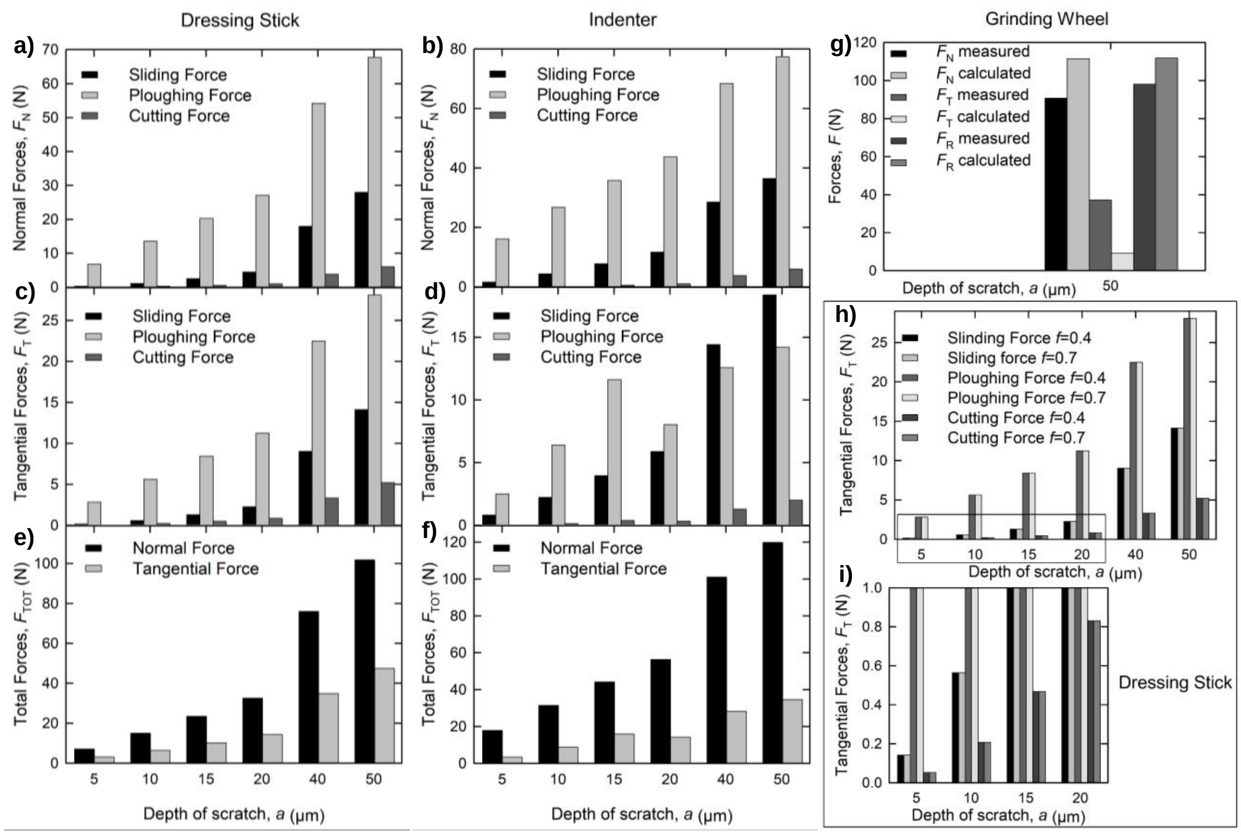

Figure 5.2.1 Calculated a), b) Normal forces, c), d) Tangential forces, e), f) Total normal and tangential forces, g) Calculated and measured forces comparison for the grinding wheel, h) Tangential forces comparison for two interfacial friction factors, and i) enlargement of the square

For the dressing stick, the larger component of the normal and tangential forces was the ploughing force followed by the sliding force and the chip formation force which remained lower than 5 N regardless of the depth of scratch. For the indenter, the trend was comparable to that of the dressing stick only for the components of the normal force. An increase in depth of scratch led an increase in the sliding component which became higher than the ploughing component for a depth of scratch of 40 µm. The trend change occurred between 15 and 40 µm in depth of scratch (in Figure 5.2.1 d)). This trend change highlighted the effect of the attack angle α on the sliding and ploughing components of the tangential force. The scratch depth from which the attack angle was considered equal to 30° (spherical-conical indenter) correspond to the scratch depth of the trend change (one-third of the sphere diameter). Below this scratch depth, the attack angle evolved according to the latter.

The analytical calculation of the normal and tangential forces presented in in Figure 5.2.1 a) to f) for the dressing stick and the indenter showed that the chip formation component is the smallest one. The observations made in paper 2 (Chapter 4) in which chip re-deposition at the bottom of the scratches for the dressing tool with grinding fluid was not present with grinding fluid, and minimal without the use of grinding fluid were supported by the analytical calculation result. Also, it was experimentally observed that increasing the depth of scratch did not increase the quantity of chips produced. The quantity of chips sticking on the tools and deposited on the edges of the scratches did not increase at larger depths of scratch either. Finally, the observations at the bottom of the scratches revealed that the layer of the plastic flow of the matrix was thicker. The results of the analytical calculations confirmed the experimental observations for chips production, and for the large amount of mixture of matrix and broken particles ploughed and re-deposited, as the ploughing component was the highest and the chip formation component the lowest. The effect of the interfacial friction factor on the tangential force components is presented in in Figure 5.2.1 h) and i). Compared to the literature [103], the use of the interfacial friction factor did not induce a significant difference between the results of the analytical calculation. The use of the grinding fluid or not when calculating tangential force components cannot be distinguished when using this model. There was no difference between the results of the calculation of the tangential force components with or without grinding fluid.

Finally, the results of the analytical calculation for the grinding wheel are presented in Figure 5.2.1 g). The values of the normal and tangential resultant forces calculated were compared to the values of the experimental forces measured for paper 1 (Chapter 3). The calculated normal resultant force was overestimated compared to the measured normal force. For the tangential resultant force, the opposite trend was observed. The comparison of the resultant forces showed a decrease in the difference between the calculated and measured forces. The root mean squared error was calculated to evaluate the accuracy of the model used in this study by using the root mean square function on the resultant of the forces:

$$RMSE = \sqrt{\frac{\sum_{i=1}^{n}(F_c - F_e)^2}{n}} \quad (21)$$

Where F_e and F_c were respectively the experimental and calculated values of the forces for the grinding wheel. The accuracy of the calculated values for the resultant of the forces was 13.80%. This value was lower than that obtained in a previous study (17.36%) on the analytical simulation of grinding forces [103]. It was important to specify that the error obtained for the normal and tangential forces was respectively 20.77% and 28.14%. These values showed that the analytical model used was accurate.

5.2.4 Conclusion

An analytical methodology was proposed to calculate the normal and tangential forces for scratching and grinding tests. The results of the analytical calculations were in agreement with the experimental observations made in paper 2 (Chapter 4). The low chip production was verified by a very low chip formation component compared to the sliding and ploughing components. The large amount of mixture of matrix and broken particles ploughed and re-deposited, were verified by a very high ploughing component as well. The estimation of the accuracy of the model was calculated using the analytical calculation of the forces for the grinding wheel and the experimental results obtained in paper 1 (Chapter 3). The accuracy of the proposed analytical model is 13.80% on the resultant force for the grinding forces.

CHAPTER 6 GENERAL DISCUSSION

The general discussion of the thesis highlights the most important results of each phase of the study and proposes a second interpretation of the results presented in Figure 3.3.2 (Chapter 3), following the additional results and paper 2.

The first phase of this work focussed on the grinding performance of a TiMMC with a diamond wheel in terms of grinding force, tool wear, surface roughness, and microstructure. The results showed lower consumption of power and specific energy, as well as lower wheel wear for the TiMMC compared to grinding under identical conditions for the Ti alloy. These differences were attributed to the presence of TiC and the three-body abrasion, which in the case of grinding with a diamond wheel, will help to erode the workpiece. This effect has also been used to explain the decrease in surface roughness with increasing workspeed. The trend observed is inconsistent with the general findings of the roughness and workspeed relationship.

In the second phase of this study, the evaluation of the morphology and integrity of the scratched surfaces was performed. The behavior of the TiC particles and the matrix was highlighted for different scratching test conditions. It made it possible to identify by comparison the morphology and integrity of the ground surfaces obtained in phase 1. Observations showed that the matrix was mainly pushed, mixed with the broken TiC particles, and redeposited on the surface, a phenomenon known as ploughing. The presence of chips was very low whatever the tested conditions.

The third phase corresponds to a complementary analysis which completes the understanding of the morphology and integrity of the scratched surfaces identified in phase 2. The calculation of the normal and tangential forces was performed for the scratching and the grinding tests. The comparison of the theoretical and experimental results helped to determine the accuracy of the model used.

The combination of the results of these three phases makes it possible to discuss a second hypothesis for the decrease in roughness with the increase in the workspeed shown in Figure 3.3.2. It was seen in phase 1 that the increase in workspeed induces an increase in undeformed chip thickness, and therefore an increase in broken TiC particle content at the interface between the grinding wheel and the workpiece. During phase 2, observations showed that the matrix and the broken particles were dragged, and redeposited on the surface, thus forming a mixture of matrix/broken particles. This mixture, which is denser than the matrix alone (in the case of TiMMC vs Ti alloy), is redeposited on the surface workpiece, thus hiding, and minimizing surface defects. An increase in workspeed induces according to phase 1 a denser mixture of broken TiC particles, due to the increase in the undeformed chip thickness. A mixture containing more broken particles will be denser and able to fill more surface defects. This effect combined with three-body abrasion can explain the surface roughness decreases with increasing workspeed. This hypothesis is supported by the results presented in the additional results. Indeed, they demonstrate a predominance of the ploughing phenomenon during scratching and grinding tests. The components of sliding and chip formation were very low. As experimentally the material could not be disposed of, it was ploughed to the surface of the workpiece.

CHAPTER 7 CONCLUSION AND RECOMMENDATIONS

7.1 Conclusion

As a concerned by the improvement of the grinding performance on heat sensitive and fast wear materials, namely the TiMMCs, the aim of this study was to provide insights and understanding of the grinding performance of TiMMC with electroplated diamond wheels. The grindability study of the grinding of TiMMCs with a diamond wheel were conducted in terms of forces, power consumption, wheel wear, surface roughness, microstructure. The results were compared with those obtained on a Ti alloy under identical grinding and wheel wear conditions. For the TiMMC, the consumption in power, specific energy, the electroplated diamond wheel wear, and the surface roughness as a function of the workspeed were lower than that of the Ti alloy. Also, the surface roughness was found to decrease with the increase in workspeed. This trend might be attributed to the three-body abrasion occurring during the grinding of the TiMMC, and to the cover up of the broken particles by the matrix ploughed at the bottom of the scratches. The limits of the process showed that a higher material removal rate can be achieved by decreasing the depth of cut while increasing the workspeed or by increasing the grinding fluid pressure. Specific energy values were ranging from 16 to 34 J/mm^3 under all the tested conditions due to the usage of high-pressure grinding fluid.

The experimental study on the morphology and integrity of scratched surfaces on TiMMCs showed that the morphology at the bottom of the scratches was affected by the geometry of the tool tips and by the application of grinding fluid. The application of grinding fluid mainly affected the severity of the particle breakage. The ploughing and re-deposition of the matrix on the scratched surface were found to led to the matrix mixing with broken TiC particles. The comparison of the morphology observed for the scratching and for the ground surfaces, revealed that the morphology and integrity of surfaces were dependent on the wear of the grinding wheel. Finally, the analytical investigation of the normal and tangential forces was of interest to verify that the ploughing of the matrix was prevailing over the sliding of the tool on the workpiece surface or the chip formation. Also, the comparison of the experimental and calculating grinding forces has shown the accuracy of the model used.

7.2 Recommendations

The analytical model used was not able to predict the difference in normal and tangential forces with or without lubrication. As the experimental observations showed a difference in the morphology and surface integrity according to the use of grinding fluid, it is an interesting subject to implement the model used for the calculation of the grinding forces with the data related to the observed morphology and integrity of the ground surfaces.

Also, an experimental study focused on the determination and description of material removal mechanisms would complement the observations related to the morphology and surface integrity of the ground surface obtained in the present study.

REFERENCES

[1] Z. Shi and H. Attia, "High performance grinding of titanium alloys with electroplated diamond wheels," *Procedia CIRP,* vol. 101, pp. 178-181, 2021.

[2] M. D. Hayat, H. Singh, Z. He, and P. Cao, "Titanium metal matrix composites: An overview," *Composites Part A: Applied Science and Manufacturing,* 2019.

[3] T. Thepsonthi and T. Özel, "3-D finite element process simulation of micro-end milling Ti-6Al-4V titanium alloy: experimental validations on chip flow and tool wear," *Journal of Materials Processing Technology,* vol. 221, pp. 128-145, 2015.

[4] Z. Li, W. Ding, L. Shen, X. Xi, and Y. Fu, "Comparative investigation on high-speed grinding of TiCp/Ti–6Al–4V particulate reinforced titanium matrix composites with single-layer electroplated and brazed CBN wheels," *Chinese Journal of Aeronautics,* vol. 29, no. 5, pp. 1414-1424, 2016.

[5] J. Monaghan and P. O'reilly, "The drilling of an Al/SiC metal-matrix composite," *Journal of materials processing technology,* vol. 33, no. 4, pp. 469-480, 1992.

[6] Z. Li, W. Ding, C. Liu, and H. Su, "Grinding performance and surface integrity of particulate-reinforced titanium matrix composites in creep-feed grinding," *The International Journal of Advanced Manufacturing Technology,* vol. 94, no. 9-12, pp. 3917-3928, 2018.

[7] Z. Li, W. Ding, C. Liu, and H. Zhou, "Grinding performance of TiCp/Ti-6Al-4V composites with CBN wheels, part I: experimental investigation and surface features," *Procedia CIRP,* vol. 77, pp. 525-528, 2018.

[8] X. Xi, W. Ding, Z. Li, and J. Xu, "High speed grinding of particulate reinforced titanium matrix composites using a monolayer brazed cubic boron nitride wheel," *The International Journal of Advanced Manufacturing Technology,* vol. 90, no. 5-8, pp. 1529-1538, 2017.

[9] N. Hung, Z. Zhong, and C. Zhong, "Grinding of metal matrix composites reinforced with silicon-carbide particles," *MATERIAL AND MANUFACTURING PROCESS,* vol. 12, no. 6, pp. 1075-1091, 1997.

[10] M. Cook, "Diamond grinding and PCD machining of MMC engineering components," *Powder metallurgy,* vol. 41, no. 2, pp. 87-89, 1998.

[11] Z. Zhong and N. P. Hung, "Grinding of alumina/aluminum composites," *Journal of materials processing technology,* vol. 123, no. 1, pp. 13-17, 2002.

[12] H. Chandrasekaran and J. Johansson, "Role of material and grinding parameters in grinding of alumina fiber-reinforced aluminum alloys," *NIST Spec. Publ., 847 pp.,* vol. 55, 1993.

[13] A. Di Ilio and A. Paoletti, "A comparison between conventional abrasives and superabrasives in grinding of SiC-aluminium composites," *International Journal of Machine Tools and Manufacture,* vol. 40, no. 2, pp. 173-184, 2000.

[14] M. Aramesh, "Machinability of titanium metal matrix composites (Ti-MMCs)," École Polytechnique de Montréal, 2015.

[15] S. SESHAN, A. GURUPRASAD, M. PRABHA, and A. SUDHAKAR, "Fibre-reinforced metal matrix composites—• a review," *J. Indian Inst. Sci*, vol. 76, pp. 1-14, 1996.

[16] T. Srivatsan and J. Lewandowski, "Metal matrix composites: types, reinforcement, processing, properties and applications," *MATERIALS ENGINEERING-NEW YORK-*, vol. 32, p. 275, 2006.

[17] L. Geng, D. Ni, J. Zhang, and Z. Zheng, "Hybrid effect of TiBw and TiCp on tensile properties of in situ titanium matrix composites," *Journal of alloys and compounds,* vol. 463, no. 1-2, pp. 488-492, 2008.

[18] K. Morsi and V. Patel, "Processing and properties of titanium–titanium boride (TiB w) matrix composites—a review," *Journal of materials science,* vol. 42, no. 6, pp. 2037-2047, 2007.

[19] T. Dougherty, Y. Xu, and A. Hanizan, "Mechanical Properties and Microstructure of PM Ti-Si 3 N 4 Discontinuous Fibre Composite," in *TMS 2016 145th Annual Meeting & Exhibition*, 2016: Springer, pp. 721-728.

[20] G. Sivakumar, V. Ananthi, and S. Ramanathan, "Production and mechanical properties of nano SiC particle reinforced Ti–6Al–4V matrix composite," *Transactions of Nonferrous Metals Society of China,* vol. 27, no. 1, pp. 82-90, 2017.

[21] N. Shivakumar, V. Vasu, and N. Narasaiah, "Synthesis and characterization of nano-sized Al2O3 particle reinforced ZA-27 metal matrix composites," *Procedia Materials Science,* vol. 10, pp. 159-167, 2015.

[22] T. Saito, "The automotive application of discontinuously reinforced TiB-Ti composites," *JOM,* vol. 56, no. 5, pp. 33-36, 2004.

[23] M. A. Shypitsa and A. A. Dmitrovitch, "Influence of hard inclusions on mechanical properties of materials on the base sintered steels " in *Proceding of World Congress & Exhibition Euro PM 2005*, vol. 99. Prague, Czech Republic, 2-5 october 2005, p. 285.

[24] N. Chawla and Y. L. Shen, "Mechanical behavior of particle reinforced metal matrix composites," *Advanced engineering materials,* vol. 3, no. 6, pp. 357-370, 2001.

[25] B. Harris, *Fatigue in composites: science and technology of the fatigue response of fibre-reinforced plastics*. Woodhead Publishing, 2003.

[26] L. Huang and L. Geng, *Discontinuously reinforced titanium matrix composites*. Springer, 2017.

[27] A. Jain, M. Hack, I. Verpoest, S. V. Lomov, W. Van Paepegem, and I. Seyfarth, "Fatigue evaluation of composite materials-overview and industrial applications," in *Tagung AK Betriebsfestigkeit, Werkstoffe und Fügeverfahren-Neue Herausforderungen für die Betriebsfestigkeit, Date: 2012/10/10-2012/10/11, Location: Paderborn, Germany*, 2012.

[28] E. Bayraktar, J. Masounave, R. Caplain, and C. Bathias, "Manufacturing and damage mechanisms in metal matrix composites," *Journal of Achievements in Materials and Manufacturing Engineering,* vol. 31, no. 2, pp. 294-300, 2008.

[29] A. Designation, "E466-15, Standard practice for conducting force controlled constant amplitude axial fatigue tests of metallic materials," *ASTM International*, 2015.

[30] A. E606/E606M-12, "Standard test method for strain-controlled fatigue testing," ed: ASTM International West Conshohocken, PA, 2012.

[31] Z. Wang and H. Xiao, "A Simulation of Low and High Cycle Fatigue Failure Effects for Metal Matrix Composites Based on Innovative J2-Flow Elastoplasticity Model," *Materials*, vol. 10, no. 10, p. 1126, 2017.

[32] M. Premkumar and M. Chu, "Al□ TiC particulate composite produced by a liquid state in situ process," *Materials Science and Engineering: A*, vol. 202, no. 1-2, pp. 172-178, 1995.

[33] S. Hashimoto, A. Yamaguchi, and M. Koshino, "Fabrication and characterization of TiC/Al composites," *Materials Science and Engineering: A*, vol. 265, no. 1-2, pp. 71-76, 1999.

[34] R. Ritchie, C. Gilbert, and J. McNaney, "Mechanics and mechanisms of fatigue damage and crack growth in advanced materials," *International Journal of Solids and Structures*, vol. 37, no. 1-2, pp. 311-329, 2000.

[35] T. Tagawa, E. Wadahara, and T. Miyala, "Fatigue crack initiation and growth in titanium alloy matrix composite," in *ICF 9-Sydney, Australia-1997*, 1997.

[36] S. C. Tjong and Y.-W. Mai, "Processing-structure-property aspects of particulate-and whisker-reinforced titanium matrix composites," *Composites Science and Technology*, vol. 68, no. 3-4, pp. 583-601, 2008.

[37] W. Soboyejo, W. Shen, and T. S. Srivatsan, "An investigation of fatigue crack nucleation and growth in a Ti–6Al–4V/TiB in situ composite," *Mechanics of Materials*, vol. 36, no. 1-2, pp. 141-159, 2004.

[38] H. Tsang, C. Chao, and C. Ma, "Effects of volume fraction of reinforcement on tensile and creep properties of in-situ TiB/Ti MMC," *Scripta Materialia*, vol. 37, no. 9, pp. 1359-1365, 1997.

[39] S. Zhu, Y. Lu, Z. Wang, and J. Bi, "Creep behavior of TiC-particulate-reinforced Ti alloy composite," *Materials Letters*, vol. 13, no. 4-5, pp. 199-203, 1992.

[40] S. Wang, L. Huang, L. Geng, F. Scarpa, Y. Jiao, and H. Peng, "Significantly enhanced creep resistance of low volume fraction in-situ TiBw/Ti6Al4V composites by architectured network reinforcements," *Scientific reports*, vol. 7, p. 40823, 2017.

[41] M. Thomas, "Charpy impact behaviour of Sigma fibre reinforced titanium composites," *Materials science and technology*, vol. 16, no. 7-8, pp. 882-886, 2000.

[42] R. Chaudhari and R. Bauri, "A novel functionally gradient Ti/TiB/TiC hybrid composite with wear resistant surface layer," *Journal of Alloys and Compounds*, vol. 744, pp. 438-444, 2018.

[43] I. Kim, B. Choi, Y. Kim, and Y. Lee, "Friction and wear behavior of titanium matrix (TiB+ TiC) composites," *Wear*, vol. 271, no. 9-10, pp. 1962-1965, 2011.

[44] B.-J. Choi and Y.-J. Kim, "In-Situ (TiB+ TiC) particulate reinforced titanium matrix composites: Effect of B 4 C size and content," *Metals and Materials International,* vol. 19, no. 6, pp. 1301-1307, 2013.

[45] L. Huang, L. Geng, and H. Peng, "Microstructurally inhomogeneous composites: is a homogeneous reinforcement distribution optimal?," *Progress in Materials Science,* vol. 71, pp. 93-168, 2015.

[46] C. Liu, L. Huang, L. Geng, Y. Jiao, and A. Tang, "In Situ Synthesis of (TiC+ Ti3SiC2+ Ti5Si3)/Ti6Al4V Composites with Tailored Two‐scale Architecture," *Advanced Engineering Materials,* vol. 17, no. 7, pp. 933-941, 2015.

[47] Y. Zi-Run, H. Hai-Xiang, C.-F. Jiang, W.-M. Li, X.-R. Liu, and S. Lyu, "Evaluation on dry sliding wear behavior of (TiB+ TiC)/Ti-6Al-4V matrix composite," *International Journal of Precision Engineering and Manufacturing,* vol. 18, no. 8, pp. 1139-1146, 2017.

[48] N. Kang, P. Coddet, Q. Liu, H. Liao, and C. Coddet, "In-situ TiB/near α Ti matrix composites manufactured by selective laser melting," *Additive Manufacturing,* vol. 11, pp. 1-6, 2016.

[49] J.-S. Kim, K.-M. Lee, D.-H. Cho, and Y.-Z. Lee, "Fretting wear characteristics of titanium matrix composites reinforced by titanium boride and titanium carbide particulates," *Wear,* vol. 301, no. 1-2, pp. 562-568, 2013.

[50] H. Singh, M. D. Hayat, H. Zhang, and P. Cao, "The decomposition of Si3N4 in titanium and its effect on wear properties," *Wear,* vol. 420, pp. 87-95, 2019.

[51] H. Attar *et al.*, "Nanoindentation and wear properties of Ti and Ti-TiB composite materials produced by selective laser melting," *Materials Science and Engineering: A,* vol. 688, pp. 20-26, 2017.

[52] Q. An *et al.*, "Dry sliding wear characteristics of in-situ TiBw/Ti6Al4V composites with different network parameters," *Tribology International,* vol. 121, pp. 252-259, 2018.

[53] S. Kamalizadeh, S. A. Niknam, A. Asgari, and M. Balazinski, "Tool wear characterization in high-speed milling of titanium metal matrix composites," *The International Journal of Advanced Manufacturing Technology,* vol. 100, no. 9-12, pp. 2901-2913, 2019.

[54] A. Asgari, "Cutting Conditions Optimisation of Titanium Metal Matrix Composites in Turning and Face Milling," École Polytechnique de Montréal, 2015.

[55] D. Zhu, X. Zhang, and H. Ding, "Tool wear characteristics in machining of nickel-based superalloys," *International Journal of Machine Tools and Manufacture,* vol. 64, pp. 60-77, 2013.

[56] W. Konig, "Applied research on the machinability of titanium and its alloys," p. 1979, 1978. Proc. AGARD Conf. Advanced Fabrication Processes.

[57] J. P. Davim, *Tribology in manufacturing technology*. Springer, 2012.

[58] G. Li, K. Munir, C. Wen, Y. Li, and S. Ding, "Machinablility of titanium matrix composites (TMC) reinforced with multi-walled carbon nanotubes," *Journal of Manufacturing Processes,* vol. 56, pp. 131-146, 2020.

[59] G. r. Poulachon and A. L. Moisan, "Hard turning: chip formation mechanisms and metallurgical aspects," *J. Manuf. Sci. Eng.,* vol. 122, no. 3, pp. 406-412, 2000.

[60] R. Bejjani, M. Balazinski, B. Shi, H. Attia, and H. Kishawy, "Machinability and chip formation of titanium metal matrix composites," *International Journal of Advance Manufacturing System, IJAMS,* vol. 13, no. 1, 2011.

[61] R. Bejjani, "Machinability and modeling of cutting mechanism for titanium metal matrix composites," École Polytechnique de Montréal, 2012.

[62] R. Bejjani, B. Shi, H. Attia, and M. Balazinski, "Laser assisted turning of titanium metal matrix composite," *CIRP annals,* vol. 60, no. 1, pp. 61-64, 2011.

[63] X. Duong, J. Mayer, and M. Balazinski, "Initial tool wear behavior during machining of titanium metal matrix composite (TiMMCs)," *International Journal of Refractory Metals and Hard Materials,* vol. 60, pp. 169-176, 2016.

[64] R. Bejjani, M. Balazinski, H. Attia, P. Plamondon, and G. L'Éspérance, "Chip formation and microstructure evolution in the adiabatic shear band when machining titanium metal matrix composites," *International Journal of Machine Tools and Manufacture,* vol. 109, pp. 137-146, 2016.

[65] A. Di Ilio, A. Paoletti, V. Tagliaferri, and F. Veniali, "An experimental study on grinding of silicon carbide reinforced aluminium alloys," *International journal of Machine tools and Manufacture,* vol. 36, no. 6, pp. 673-685, 1996.

[66] A. Di Ilio, A. Paoletti, V. Tagliaferri, and F. Veniali, "Grindability evaluation of SiC reinforced aluminium alloys," in *XIX Sci. Conf. of Abrasive Technology,* 1996.

[67] C. Thiagarajan, R. Sivaramakrishnan, and S. Somasundaram, "Experimental evaluation of grinding forces and surface finish in cylindrical grinding of Al/SiC metal matrix composites," *Proceedings of the Institution of Mechanical Engineers, Part B: Journal of Engineering Manufacture,* vol. 225, no. 9, pp. 1606-1614, 2011.

[68] R. Hood, D. Aspinwall, and W. Voice, "Creep feed grinding of a gamma titanium aluminide intermetallic alloy using SiC abrasives," *Journal of Materials Processing Technology,* vol. 191, no. 1-3, pp. 210-214, 2007.

[69] R. Hood, P. Cooper, D. Aspinwall, S. Soo, and D. Lee, "Creep feed grinding of γ-TiAl using single layer electroplated diamond superabrasive wheels," *CIRP Journal of Manufacturing Science and Technology,* vol. 11, pp. 36-44, 2015.

[70] A. Abdullah, A. Pak, M. Farahi, and M. Barzegari, "Profile wear of resin-bonded nickel-coated diamond wheel and roughness in creep-feed grinding of cemented tungsten carbide," *Journal of Materials Processing Technology,* vol. 183, no. 2-3, pp. 165-168, 2007.

[71] S. Huang, X. Yu, F. Wang, and L. Xu, "A study on chip shape and chip-forming mechanism in grinding of high volume fraction SiC particle reinforced Al-matrix composites," *The International Journal of Advanced Manufacturing Technology,* vol. 80, no. 9-12, pp. 1927-1932, 2015.

[72] A. Di Ilio, A. Paoletti, and D. D'Addona, "Characterization and modelling of the grinding process of metal matrix composites," *CIRP annals,* vol. 58, no. 1, pp. 291-294, 2009.

[73] S. Joshi, N. Ramakrishnan, and P. Ramakrishnan, "Analysis of chip breaking during orthogonal machining of Al/SiCp composites," *Journal of Materials Processing Technology,* vol. 88, no. 1-3, pp. 90-96, 1999.

[74] Z. Zhang, P. Yao, J. Wang, C. Huang, R. Cai, and H. Zhu, "Analytical modeling of surface roughness in precision grinding of particle reinforced metal matrix composites considering nanomechanical response of material," *International Journal of Mechanical Sciences,* vol. 157, pp. 243-253, 2019.

[75] S. Malkin, "Grinding technology-theory and applications of machining with abrasives ", ed. Series in Mechanical Engineering: Elsevier, 1989.

[76] P. J. Blau and B. C. Jolly, "Relationships between abrasive wear, hardness, and grinding characteristics of titanium-based metal-matrix composites," *Journal of materials engineering and performance,* vol. 18, no. 4, p. 424, 2009.

[77] Z. Li, W. Ding, C. Liu, and H. Su, "Prediction of grinding temperature of PTMCs based on the varied coefficients of friction in conventional-speed and high-speed surface grinding," *The International Journal of Advanced Manufacturing Technology,* vol. 90, no. 5-8, pp. 2335-2344, 2017.

[78] Z. Zhang, D. Guo, R. Kang, H. Gao, Z. Jin, and Y. Meng, "Subsurface crystal lattice deformation machined by ultraprecision grinding of soft-brittle CdZnTe crystals," *The International Journal of Advanced Manufacturing Technology,* vol. 47, no. 9-12, pp. 1065-1081, 2010.

[79] Z. Zhang, Y. Meng, D. Guo, R. Kang, and H. Gao, "Nanoscale machinability and subsurface damage machined by CMP of soft-brittle CdZnTe crystals," *The International Journal of Advanced Manufacturing Technology,* vol. 47, no. 9-12, pp. 1105-1112, 2010.

[80] W. Ding, Z. Li, C. Liu, and H. Zhou, "Grinding performance of TiCp/Ti-6Al-4V composites with CBN wheels, part II: material removal behavior based on FEM," *Procedia CIRP,* vol. 77, pp. 529-532, 2018.

[81] X. X. Xi, W. F. Ding, Z. Li, J. H. Xu, and X. Y. Wang, "A Study on Heat Transfer in High-Speed Grinding of Titanium Matrix Composites," in *Key Engineering Materials*, 2016, vol. 693: Trans Tech Publ, pp. 1003-1008.

[82] C. Escaich, Z. Shi, L. Baron, and M. Balazinski, "Machining of Titanium Metal Matrix Composites: Progress Overview," *Materials,* vol. 13, no. 21, p. 5011, 2020.

[83] C. Guo, Z. Shi, H. Attia, and D. McIntosh, "Power and Wheel Wear for Grinding Nickel Alloy with Plated CBN Wheels," *CIRP Annals,* vol. 56, no. 1, pp. 343-346, 2007/01/01/ 2007, doi: https://doi.org/10.1016/j.cirp.2007.05.079.

[84] Z. Shi and H. Attia, "High removal rate grinding of titanium alloys with electroplated CBN wheels," *International Journal of Abrasive Technology 16,* vol. 6, no. 3, pp. 243-255, 2014.

[85] Z. Shi and H. Attia, "High performance of titanium alloys with electroplated diamond wheel," presented at the 9th CIRP Conference on High Performance Cutting, 2019.

[86] C. S. Escaich, Zhongde; Baron, Luc; Balazinski,Marek "Performance of Electroplated Diamond Wheels in Grinding Titanium Metal Matrix Composites," presented at the The

23rd International Symposium on Advances in Abrasive Technology, Sapporo, Japan, 2021.

[87] M. Deja and D. Zieliński, "Wear of electroplated diamond tools in lap-grinding of Al2O3 ceramic materials," *Wear,* vol. 460, p. 203461, 2020.

[88] H. Li, L. Zou, Z. Li, W. Wang, and Y. Huang, "Investigation on abrasive wear of electroplated diamond belt in grinding nickel-based superalloys," *The International Journal of Advanced Manufacturing Technology,* vol. 121, no. 7, pp. 4419-4429, 2022.

[89] J. P. Davim and A. M. Baptista, "Relationship between cutting force and PCD cutting tool wear in machining silicon carbide reinforced aluminium," *Journal of materials processing technology,* vol. 103, no. 3, pp. 417-423, 2000.

[90] H. Kishawy, S. Kannan, and M. Balazinski, "Analytical modeling of tool wear progression during turning particulate reinforced metal matrix composites," *CIRP annals,* vol. 54, no. 1, pp. 55-58, 2005.

[91] Y. Sahin and G. Sur, "The effect of Al2O3, TiN and Ti (C, N) based CVD coatings on tool wear in machining metal matrix composites," *Surface and Coatings Technology,* vol. 179, no. 2-3, pp. 349-355, 2004.

[92] X. Li and W. Seah, "Tool wear acceleration in relation to workpiece reinforcement percentage in cutting of metal matrix composites," *Wear,* vol. 247, no. 2, pp. 161-171, 2001.

[93] E. Rabinowicz, L. Dunn, and P. Russell, "A study of abrasive wear under three-body conditions," *wear,* vol. 4, no. 5, pp. 345-355, 1961.

[94] C. Guo *et al.*, "Recent advancements in machining with abrasives," *Journal of Manufacturing Science and Engineering,* vol. 142, no. 11, 2020.

[95] H. Zhou, W. Ding, and C. Liu, "Material removal mechanism of PTMCs in high-speed grinding when considering consecutive action of two abrasive grains," *The International Journal of Advanced Manufacturing Technology,* vol. 100, no. 1-4, pp. 153-165, 2019.

[96] W. D. Callister and D. G. Rethwisch, *Fundamentals of materials science and engineering*. Wiley London, 2000.

[97] J. Ding *et al.*, "Dynamic modeling of ultra-precision fly cutting machine tool and the effect of ambient vibration on its tool tip response," *International Journal of Extreme Manufacturing,* vol. 2, no. 2, p. 025301, 2020.

[98] G. Werner, "Influence of work material on grinding forces," *Annals of the CIRP,* vol. 27, no. 1, pp. 243-248, 1978.

[99] S. Malkin and C. Guo, *Grinding technology: theory and application of machining with abrasives*. Industrial Press Inc., 2008.

[100] L. Lichun, F. Jizai, and J. Peklenik, "A study of grinding force mathematical model," *CIRP Annals,* vol. 29, no. 1, pp. 245-249, 1980.

[101] Q. Liu, X. Chen, Y. Wang, and N. Gindy, "Empirical modelling of grinding force based on multivariate analysis," *Journal of Materials Processing Technology,* vol. 203, no. 1-3, pp. 420-430, 2008.

[102] M. Guo, B. Li, Z. Ding, and S. Y. Liang, "Empirical modeling of dynamic grinding force based on process analysis," *The International Journal of Advanced Manufacturing Technology,* vol. 86, pp. 3395-3405, 2016.

[103] H. Adibi, F. Jamaati, and A. Rahimi, "Analytical simulation of grinding forces based on the micro-mechanisms of cutting between grain-workpiece," *The International Journal of Advanced Manufacturing Technology,* vol. 119, no. 7, pp. 4781-4801, 2022.

[104] M. Younis, M. Sadek, and T. El-Wardani, "A new approach to development of a grinding force model," 1987.

[105] U. P. Durgumahanti, V. Singh, and P. V. Rao, "A new model for grinding force prediction and analysis," *International Journal of Machine Tools and Manufacture,* vol. 50, no. 3, pp. 231-240, 2010.

[106] Y. Zhang, C. Fang, G. Huang, and X. Xu, "Modeling and simulation of the distribution of undeformed chip thicknesses in surface grinding," *International Journal of Machine Tools and Manufacture,* vol. 127, pp. 14-27, 2018.

[107] M. Yang *et al.*, "Maximum undeformed equivalent chip thickness for ductile-brittle transition of zirconia ceramics under different lubrication conditions," *International Journal of Machine Tools and Manufacture,* vol. 122, pp. 55-65, 2017.

[108] S. Agarwal and P. V. Rao, "Predictive modeling of force and power based on a new analytical undeformed chip thickness model in ceramic grinding," *International Journal of Machine Tools and Manufacture,* vol. 65, pp. 68-78, 2013.

[109] K. Salonitis, P. Stavropoulos, and A. Kolios, "External grind-hardening forces modelling and experimentation," *The International Journal of Advanced Manufacturing Technology,* vol. 70, pp. 523-530, 2014.

[110] W. Rowe, J. Pettit, A. Boyle, and J. Moruzzi, "Avoidance of thermal damage in grinding and prediction of the damage threshold," *CIRP Annals,* vol. 37, no. 1, pp. 327-330, 1988.

[111] W. B. Rowe and X. Chen, "Characterization of the size effect in grinding and the sliced bread analogy," *International Journal of Production Research,* vol. 35, no. 3, pp. 887-899, 1997.

[112] J. Tang, J. Du, and Y. Chen, "Modeling and experimental study of grinding forces in surface grinding," *Journal of materials processing technology,* vol. 209, no. 6, pp. 2847-2854, 2009.

[113] !!! INVALID CITATION !!! .

[114] K. L. Johnson and K. L. Johnson, *Contact mechanics*. Cambridge university press, 1987.

[115] A. Jourani, "Modelling of ploughing-cutting transition regime during abrasive manufacturing process," *International Journal of Mechatronics and Manufacturing Systems,* vol. 8, no. 1-2, pp. 19-32, 2015.

[116] H. N. Li, T. B. Yu, Z. X. Wang, L. Da Zhu, and W. S. Wang, "Detailed modeling of cutting forces in grinding process considering variable stages of grain-workpiece micro interactions," *International Journal of Mechanical Sciences,* vol. 126, pp. 319-339, 2017.

[117] F. P. Bowden and D. Tabor, *Friction: an introduction to tribology*. Anchor, 1973.

[118] E. Rabinowicz and R. Tanner, "Friction and wear of materials," *Journal of Applied Mechanics,* vol. 33, no. 2, p. 479, 1966.

[119] J. Challen and P. Oxley, "An explanation of the different regimes of friction and wear using asperity deformation models," *Wear,* vol. 53, no. 2, pp. 229-243, 1979.

[120] M. Winter, S. Thiede, and C. Herrmann, "Influence of the cutting fluid on process energy demand and surface roughness in grinding—a technological, environmental and economic examination," *The International Journal of Advanced Manufacturing Technology,* vol. 77, no. 9, pp. 2005-2017, 2015.

[121] E. van der Heide and D. J. Schipper, "Galling initiation due to frictional heating," *Wear,* vol. 254, no. 11, pp. 1127-1133, 2003.

APPENDIX A ARTICLE 3: MACHINING OF TITANIUM METAL MATRIX COMPOSITES

Coauthors: Zhongde Shi, Luc Baron, and Marek Balazinski

Published on November 6, 2020.

Multidisciplinary Digital Publishing Institute, Materials

Abstract: The TiC particles in titanium metal matrix composites (TiMMCs) make them difficult to machine. As a specific MMC, it is legitimate to wonder if the cutting mechanisms of TiMMCs are the same as or similar to those of MMCs. For this purpose, the tool wear mechanisms for turning, milling, and grinding are reviewed in this paper and compared with those for other MMCs. In addition, the chip formation and morphology, the material removal mechanism and surface quality are discussed for the different machining processes and examined thoroughly. Comparisons of the machining mechanisms between the TiMMCs and MMCs indicate that the findings for other MMCs should not be taken for granted for TiMMCs for the machining processes reviewed. The increase in cutting speed leads to a decrease in roughness value during grinding and an increase of the tool life during turning. Unconventional machining such as laser-assisted turning is effective to increase tool life. Under certain conditions, a "wear shield" was observed during the early stages of tool wear during turning, thereby increasing tool life considerably. The studies carried out on milling showed that the cutting parameters affecting surface roughness and tool wear are dependent on the tool material. The high temperatures and high shears that occur during machining lead to microstructural changes in the workpiece during grinding, and in the chips during turning. The adiabatic shear band (ASB) of the chips is the seat of the sub-grains' formation. Finally, the cutting speed and lubrication influenced dust emission during turning but more studies are needed to validate this finding. For the milling or grinding, there are major areas to be considered for thoroughly understanding the machining behavior of TiMMCs (tool wear mechanisms, chip formation, dust emission, etc.).

Keywords: titanium metal matrix composites; material removal mechanisms; tool wear; surface quality

1. Introduction

Titanium and its alloys have been the subject of significant research interest in different fields. The unique properties of these alloys such as high specific strength, lightweight, chemical resistance, and biocompatibility make them ideal candidates for biomedical, automotive, petrochemical, and aerospace industries [1–3]. Titanium metal matrix composites (TiMMCs) are made of a titanium alloy matrix reinforced with fibers, particles, or whiskers [3] which provide them exceptional properties such as a high specific modulus, high specific strength, high-temperature and wear resistance, and potential decreased weight. In the last 30 years, TiMMCs have emerged as an alternative to Ni-based alloys in aerospace applications [3–5]. They are suitable for high-performance applications such as rotating components of jet engine compressors [6]. However, the complexities of fabrication and high material and processing costs limit their wide industrial applications. Recent research efforts by

NASA, made it possible to implement their use in large gas turbine engines [7,8] resulting in successful applications of TiMMCs. However, research efforts are still required on the precision machining of TiMMCs. TiMMCs reinforced with fibers are difficult and expensive to fabricate, industries prefer TiMMCs reinforced with particles or whiskers which have equivalent performances but without the disadvantages of anisotropic strength. The difference in mechanical properties between the matrix (ductile) and the particle reinforcements (brittle, hard, and abrasive), and the high strength and low heat transfer of TiMMCs present challenges during machining [9]. Therefore, TiMMCs parts are generally made near net shape to avoid heavy machining operations. The issues in finishing TiMMC parts include high tool wear [10] and poor surface finish with voids, micro-cracks, and broken particles. The surface defects constitute crack initiation sites rendering the workpieces vulnerable to fatigue resistance [11,12], which is essential for use in high-performance applications of TiMMCs.

The literature contains a substantial amount of information regarding the machining of metal matrix composites (MMCs). Almost all typical machining methods have been studied in the literature, whether it is a conventional or unconventional machining methods. The main tool wear mechanisms were identified as abrasive wear [13], flank wear, and built-up edge [14]. The predominant tool wear mechanism for machining MMCs is two-body abrasion and three-body abrasion [15]. The effectiveness of different tool materials for a multitude of MMCs with reinforcing particles was also studied. Polycrystalline diamond (PCD) tools are more suitable than polycrystalline cubic boron nitride (PCBN) or carbide-based tool materials [16–18]. In general, studies have shown that the tool life of cutting tools made with a material less hard than SiC particles is very limited [19]. Machining of MMCs has shown that cutting speed is the parameter with the greatest impact. Both tool wear and roughness surface are greatly influenced by cutting speed, in various studies [14,20–25]. Laser machining has no advantage for the machining of MMCs. The excessive heat produced during machining negatively affects the surface finish [26]. Even though TiMMCs are an integral part of MMCs, the substantial information regarding the machining of MMCs is mainly focused on aluminum alloy matrix MMCs with SiC particle reinforcements. Lately, there has been many activities on machining TiMMCs. The present paper provides an overview of the latest advances in machining of TiMMCs. It covers the operations of turning, milling, and grinding with focus on the effect of different cutting parameters, material removal mechanisms, tool wear, and the surface finish. Comparisons of the behavior during machining between MMCs and TiMMCs are also presented and discussed throughout the paper.

2. Turning

Certain facts demonstrated for MMCs are taken for granted as being true for TiMMCs. These facts are mainly the dependence of the turning efficiency on the workpiece material [27,28], the dependence of the surface quality on the tool material, grain size, and other aspects such as the effect of the depth of cut, feed rate [29], and cutting speed [15] on tool wear and surface quality. Most studies on the turning of TiMMCs address tool wear or the quality of the machined surfaces. The difficulties related to the machining of TiMMCs guided research efforts. Studies, which are sometimes less conventional, were conducted to find cutting conditions to minimize tool wear while increasing the quality of the surface finish during turning. This section discusses these topics and some characteristics for turning the TiMMCs.

The effect of workpiece temperature on the machining performance was studied. An improvement in surface roughness was obtained when an Al-based MMC was pre-heated to 60 °C [26]. For TiMMCs, a study was carried out on laser-assisted turning [9]. The laser increases the local temperature of the TiMMCs just before cutting. During the study, the temperature was maintained below the phase change temperature of the Ti_6Al_4V matrix (882 °C), between 300–500 °C. Although the surface roughness increases by 15%, the total volume of material removal and the tool life increased. The increase in tool life is due to the fewer number of broken particles (Figure 1) and consequently, less abrasion wear. A high temperature (500 °C) coupled with a high cutting speed (v_c = 170 m/min) can induce tool diffusion wear to the point that it becomes the source of the cutting tool wear. The increase in tool life during laser-assisted turning is accompanied by reduced cutting forces. The thrust force was reduced by around 25%. The variation in cutting forces are recognized as a significant indicator of tool wear in the machining process [14]. However, cutting temperature also has effect on tool wear.

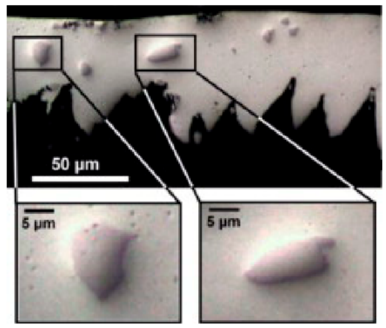

Figure 1. Unbroken particles at surface temperature 1000 °C and v_c = 100 m/min with laser-assisted machining [9].

Tool life is affected by the nature of the tool. It is shown in [20–23] that the tool life is increased for coated carbide tools used in MMC finishing compared to uncoated carbide tools. PCD tools are highly recommended in the literature for turning MMCs because they are harder than the particle reinforcements [14] and do not chemically react with the components of the part [16]. The effectiveness of coated tools on extending tool life applied to turning TiMMCs too. A comparative study conducted by Alireza [30] showed the effectiveness of different cutting tools for turning TiMMCs. The study compared the tools of tungsten carbide inserts coated with TiSiN-TiAlN, cubic boron nitride (CBN) inserts, and PCD inserts. The results showed that the carbide inserts provide a much better surface finish than the other two types of inserts. The use of CBN inserts for the same turning conditions leads to the surface being 150% rougher than carbide inserts: 2.29 µM versus 1.42 µM. The use of PCD inserts is not at all suitable for turning TiMMCs. An extremely high wear rate is observed leading to tool chipping and failure. An increase in cutting speed and depth of cut beyond 500 m/min and 0.5 mm/rev, leads to the catastrophic effect: The breakage of the insert. For other turning conditions (cutting speed between 50–120 m/min and a feed rate of 0.1 or 0.2 mm/rev) of the same TiMMCs, Bejjani [31] observed that using PCD tools led to less rough surfaces than using carbide tools, and that the surface roughness was more sensitive to the variation of cutting speed than feed rate. For high cutting speed conditions, the mechanisms change and provide a better surface finish. Moreover, beyond 170 m/min, turning can only be done with a PCD tool because the carbide tools wear rapidly [32]. Niknam et al. [33] compared carbide and CBN inserts. Their results showed that both types of inserts are subject to flank wear and the main wear mechanisms are abrasion and adhesion. The observation of a rapid increase of the cutting force from 120–500 N during turning at high speed (80 m/min) with carbide inserts revealed rapid tool wear and poor surface quality. CBN cutting tools seem to be the best choice for turning TiMMCs due to their high abrasion and resistance to thermal load.

In the literature [15,34], two- and three-body abrasion are found to be the dominant tool wear mechanisms for the MMCs. The presence of hard particles in TiMMCs leads to both two- and three-body abrasion wear. TiMMCs also exhibit strong chemical reactivity due to the chemical nature of the matrix (titanium alloy) which results in a strong affinity to almost all tool materials [35]. Adhesion is the major damage mechanism of the tool observed during the turning of TiMMCs by Alireza [30] for carbide and CBN inserts. Abrasion and diffusion are secondary wear mechanisms in this study. The tooltip is protected against abrasion due to the formation of a smooth layer of adhered material. For turning at high cutting speed, MMCs are very abrasive and tend to wear the tool rapidly [31,36]. For TiMMCs, a high cutting speed (170 m/min) tends to reduce tool wear. The increase in cutting speed above

180 m/min seems to lead to a change in the cutting mechanism causing a decrease in cutting force, and therefore a decrease in tool wear. At such a cutting speed, abrasion is the main tool wear mode. Laser-assisted turning is a good alternative to increase tool life. The tool life is linked to particle-tool interactions. When the matrix is heated by the laser (300−500 °C), the particles will move into the softer matrix instead of contributing to the abrasion wear of the tool. Even though abrasion wear mode remains the dominant wear mode, high cutting speed, and high temperature during laser-assisted turning induced diffusion wear mode at the tool chip interface. X.T. Duong et al. [37] reported that the initial tool wear mechanism would significantly affect the entire tool life when machining TiMMCs. Their subsequent study made it possible to highlight the formation of a "wear shield" on the surface of the cutting tool from the first moment of cutting. The formation of this wear shield is due to the adhesion of the tool on the workpiece (taking place at low cutting speeds), coupled with the diffusion wear (chemical reactivity of the matrix), and would make it possible to limit the tool wear during steady wear. Diffusion allows the creation of a new hard thin layer on the surface of the tool which will constitute the "wear shield". The main wear modes observed during the initial tool wear are therefore adhesion and diffusion. The wear shield protects the tool against the abrasive effect of titanium carbide particles.

The study of chip formation and particle-tool interactions clarifies the mechanisms that operate during machining. Bejjani et al. [31] investigated mechanisms due to the tool-chip interaction, and chip formation at different cutting speeds (from 60–230 m/min). The low thermal conductivity of titanium alloy matrices leads to adiabatic shear and results in segmented chips. Chip formation at different cutting speeds does not occur in the same way. At low speed (100 m/min) Bejjani et al. showed that the chip microstructure had undergone high plastic deformation, with a plastic strain over most of the area of the chip (Figure 2). The presence of these high stresses is sufficient to break the particles, resulting in the formation of a multitude of small particles which contribute to the increase of the tool wear rate (Figure 3). While at high speed (230 m/min) the microstructure shows smaller deformations, demonstrated by a larger shear angle. At these cutting speeds, particles are displaced or cut and result in less abrasion wear of the tool. The study also shows that at different cutting speeds there was no evidence of particle de-bonding. In a subsequent study, Bejjani et al. [38] investigated the nature of chip segmentation and tool-particle interactions to confirm the mechanisms reported above. The observation of the chip formation revealed a decrease in the segmentation of the chip with an increase in the cutting speed: Respectively, 150 μM and 90 μM at 50 and 150 m/min. The segmentation mechanism was observed to start from a crack on the free surface material ahead of the tool (Figure 4b). The transmission electron microscopy (TEM) and scanning transmission electron microscopy (STEM) studies revealed that there is an evolution of the microstructure in the adiabatic shear band (ASB) producing sub-grains (Figure 4a). These sub-grains exhibit misorientations characteristic of rotational dynamic recrystallization (RDX). Calculations show that the temperature in the ASB is close to the recrystallization temperature (500–690 °C). A microstructural evolution model of the chip is proposed for the first time. Otherwise, the particles present in the matrix do not interfere with the formation of the ASB.

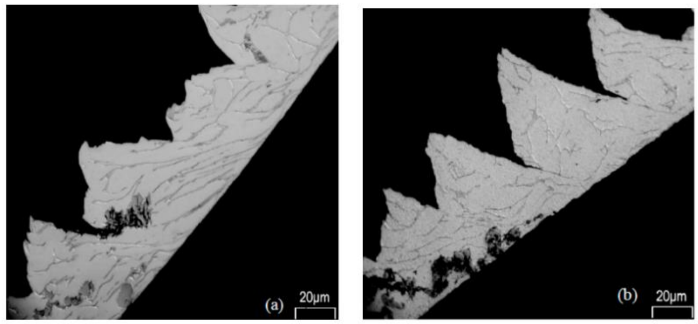

(**a**) (**b**)

Figure 2. Chip microstructure with the polycrystalline diamond (PCD) tool at (**a**) 100 m/min; and (**b**) 230 m/min [32].

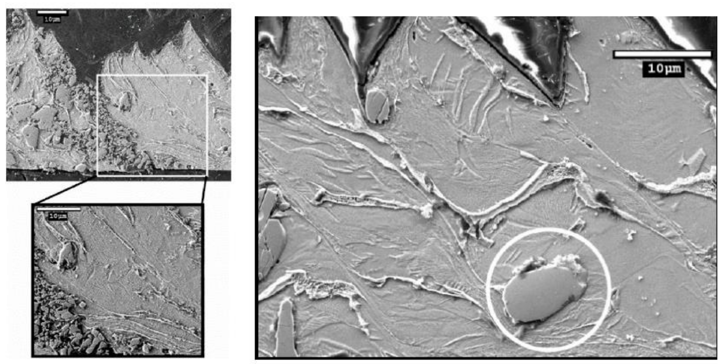

(**a**) (**b**)

Figure 3. (**a**) Particle broken into many other smaller particles during the chip formation at v_c = 60 m/min; (**b**) Unbroken particle during the chip formation at v_c = 180 m/min [32].

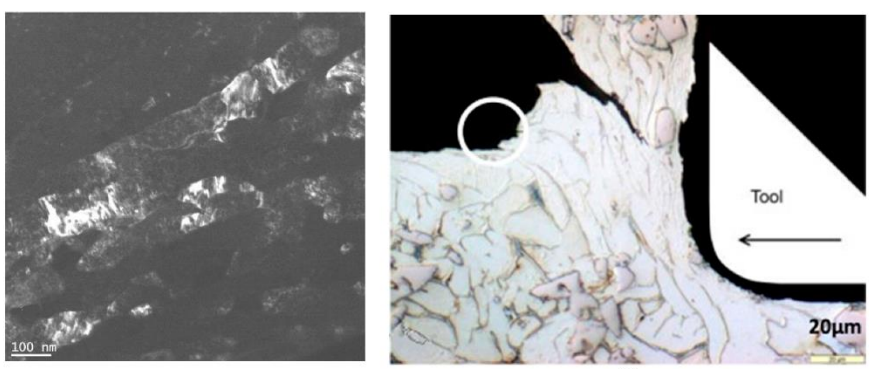

(**a**) (**b**)

Figure 4. (**a**) Darkfield imaging of sub-grains inside the adiabatic shear band (ASB); (**b**) Sign of crack initiation at the free surface ahead of the tool (v_c = 60 m/min) [38].

Dust generation during machining is a health and environmental concern that received very little attention in the current global context. Machining TiMMCs produces severe tool wear and probably a strong particulate emission. A recent study [39] reported the dust generation at micro- and nano-scales under different lubricated modes during machining of TiMMCs. The cutting speed shows a significant impact on the production of fine particles (2.5 µM aerodynamic particles diameter or less) while it does not affect the specific surface concentration and mass concentration of ultrafine particles (size range of 0.1 µM). As expected, tool lubrication reduces particle emission during turning, and high levels of flow rate (300 mL/min) combined with coated inserts lead to less ultrafine particles than with uncoated inserts. Under dry conditions, particle emission is more important, but the analysis of the cutting forces shows that at a high flow rate (300 mL/min) there is a thin film of lubricant formed. The presence of this thin film of lubricant may affect the emission of particles under high lubrication modes and high speeds (50 m/min). Finally, even if the dry condition provides a smaller roughness (around 1 µM, versus 3 µM for a flow rate of 300 mL/min) [40], the emission of ultrafine particles and fine particles with a coated tool remains significant compared to lubricated conditions.

3. Milling

Also, the numbers of publications on conventional milling of TiMMCs is fewer than turning, comparison can still be done between the different mechanisms occurring during the milling of TiMMCs and those of MMCs. As with turning, tool wear and surface roughness are the main concerns in milling TiMMCs. The studies available in the literature provide a comprehensive comparison between different tool materials during high-speed milling [30,41]. The tools compared are two carbide tools (X400 and X500) and a PCD tool. Studies on the milling of MMCs have shown that carbide tools are not very effective and have lower tool life than PCD tools [17,18]. For the milling of TiMMCs [30,41], the carbide tools demonstrated acceptable tool wear despite the occurrence of vibration. Similar to PCD tools, carbide tools have shown the possibility of an optimum tool wear and productivity under certain conditions. These optimum conditions are v_c = 45 m/min, f = 0.2 mm/rev, a_p = 0.16 mm for the X500 carbide tool, and v_c = 70 m/min, f = 0.35 mm/rev, a_p = 1.5 mm for the X400 carbide tool. The observations made during the study showed that cutting speed is the main factor influencing the tool wear rate for the PCD tool. Optimum tool wear is obtained at low cutting speeds (150 m/min). It is important to note that in the cutting speed range of 350–600 m/min, PCD tools failed. The tool wear of the carbide tools is equally highly dependent on the cutting speed, as well as the depth of cut. These two parameters govern the tool wear rate during milling with carbide tools. These observations do not match those made for the milling of MMCs. Indeed, studies have shown that the feed rate is the cutting parameter that significantly affects the tool wear [42,43]. Although the cutting conditions for both types of tools used for milling TiMMCs are similar, the wear mechanisms are not identical. Tool wear mechanisms vary depending on the type of tool. Observations showed the presence of oxidation on the edge of the carbide inserts, but adhesion was the main wear mechanism. While for PCD tools, the adhesion was very slight and the main wear mechanisms were identified as edge chipping, abrasion, and peeling.

As surface roughness is a primary concern in machining TiMMCs, cutting parameters with considerable influence on roughness were investigated. For carbide tools, statistical analyses have shown that the feed rate is the parameter having the most influence on roughness [41]. A feed rate of 0.2 mm/rev permits to obtain a roughness of 1.74 µM for a X500 carbide tool. Similarly, for milling of MMCs, the feed rate is likewise one of the cutting parameters having the most impact on roughness [24,25]. PCD tools for milling TiMMCs do not show any dependence on one specific cutting parameter, but rather on a set of different cutting parameters. Optimization of these cutting parameters is necessary to obtain a quality surface roughness. As an example, a roughness of 0.18 µM can be achieved after optimization of the parameters. An investigation on the milling of a TiMMCs reinforced with carbon nanotubes was conducted. It was found that the roughness is lower at high cutting speed

(v_c = 188.4 m/min) and low feed rate (200 mm/min). Unfortunately, the cutting tool material was not provided, which makes it impossible to compare with other investigations [44].

Chip morphology study is important in understanding the mechanisms that operate during milling just as it is in turning. In general, the study conducted by Kamalizadeh et al. [41] shows that the chips obtained during milling of TiMMCs are similar to those obtained during turning: Serrated chips. Unlike chips formed during turning, milling chips have two different chip compression ratios, thus creating two main zones. The former is the A1 zone and the later the A2 zone as shown in Figure 5a. These zones are due to either the non-linear movement of chips caused by catastrophic shearing during the segment formation (A2) or the high temperature at the tool chip interface (A1). Statistical studies conducted on the shear slip distance and slip angle show that they increase slightly with the time (Figure 5b). The authors attribute this phenomenon to a serration level which becomes more and more intense with time. This is closely linked to the increase in cutting force, friction force, as well as the rapid increase in temperature in the shearing bands characteristic of machining TiMMCs.

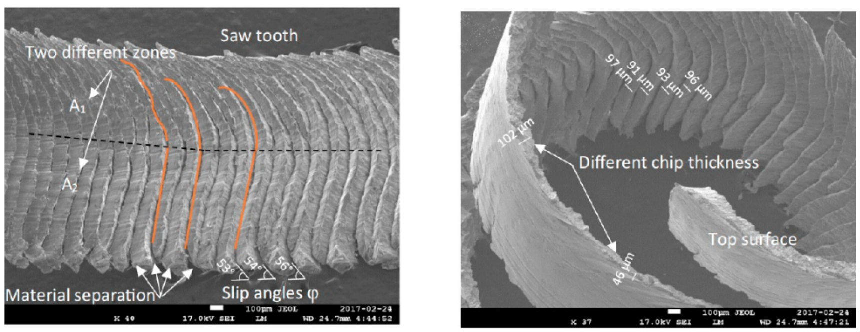

(**a**) (**b**)

Figure 5. (**a**) two distinct zones with two different compression ratios; (**b**) different shear slip distances [41].

4. Grinding

The exceptional properties of TiMMCs make them good candidates for manufacturing parts for the aerospace industry, especially for large gas turbine engines [7,8]. However, the reinforcing particles in the TiMMCs cause the defects on machined surfaces. These defects are the seat of the formation of fatigue cracks under repeated loading, leading to the fracture of the part. The fatigue resistance of aeronautical parts is essential to avoid catastrophic accidents. The surface finish is one of the main concerns for TiMMCs research. As the grinding is mainly used to increase the accuracy of the workpiece and surface quality [45,46], understanding the mechanisms operating during grinding is essential.

Several previous studies [47–50] showed that grinding forces affect roughness, work hardening, power consumption, grinding stresses, and surface defects, and give a qualitative indication of the tool wear and grindability (the ease of removal material). For MMCs, the literature has shown [51] that grinding wheel wear increases with increasing contents of the reinforcing particle because the particles are highly abrasive. In their study on TiMMC, Blau et al. [49] showed the influence of particle content on grinding parameters, including grinding forces. The results showed that when the content of TiC particles increases from 0% to 10%, the grinding force increases as does the resistance to material removal, and therefore the tool wear. The results follow the same trend as those obtained for MMCs [52,53].

Depth of cut is the grinding parameter having the most influence on cutting forces during grinding TiMMCs [54]. Comparisons of cutting force in high-speed grinding (120 m/s) and conventional-speed grinding (20 m/s) have shown that cutting forces decrease with increasing cutting speed [54,55]. Even though cutting speed is not the most influential cutting parameter, it has a significant influence on cutting forces. Different types of defects such as microcracks and pile-ups can influence roughness; in particular, through the grinding scratches and cavities related to the ductile deformation of the matrix and the fragile behavior of the reinforcing particles [55]. The grinding forces [56] and the size of the undeformed chip thickness [55] play an essential role in the propagation of microcracks, in particular lateral crack propagation. The presence of microcracks on the ground surface is due to severe residual stresses from the large mechanical-thermal loads occurring during grinding [57]. Zheng Li et al. [55] compared the ground surface morphology obtained in conventional-speed grinding (20 m/s) and high-speed grinding (120 m/s). They observed that grinding scratches and cavities are related to the ductile deformation of the matrix and the fragile behavior of the reinforcing particles. The formation of pile-ups is due to the slide flow of the material during grinding. High-speed grinding induces a decrease in the presence of pile-up thanks to the increase of active grains per unit of time. The size of the pile-up is highly dependent on the depth of cut or on the undeformed chip thickness, which is consistent with previous studies [58–60] and studies on MMCs [61].

The content of reinforcing particles in the composite also has an influence on the roughness of ground surfaces. The surface roughness of MMCs increases with the content of reinforcing particles [52]. However, the roughness for the TiMMCs decreases [49]. It can be assumed that the difference in roughness tendency is due to the nature of the particles and the matrix. TiC particles are harder than SiC particles, and Ti_6 Al_4V is more ductile compared to an Al alloy. During grinding, SiC particles can easily break up into a multitude of small particles that become encrusted in the ground surface of the Al alloy, increasing the roughness. Ti_6Al_4V is more difficult to machine due to its high ductility. Without particles, its ductility can induce the formation of pile-ups as well as numerous grooves. The presence of TiC particles limits the formations of pile-ups and grooves. The very hard nature of the TiC particles seems to promote the dislodgement of the particles instead of their breaking, which is favorable to the reduction in roughness. Table 1 presents some of the roughness measurement data from articles of interest to illustrate the point.

Table 1. Effect of particles content on roughness.

	Blau et al. [49]		**Thiagarajan et al. [52]**	
Particle %	Ti_6Al_4V + 0% TiC	Ti_6Al_4V + 10% TiC	Al alloy + 2% SiC	Al alloy + 12% SiC
Ra (µM)	1.68	0.86	0.20	0.60

One might think, instinctively, that the grinding temperature depends on the grinding forces. However, Zheng Li et al. [54,55] showed that the same cutting parameters influence the grinding temperature and the grinding forces, but in a different way. When the grinding speed increases from 20–120 m/s, the grinding forces decrease by up to 50% but the grinding temperature increases. The authors attributed the decrease in grinding force to the lower friction coefficient in high-speed grinding, which is questionable. Conversely, the grinding temperature increase is caused by the increased action of the grinding grains in the contact zone per unit of time coupled with the drop-in efficiency of the coolant. The drop-in efficiency of the coolant is due to an air barrier that forms around the abrasive wheel, thus preventing the cooling fluid from entering the grinding zone leading to very poor efficiency of the coolant and at an increase in the grinding temperature. The effect of the different grinding parameters on the grinding temperature is shown in Figure 6. Different from grinding speed, the parameters of workpiece speed and the depth of cut have the same effect on both grinding forces and grinding temperature.

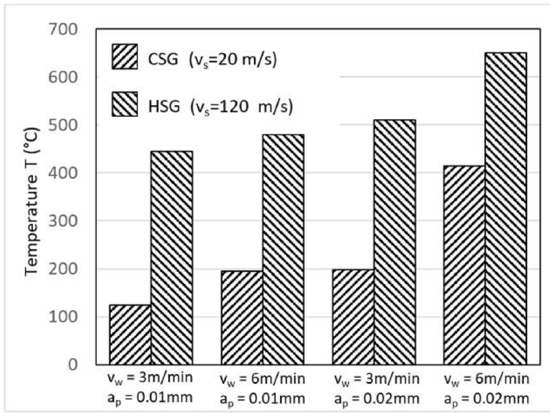

Figure 6. Effects of grinding parameter in high (HSG) and conventional (CSG) speed grinding on grinding temperature [55].

Temperature variations during grinding can have significant impacts on the microstructural or mechanical integrity of the material. Large temperature variations can lead to the presence of residual stresses on the subsurface as well as microstructural transformations [62–64]. The presence of micro-cracks on the ground surface is characteristic of severe residual stresses [57]. Zheng Li et al. [62] observed residual compressive stress, work hardening on the ground surface, and microstructural changes in the subsurface. The microstructural changes observed are the bending and elongation of the crystal lattice as shown in Figure 7. These changes are mainly related to the strong plastic deformations and rapid cooling effects that occur on the surface during grinding. The authors showed that the depth of cut is the parameter that induces the higher variation in the microstructure.

(**a**) (**b**)

Figure 7. Changes in microstructure: (**a**) v_s = 25 m/s, v_w = 300 mm/s, a_p = 0.3 mm; (**b**) v_s = 20 m/s, vw = 300 mm/s, a_p = 1.0 mm (v_s = cutting speed, v_w = speed of the workpiece, and a_p = cutting depth) [62].

Microstructural changes were also observed in the study by Xinxin Xi et al. [65]. Microstructural changes were highly dependent on the same grinding parameter, or the depth of cut. When the depth of cut is 0.020 mm, the distinction of the grain boundary is difficult due to the microstructural changes (up to a thickness of about 20 µM), when the depth of cut is 0.002 mm the microstructure is slightly altered (up to 5 µM) deep below the surface. Microhardness tests were also carried out by the authors to validate their microstructural observations. The results showed that microhardness increases (from 250–425 HV) with the decreasing depth below the ground surface (from 225–10 μM, respectively). This increase in hardness reflects significant residual stresses and/or a microstructural change linked to grinding.

Similar to turning and milling, the understanding of chip morphology and the material removal mechanisms in grinding is important for the optimization of grinding parameters. Ding et al. [56] studied the material removal behavior. Their results show that the material removal behavior is divided into three stages. Stages one and three belong to ductile regime removal of the matrix, dominated by serrated chip formation. Meanwhile, stage two belongs to the brittle regime removal dominated by brittle fracture, crack initiation, and crack propagation. The authors extended their study to investigate the effect of grinding speed on material removal mechanisms. The results show that the chip morphology varies with the grinding speed. The chip morphology is continuous and thicker at the speed of 20 m/s. It becomes discontinuous and thinner at 120 m/s. At high-speed grinding (120 m/s), the material removal behavior is dominated by a high strain and strain-rate hardening which induces a weakened and brittle plastic flow. Similar results were obtained by Xinxin Xi et al. [65]. Specifically, the material removals behavior observed are the same, namely: The ductile removal of the matrix, ductile removal of the particle and brittle behavior, fracture, and crack propagation for the particles. Moreover, these different stages of material removal mechanism are the same as those observed for MMCs in the study conducted by Huang et al. [66].

Most studies on material removal mechanisms of grinding are based on experimentally validated finite element (FE) models. The work of Huan et al. [67] modeled for the first time the simultaneous action of two abrasive grains of a CBN wheel in high-speed grinding (120−140 m/s). All relevant details of the material removal behavior during grinding are developed. During the grinding by the first grain of CBN, there are two possible outcomes: Either the TiC reinforcement has a residual crack, or it does not. In the case of a residual crack during the passage of the second grain, the FE simulation showed that the maximum stress of Mises was located at the point of the crack in the reinforcement particle, regardless of the distance between the grain of the grinding wheel and the interface. The residual crack spreads during the passage of the second grain of the wheel until the tensile failure of the TiC particle. Then the reinforcement particle breaks off the matrix. During these conditions, stress concentrations are present but do not continuously exchange between the matrix and the reinforcement. These mechanisms are illustrated in Figure 8. In the case of no residual crack, there is no stress concentration which leads to the tensile failure of the particle. The position of the maximum Mises strain is located at the point of contact between the grain of the wheel and the workpiece. The grinding action of the second grain therefore causes the plastic removal of the matrix as well as the brittle removal of the TiC particle. Figure 9 shows a schematic of the mechanism. The results also show that for the passage of the first grain of the wheel that the crushing depth is affected by the undeformed chip thickness. The more the undeformed chip thickness increases, the more the crushing depth of the particles increases in high speed grinding.

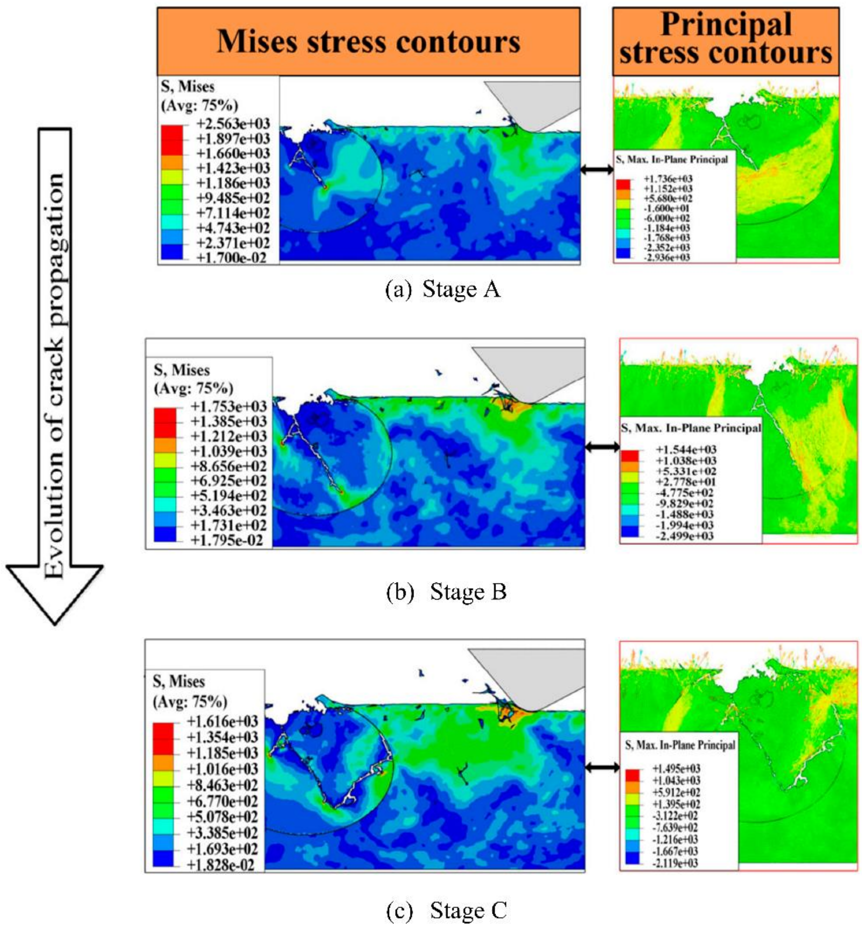

Figure 8. Evolution of the crack propagation for the second grinding grain. (**a**) initial stage, (**b**) developing and (**c**) complete [67].

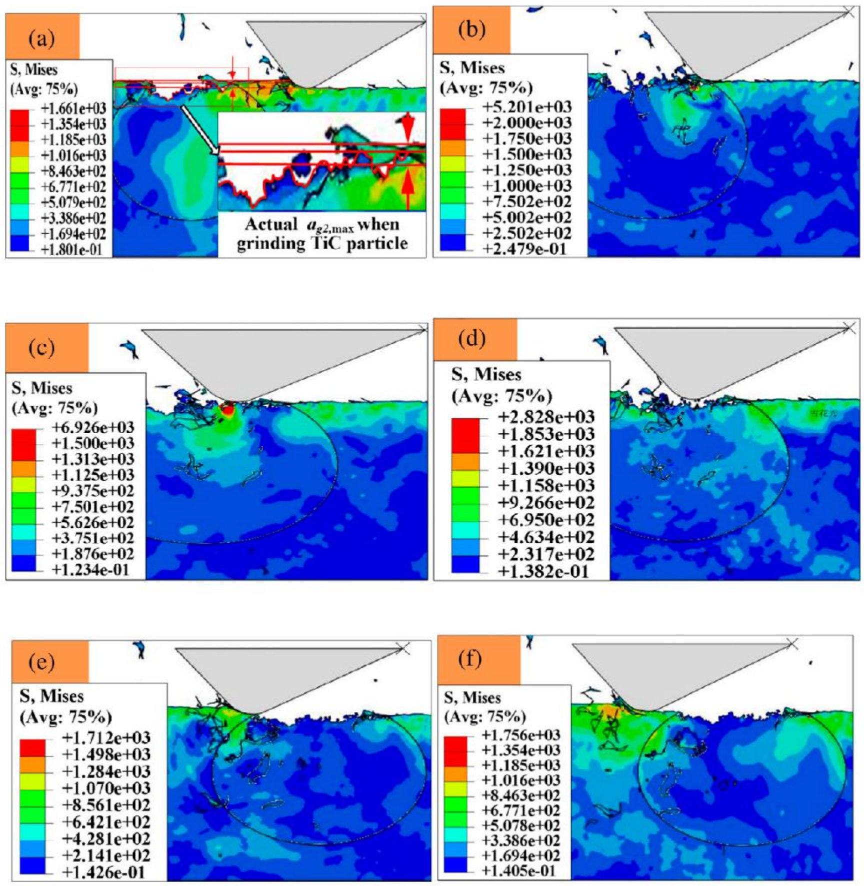

Figure 9. Material removal mechanism details from stage (**a**) to (f); (**a**) grinding the matrix, (**b**) the initial contact between the CBN grain and the TiC particle, (**c**) initial grinding of the particle, (**d**) particle removal process, (**e**) particle failure completed, (**f**) grinding the matrix [67]

Other studies have shown that the undeformed chip thickness influences many parameters, notably the grinding force, grinding temperature, surface roughness, and material removal mechanism [55–57]. The trend of the results obtained showed that the grinding forces decrease and that the grinding temperature increases with the decrease in the undeformed chip thickness. Observations of the surfaces after grinding revealed that when a small undeformed chip thickness (0.3 μM) is employed, the particles are subject to a tiny fracture which generates a small and shallow cavity on the ground surface. When the undeformed chip thickness is large (1.2 μM), the cavities of the ground surface are deep and wide. These differences in material removal mechanism result in the differences in the ground surface roughness. A wide undeformed chip thickness will increase surface roughness [55]. Besides, they observed that the lateral crack formation is dependent of the undeformed chip thickness. The larger the undeformed chip thickness, the deeper the depth of the lateral crack becomes. A deeper depth of the lateral crack leads to an increase of the interactions between cracks which can cause them to emerge on the ground surface and alter the roughness [55]. The influence of the undeformed chip thickness on the depth of the voids left by the fragile rupture of the particles was also observed by Xinxin et al. [65]. Their study in high-speed grinding showed that the bigger the undeformed chip thickness, the larger and deeper the cavity produced on the ground surface. The results of the finite element modeling were verified experimentally for similar grinding conditions and presented in Figure 10.

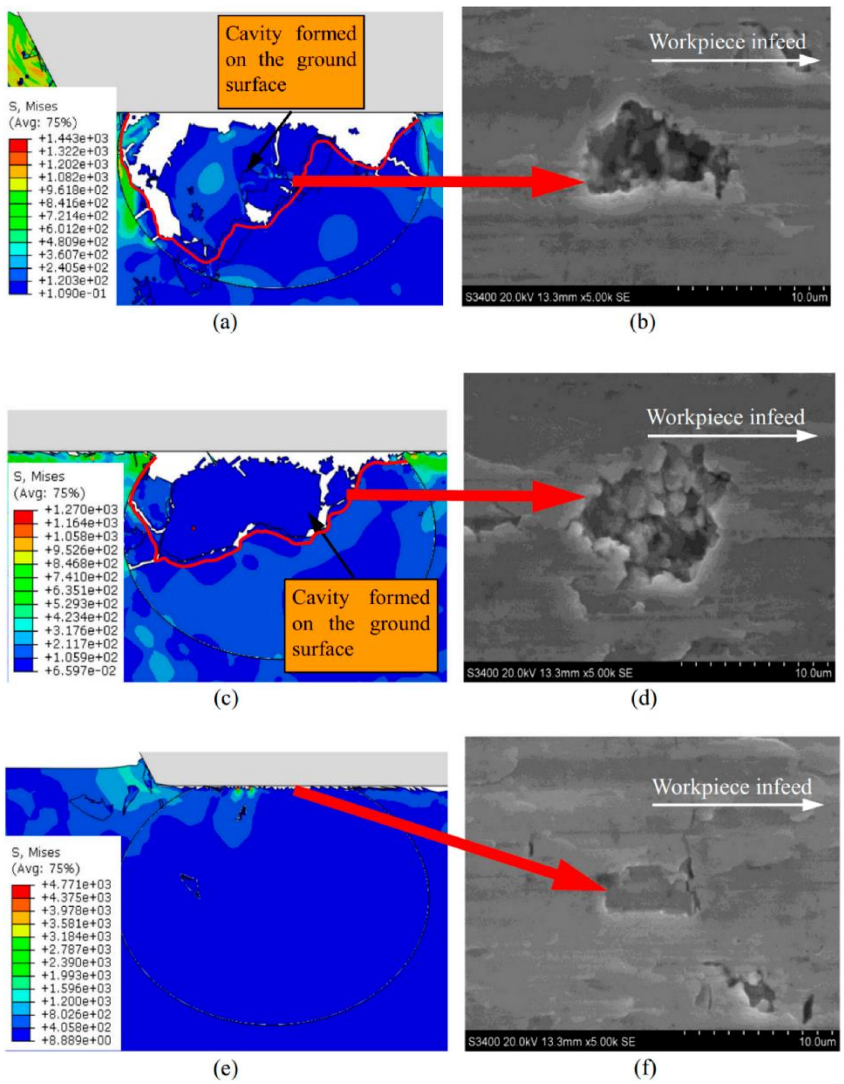

Figure 10. Effect of undeformed chip thickness on ground surface. Experiment versus simulation. (**a**) and (**b**) a_p = 1.2 μM, (**c**) and (**d**) a_p = 0.7 μM, and (**e**) and (**f**) a_p = 0.2 μM [65].

Ding et al. [50] employed the undeformed chip thickness to study the specific grinding energy which is a fundamental parameter for the characterization of the grinding process. The results showed that the specific grinding energy is slightly smaller for the TiMMC compared to Ti_6Al_4V (around 20 J/mm^3 lower). They highlighted the fact that the specific grinding energy is dependent on the mechanical properties of the material under grinding conditions [68]. It is well known in the literature that the complete ductile-mode removal of the material during the grinding requires a higher specific grinding energy compared to brittle-mode removal. As presented by Malkin et al. [69], when brittle fracture takes place during grinding, the specific grinding energy is lower than that for ductile behavior. The presence of brittle breaking of the reinforcements in the TiMMCs explains the observations made by the authors. The results also showed that the more the undeformed chip thickness increases, the more the specific grinding energy decreases. This is explained by the dependence of specific grinding energy on the following parameters: Energies consumed in chip formation, elastic deformation of the workpiece, sliding, and plowing [50,69].

The grinding wheel performance in terms of wheel life, grinding performance (forces, temperature, energy), and ground surface finish is one of the main concerns in machining TiMMCs. Zheng Li et al. [62] compared three types of conventional wheels: White alumina (WA), pink fused alumina (PA), and micro-crystal corundum (SG) grinding wheels. The SG wheel showed better performance, with the lowest grinding forces and force ratio, grinding temperature, specific energy, and surface roughness. The ground surface obtained with the SG wheel contains only a few voids and slight grooves, while the other two wheels which presented voids, debris, adherence, grooves, and delamination zone. The grinding temperature is closely related to the thermal conductivity of the grinding wheel. Indeed, Xin-Xin Xi et al. [70] compared the heat transfer characteristic of electroplated CBN wheel and vitrified CBN wheel for high-speed grinding. It was shown that the grinding temperature was lower with an electroplated CBN wheel due to its high thermal conductivity. Other authors [57] compared the performance of wheels on TiMMCs with randomly distributed grains and linearly organized grains (spaced 1.2 mm apart). The former is a single layer electroplated wheel and the latter is a brazed CBN wheel. The brazed wheel showed a removal rate twice as high as that of the electroplated wheel, it had the lowest grinding forces, grinding temperature, and less ground surface defects as well. The brazed wheel showed a better potential for high-speed grinding, without burning at the ground surface.

5. Conclusions

This paper presents a critical review on the machining of TiMMCs with focus on tool wear mechanisms, material removal and chip formation mechanisms, and machined surface quality for turning, milling, and grinding operations. The following conclusions can be drawn:

- Machining of TiMMCs presents challenges due to the presence of hard abrasive particles in a softer and sticky matrix and the low thermal conductivity of the matrix material. TiMMCs are significantly different from other types of MMCs. The findings from the machining of other MMCs cannot be taken for granted for machining of TiMMCs.
- The information in the literature about the turning of TiMMCs is quite comprehensive and the mechanisms that operate during the process are well understood. However, research efforts still need to be made regarding the emission of particles. In the milling and grinding of TiMMCs, the literature is very limited. There is a bright future for further investigations.
- For turning operations, tool wear tends to decrease in high-speed turning. No evidence of particle de-bonding was observed in turning of TiMMCs regardless of the cutting speed. The segmentation of the chip starts at the free surface ahead of the tool. The tool wear mechanisms are dependent on the cutting speed. Adhesion wear is the main wear mode and abrasion, and diffusion are secondary mode in conventional speed turning. Abrasion wear is the main wear mode in high speed turning of TiMMCs. The formation of a "wear shield" on the surface of the cutting tool from the first moment of cutting and under specific conditions results in enhanced tool life.
- For milling operations, surface roughness dependency on the cutting parameters varies with the cutting tool. The main wear mode is dependent on the cutting tool.
- For grinding, wheel wear increases with increasing contents of the reinforcing particle for both TiMMCs and MMCs. Surface roughness, however, decreases with the increase of in the percentage

of hard particles. The undeformed chip thickness is the most important parameter which affects the material removal mechanisms, ground surface microstructure, lateral cracks, surface cavities, and surface roughness.

In the future, to find the effect on grinding or milling condition on tool wear would be of major interest. The study of the efficiency of other cutting tools such as diamond tools could provide interesting insights in terms of TiMMCs machinability. Dust emission is also a field of study which should not be left aside in order to comply with occupational safety standards and to limit the pollution resulting from the processing of TIMMCs.

Author Contributions: Writing—original draft preparation, C.E.; writing—review and editing, Z.S.; writing—review and editing, L.B.; supervision and writing—review and editing, M.B. All authors have read and agreed to the published version of the manuscript.

Funding: This research received no external funding.

Conflicts of Interest: The authors declare no conflict of interest.

References

1. Boyer, R.; Welsch, G.; Collings, E. *Titanium Alloys, Materials Properties Handbook*; ASM Int: Russell Township, OH, USA, 1994.
2. Leyens, C.; Peters, M. *Titanium and Titanium Alloys: Fundamentals and Applications*; John Wiley & Sons: Hoboken, NJ, USA, 2003.
3. Hayat, M.D.; Singh, H.; He, Z.; Cao, P. Titanium metal matrix composites: An overview. *Compos. Part A Appl. Sci. Manuf.* **2019**, *121*, 418–438. [CrossRef]
4. Li, S.; Sun, B.; Imai, H.; Mimoto, T.; Kondoh, K. Powder metallurgy titanium metal matrix composites reinforced with carbon nanotubes and graphite. *Compos. Part A Appl. Sci. Manuf.* **2013**, *48*, 57–66. [CrossRef]
5. Kuzumaki, T.; Ujiie, O.; Ichinose, H.; Ito, K. Mechanical characteristics and preparation of carbon nanotube fiber-reinforced Ti composite. *Adv. Eng. Mater.* **2000**, *2*, 416–418. [CrossRef]
6. Chawla, N.; Shen, Y.L. Mechanical behavior of particle reinforced metal matrix composites. *Adv. Eng. Mater.* **2001**, *3*, 357–370. [CrossRef]
7. Singerman, S.; Jackson, J. *Superalloys 1996*; The Minerals, Metals & Materials Society: Pittsburgh, PA, USA, 1996; pp. 579–586.
8. Anderson, R.E. *Titanium Matrix Composite Turbine Engine Component Consortium (TMCTECC)*; Advanced Materials and Process Technology Information Analysis Center (AMPTIAC) Newsletter: Rome, NY, USA, 1998.
9. Bejjani, R.; Shi, B.; Attia, H.; Balazinski, M. Laser assisted turning of titanium metal matrix composite. *CIRP Ann.* **2011**, *60*, 61–64. [CrossRef]
10. Thepsonthi, T.; Özel, T. 3-D finite element process simulation of micro-end milling Ti-6Al-4V titanium alloy: Experimental validations on chip flow and tool wear. *J. Mater. Process. Technol.* **2015**, *221*, 128–145. [CrossRef]
11. Tu, S.-T.; Zhang, X.-C. Fatigue Crack Initiation Mechanisms. *Ref. Modul. Mater. Sci. Mater. Eng.* **2016**. [CrossRef]
12. Przybyla, C.; Prasannavenkatesan, R.; Salajegheh, N.; McDowell, D.L. Microstructure-sensitive modeling of high cycle fatigue. *Int. J. Fatigue* **2010**, *32*, 512–525. [CrossRef]
13. Di Ilio, A.; Paoletti, A. Machinability aspects of metal matrix composites. In *Machining of Metal Matrix Composites*; Springer: London, UK, 2012; pp. 63–77.
14. Li, J.; Laghari, R.A. A review on machining and optimization of particle-reinforced metal matrix composites. *Int. J. Adv. Manuf. Technol.* **2019**, *100*, 2929–2943. [CrossRef]
15. Davim, J.P.; Baptista, A.M. Relationship between cutting force and PCD cutting tool wear in machining silicon carbide reinforced aluminium. *J. Mater. Process. Technol.* **2000**, *103*, 417–423. [CrossRef]
16. Jani, D. Machining of Sic—metal matrix composite (MMC) by polycrystalline diamond (PCD) tools and effect on quality of surface by changing machining parameters. *Int. J. Sci. Res. Dev.* **2014**, *2*, 106–108.
17. Markopoulos, A.P.; Pressas, I.S.; Papantoniou, I.G.; Karkalos, N.E.; Davim, J.P. Machining and machining modeling of metal matrix composites—A review. In *Modern Manufacturing Engineering*; Springer: Cham, Switzerland, 2015; pp. 99–141.
18. Davim, J.P. *Machining Composites Materials*; John Wiley & Sons: Hoboken, NJ, USA, 2013.

19. Teti, R.; Jemielniak, K.; O'Donnell, G.; Dornfeld, D. Advanced monitoring of machining operations. *CIRP Ann.* **2010**, *59*, 717–739. [CrossRef]
20. Ciftci, I.; Turker, M.; Seker, U. Evaluation of tool wear when machining SiCp-reinforced Al-2014 alloy matrix composites. *Mater. Des.* **2004**, *25*, 251–255. [CrossRef]
21. Kılıckap, E.; Cakır, O.; Aksoy, M.; Inan, A. Study of tool wear and surface roughness in machining of homogenised SiC-p reinforced aluminium metal matrix composite. *J. Mater. Process. Technol.* **2005**, *164*, 862–867. [CrossRef]
22. Bansal, P.; Upadhyay, L. Experimental investigations to study tool wear during turning of alumina reinforced aluminium composite. *Procedia Eng.* **2013**, *51*, 818–827. [CrossRef]
23. Yanming, Q.; Zehua, Z. Tool wear and its mechanism for cutting SiC particle-reinforced aluminium matrix composites. *J. Mater. Process. Technol.* **2000**, *100*, 194–199. [CrossRef]
24. Arokiadass, R.; Palaniradja, K.; Alagumoorthi, N. Surface roughness prediction model in end milling of Al/SiC p MMC by carbide tools. *Int. J. Eng. Sci. Technol.* **2011**, *3*, 78–87. [CrossRef]
25. Arokiadass, R.; Palaniradja, K.; Alagumoorthi, N. Prediction and optimization of end milling process parameters of cast aluminium based MMC. *Trans. Nonferrous Met. Soc. China* **2012**, *22*, 1568–1574. [CrossRef]
26. Dabade, U.; Jadhav, M. Experimental study of surface integrity of Al/SiC particulate metal–matrix composites in hot machining. *Procedia CIRP* **2016**, *41*, 914–919. [CrossRef]
27. Dandekar, C.R.; Shin, Y.C. Modeling of machining of composite materials: A review. *Int. J. Mach. Tools Manuf.* **2012**, *57*, 102–121. [CrossRef]
28. Das, D.; Thakur, R.K.; Chaubey, A.K.; Sahoo, A.K. Optimization of machining parameters and development of surface roughness models during turning Al-based metal matrix composite. *Mater. Today Proc.* **2018**, *5*, 4431–4437. [CrossRef]
29. Tomac, N.; Tannessen, K.; Rasch, F.O. Machinability of particulate aluminium matrix composites. *CIRP Ann.* **1992**, *41*, 55–58. [CrossRef]
30. Asgari, A. Cutting Conditions Optimisation of Titanium Metal Matrix Composites in Turning and Face Milling. Master's Thesis, École Polytechnique de Montréal, Montreal, QC, Canada, 2015.
31. Bejjani, R.; Balazinski, M.; Shi, B.; Attia, H.; Kishawy, H. Machinability and chip formation of titanium metal matrix composites. *Int. J. Adv. Manuf. Syst. IJAMS* **2011**, *13*, 75–90.
32. Bejjani, R. Machinability and Modeling of Cutting Mechanism for Titanium Metal Matrix Composites. Ph.D. Thesis, École Polytechnique de Montréal, Montreal, QC, Canada, 2012.
33. Niknam, S.A.; Kamalizadeh, S.; Asgari, A.; Balazinski, M. Turning titanium metal matrix composites (Ti-MMCs) with carbide and CBN inserts. *Int. J. Adv. Manuf. Technol.* **2018**, *97*, 253–265. [CrossRef]
34. Kishawy, H.; Kannan, S.; Balazinski, M. Analytical modeling of tool wear progression during turning particulate reinforced metal matrix composites. *CIRP Ann.* **2005**, *54*, 55–58. [CrossRef]
35. Machado, A.; Wallbank, J. Machining of titanium and its alloys—A review. *Proc. Inst. Mech. Eng. Part B J. Eng. Manuf.* **1990**, *204*, 53–60. [CrossRef]
36. Basavarajappa, S.; Chandramohan, G.; Rao, K.N.; Radhakrishanan, R.; Krishnaraj, V. Turning of particulate metal matrix composites—Review and discussion. *Proc. Inst. Mech. Eng. Part B J. Eng. Manuf.* **2006**, *220*, 1189–1204. [CrossRef]
37. Duong, X.-T.; Balazinski, M.; Mayer, R. Chaotic tool wear during machining of titanium metal matrix composite (TiMMCs). In Proceedings of the ASME International Mechanical Engineering Congress and Exposition, Montreal, QC, Canada, 14–20 November 2014; p. V02BT02A018.
38. Bejjani, R.; Balazinski, M.; Attia, H.; Plamondon, P.; L'Éspérance, G. Chip formation and microstructure evolution in the adiabatic shear band when machining titanium metal matrix composites. *Int. J. Mach. Tools Manuf.* **2016**, *109*, 137–146. [CrossRef]
39. Niknam, S.A.; Saberi, M.; Kouam, J.; Hashemi, R.; Songmene, V.; Balazinski, M. Ultrafine and fine particle emission in turning titanium metal matrix composite (Ti-MMC). *J. Cent. South Univ.* **2019**, *26*, 1563–1572. [CrossRef]
40. Niknam, S.A.; Kouam, J.; Songmene, V.; Balazinski, M. Dry and Semi-Dry turning of titanium metal matrix composites (Ti-MMCs). *Procedia CIRP* **2018**, *77*, 62–65. [CrossRef]
41. Kamalizadeh, S.; Niknam, S.A.; Asgari, A.; Balazinski, M. Tool wear characterization in high-speed milling of titanium metal matrix composites. *Int. J. Adv. Manuf. Technol.* **2019**, *100*, 2901–2913. [CrossRef]

42. Chandrasekaran, H.; Johansson, J.-O. Influence of processing conditions and reinforcement on the surface quality of finish machined aluminium alloy matrix composites. *CIRP Ann.* **1997**, *46*, 493–496. [CrossRef]
43. Songmene, V.; Balazinski, M. Machining of a graphitic SiC-reinforced aluminium metal matrix composites with diamond tools. In Proceedings of the CIRP International Seminar on Progress in Innovative Manufacturing Engineering—PRIME, Sestri Levante, Italy, 20–22 June 2001; pp. 73–76.
44. Li, G.; Munir, K.; Wen, C.; Li, Y.; Ding, S. Machinablility of titanium matrix composites (TMC) reinforced with multi-walled carbon nanotubes. *J. Manuf. Process.* **2020**, *56*, 131–146. [CrossRef]
45. Monaghan, J.; O'reilly, P. The drilling of an Al/SiC metal-matrix composite. *J. Mater. Process. Technol.* **1992**, *33*, 469–480. [CrossRef]
46. Thiagarajan, C.; Sivaramakrishnan, R.; Somasundaram, S. Modeling and optimization of cylindrical grinding of Al/SiC composites using genetic algorithms. *J. Braz. Soc. Mech. Sci. Eng.* **2012**, *34*, 32–40.
47. Amamou, R.; Fredj, N.B.; Fnaiech, F. Improved method for grinding force prediction based on neural network. *Int. J. Adv. Manuf. Technol.* **2008**, *39*, 656–668. [CrossRef]
48. Li, Z.; Lin, B.; Xu, Y.; Hu, J. Experimental studies on grinding forces and force ratio of the unsteady-state grinding technique. *J. Mater. Process. Technol.* **2002**, *129*, 76–80. [CrossRef]
49. Blau, P.J.; Jolly, B.C. Relationships between abrasive wear, hardness, and grinding characteristics of titanium-based metal-matrix composites. *J. Mater. Eng. Perform.* **2009**, *18*, 424. [CrossRef]
50. Ding, W.; Zhao, B.; Xu, J.; Yang, C.; Fu, Y.; Su, H. Grinding behavior and surface appearance of (TiCp+ TiBw)/Ti-6Al-4V titanium matrix composites. *Chin. J. Aeronaut.* **2014**, *27*, 1334–1342. [CrossRef]
51. Muthukrishnan, N.; Davim, J.P. An investigation of the effect of work piece reinforcing percentage on the machinability of Al-SiC metal matrix composites. *J. Mech. Eng. Res.* **2011**, *3*, 15–24.
52. Thiagarajan, C.; Sivaramakrishnan, R.; Somasundaram, S. Experimental evaluation of grinding forces and surface finish in cylindrical grinding of Al/SiC metal matrix composites. *Proc. Inst. Mech. Eng. Part B J. Eng. Manuf.* **2011**, *225*, 1606–1614. [CrossRef]
53. Bains, P.S.; Sidhu, S.S.; Payal, H. Fabrication and machining of metal matrix composites: A review. *Mater. Manuf. Process.* **2016**, *31*, 553–573. [CrossRef]
54. Li, Z.; Ding, W.; Liu, C.; Su, H. Prediction of grinding temperature of PTMCs based on the varied coefficients of friction in conventional-speed and high-speed surface grinding. *Int. J. Adv. Manuf. Technol* **2017**, *90*, 2335–2344. [CrossRef]
55. Li, Z.; Ding, W.; Liu, C.; Zhou, H. Grinding performance of TiCp/Ti-6Al-4V composites with CBN wheels, part I: Experimental investigation and surface features. *Procedia CIRP* **2018**, *77*, 525–528. [CrossRef]
56. Ding, W.; Li, Z.; Liu, C.; Zhou, H. Grinding performance of TiCp/Ti-6Al-4V composites with CBN wheels, part II: Material removal behavior based on FEM. *Procedia CIRP* **2018**, *77*, 529–532. [CrossRef]
57. Li, Z.; Ding, W.; Shen, L.; Xi, X.; Fu, Y. Comparative investigation on high-speed grinding of TiCp/Ti–6Al–4V particulate reinforced titanium matrix composites with single-layer electroplated and brazed CBN wheels. *Chin. J. Aeronaut.* **2016**, *29*, 1414–1424. [CrossRef]
58. Öpöz, T.T.; Chen, X. Experimental investigation of material removal mechanism in single grit grinding. *Int. J. Mach. Tools Manuf.* **2012**, *63*, 32–40. [CrossRef]
59. Brinksmeler, E.; Glwerzew, A. Chip formation mechanisms in grinding at low speeds. *CIRP Ann.* **2003**, *52*, 253–258. [CrossRef]
60. Durgumahanti, U.P.; Singh, V.; Rao, P.V. A new model for grinding force prediction and analysis. *Int. J. Mach. Tools Manuf.* **2010**, *50*, 231–240. [CrossRef]
61. Thiagarajan, C.; Sivaramakrishnan, R.; Somasundaram, S. Cylindrical grinding of SiC particles reinforced aluminium metal matrix composites. *ARPN J. Eng. Appl. Sci.* **2011**, *6*, 14–20.
62. Li, Z.; Ding, W.; Liu, C.; Su, H. Grinding performance and surface integrity of particulate-reinforced titanium matrix composites in creep-feed grinding. *Int. J. Adv. Manuf. Technol.* **2018**, *94*, 3917–3928. [CrossRef]
63. Zhang, Z.; Guo, D.; Kang, R.; Gao, H.; Jin, Z.; Meng, Y. Subsurface crystal lattice deformation machined by ultraprecision grinding of soft-brittle CdZnTe crystals. *Int. J. Adv. Manuf. Technol.* **2010**, *47*, 1065–1081. [CrossRef]
64. Zhang, Z.; Meng, Y.; Guo, D.; Kang, R.; Gao, H. Nanoscale machinability and subsurface damage machined by CMP of soft-brittle CdZnTe crystals. *Int. J. Adv. Manuf. Technol.* **2010**, *47*, 1105–1112. [CrossRef]
65. Xi, X.; Ding, W.; Li, Z.; Xu, J. High speed grinding of particulate reinforced titanium matrix composites using a monolayer brazed cubic boron nitride wheel. *Int. J. Adv. Manuf. Technol.* **2017**, *90*, 1529–1538. [CrossRef]

66. Huang, S.; Yu, X.; Wang, F.; Xu, L. A study on chip shape and chip-forming mechanism in grinding of high volume fraction SiC particle reinforced Al-matrix composites. *Int. J. Adv. Manuf. Technol.* **2015**, *80*, 1927–1932. [CrossRef]
67. Zhou, H.; Ding, W.; Liu, C. Material removal mechanism of PTMCs in high-speed grinding when considering consecutive action of two abrasive grains. *Int. J. Adv. Manuf. Technol.* **2019**, *100*, 153–165. [CrossRef]
68. Ren, Y.; Zhang, B.; Zhou, Z. Specific energy in grinding of tungsten carbides of various grain sizes. *CIRP Ann.* **2009**, *58*, 299–302. [CrossRef]
69. Malkin, S. *Grinding Technology-Theory and Applications of Machining with Abrasives*; Series in Mechanical Engineering; Elsevier: Amsterdam, The Netherlands, 1989.
70. Xi, X.X.; Ding, W.; Li, Z.; Xu, J.H.; Wang, X.Y. A Study on Heat Transfer in High-Speed Grinding of Titanium Matrix Composites. *Proc. Key Eng. Mater.* **2016**, *693*, 1003–1008. [CrossRef]

APPENDIX B ARTICLE 4: PERFORMANCE OF ELECTROPLATED DIAMOND WHEELS IN GRINDING TITANIUM METAL MATRIX COMPOSITES

Coauthors: Zhongde Shi, Luc Baron, and Marek Balazinski

Published on November 30, 2021.

The 23rd International Symposium on Advances in Abrasive Technology, 30 Nov. - 3 Dec. 2021

Keywords: Grinding, titanium metal matrix composite, electroplated diamond wheel, wheel wear, specific energy, surface integrity.

Abstract. This paper presents an experimental study on the grinding of a titanium metal matrix composite (TiMMC) using electroplated diamond wheels with a focus on the wheel wear and its effects on grinding forces, power, surface roughness, and microstructures under the ground surfaces. Flat up-mode surface grinding experiments were performed all at a fixed wheel speed v_s = 20 m/s. Wheel wear tests were first conducted with a brand-new wheel at a fixed depth of cut a = 0.05 mm and a workspeed v_w = 50 mm/s by up to 800 grinding passes to wear the wheel. Grinding forces, power, surface roughness, and radial wheel wear depth were measured at different grinding passes. Additional tests were conducted by varying the workspeed from 10 to 100 mm/s to explore its effect on TiMMC and titanium alloy. It was revealed that electroplated diamond wheels wear on TiMMC was comparable to titanium alloys, but it was slightly higher on TiMMCs. The specific energy calculated from measured grinding power ranged from 17 – 34 J/mm^3. It was found that surface roughness decreases for TiMMC, but increases for titanium alloy, with increasing workspeed. The plastic deformation induces microstructural change that was identified as twinning under the ground surface.

Introduction

Titanium metal matrix composites (TiMMCs) are an alternative to Ti-based alloys for use in the automotive and aerospace industries as they exhibit excellent mechanical properties because of their reinforcing particles [1, 2]. However, machining TiMMCs is difficult due to the difference in behavior between the ductile removal behavior of the matrix and the brittle removal behavior of the reinforcement particles. The presence of TiC or TiB reinforcing particles in TiMMCs increases the ratio of normal to tangential grinding forces compared to Ti_6Al_4V for similar grinding parameters [3]. The issues encountered during machining of TiMMCs include mainly premature wear of cutting tools, voids, pile ups, and grooves on the surface, not to mention micro-cracks, broken particles, and microstructural changes [4-7]. TiMMC parts are manufactured near net shape to avoid heavy machining operations. Research on machining of TiMMCs focusses on developing efficient machining processes to get high surface quality and dimension accuracy [8]. Several studies [5-7, 9] on grinding TiMMCs generated results regarding the improvement of the surface finish with respect to the grinding wheel used or the wear of the wheel. They were mainly carried out with cubic boron nitride (CBN) wheels or conventional wheels such as white alumina, pink fused alumina, or micro-crystal corundum. However, both grinding approaches result in numerous surface defects (i.e., high surface roughness). Furthermore, the wear of the grinding wheels has not been studied on TiMMCs.

It was showed that grinding metal matrix composites with a diamond wheel significantly reduced grinding force [10]. It was revealed that the surface finish was not strongly dependent on the grinding parameters when grinding with superabrasives [11]. It was recommended to use diamond abrasives to obtain ultra-smooth surface finish in grinding MMCs (Metal Matrix Composites) [12]. However, this contradicts the results obtained by another study [13], which showed lower grinding forces, surface roughness, and percentage of wear flat area with conventional wheels (SiC and Al_2O_3) instead of superabrasives wheels (diamond or CBN). Another study recommended to apply first the SiC wheels and fine-grained diamond wheels for finishing operations [14]. Studies carried out on the grinding of MMCs with diamond grinding wheels are very limited. Diamond is harder than CBN, it is worth investigating whether diamond wheels provide better grinding performance, especially in wheel wear resistance, than CBN wheels.

The present paper is concerned mainly with the grinding performance in terms of forces, power consumption, and wheel wear of TiMMCs with diamond wheel. The objective is to explore the feasibility to grind TiMMCs with diamond wheels and enhance the knowledges on the grinding performance of TiMMCs. The aforementioned grinding parameters are also compared to a titanium alloy throughout the paper.

Experimental Setup and Test Conditions

In the present work, the TiMMC chosen is composed of Ti6Al4V matrix reinforced with 10 - 12%vol of TiC particles. The average size of TiC reinforcing particles is 10 – 20 µm. Fig.1. a. shows the material microstructure which is bimodal: the globular α phase (the lightest one) is surrounded by Widmanstätten platelets. Widmanstätten structure (α+β) is composed of retained β phase (brown) lying between the α platelets. TiC reinforcing particles are distributed in the material. The workpieces were rectangular blocks with a length of 76.2 mm along the grinding direction and a width of 12.7 mm.

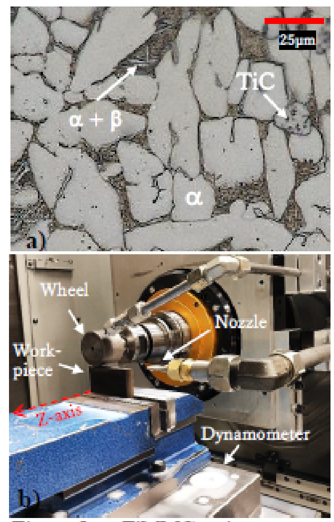

Figure 1. a. TiMMCs microstructure, b. Experimental set-up

Straight surface up-grinding tests were performed on a Makino A88E high-speed and high-power machining center. The wheel was a 120-grit electroplated diamond wheels of diameter d_s = 50.8 mm and width b_s = 38 mm. Fig. 1. b. shows the experimental setup. A water-based grinding fluid of 7% soluble oil was applied at a flow rate of 140 liters/min and pressure of 2.8 MPa through a rectangular nozzle with an opening width of 15 mm and a height of 2.5 mm.

Two sets of tests were performed at a fixed wheel speed v_s= 20 m/s. The first set of experiments were to investigate the wear and the grinding performance of the wheel. The workspeed was fixed at v_w= 50 mm/s and the depth of cut at a = 0.05 mm. The second set of experiments were to explore the effects of workspeed. The workspeed was varied from v_w= 10 to 100 mm/s corresponding to a specific material removal rate of Q_w' = 0.5 - 5 mm^2/s. These experiments were also carried out on titanium alloy samples for comparisons.

Grinding Power, forces, and surface roughness were measured at different grinding intervals. A universal power cell was used to measure the electrical power of the spindle motor, and a dynamometer Kistler 9255B for the forces. The net components of power and forces were obtained following the approach applied in [15]. The roughness was measured with a Taylor-Hobson Surtronic 3+ surface roughness checker. Radial wheel wear was measured by taking a grinding pass in a graphite sample with a profilometer (Form Talysurf Series 2), as presented in [16]. The microstructural observation was done on an optical microscope Keyence VHX-7000, after mirror polishing and chemical attack with Kroll's reagent.

Results and discussion

A total of 800 passes were conducted for the wheel wear tests. It is well known that experimental measurements of grinding force and power components involve non-grinding components. The non-grinding components were subtracted from the total components to obtain the net value. These components are recorded in a complete spark-out pass. An example showing the total components of forces and power, the non-grinding components, and the net components for the 100^{th} pass is presented in Fig.2. a. The peaks at the beginning and the valleys the end of the total and net power signals reflects the actual electrical power of the motor which are due to the transient behavior of the spindle motor when the wheel started to cut in and cut out the workpiece. For this example, the average net horizontal and vertical forces were F_h = 36 N and F_v = 89 N, respectively. The average net power was P = 0.56 kW for a corresponding specific energy of u = 17.6 J/mm^3. The application of the high-pressure grinding fluid is responsible for such large non-grinding forces. An example of the radial wheel wear profile is presented at the Fig.2. b. This profile was measured after 100 wear passes and shows a wear depth of about 20 µm.

The results of the wear tests are summarized in Fig.2. c. Vertical F_v and horizontal forces F_h, power P, surface roughness R_a and radial wear depth w are presented depending on the number of passes. The radial wear exhibited several transient run-ins at the 100^{th}, 400^{th}, and 800^{th} pass without reaching a clear steady state wear rate. The initial radial wheel wear after the first pass was about w = 16 µm, which is 6 µm higher than observed after one grinding pass on titanium alloy [17]. It can be attributed to the pull-outs of weakly bound diamond grains. The presence of the TiC reinforcing particles might increase this phenomenon and affect the highly protruded diamond grains. At the end of the tests, after the 800^{th} pass, the wear depth reached w = 28 µm.

Power, forces, and surface roughness have undergone gradual changes due to progressive radial wheel wear. The vertical and horizontal forces stabilize after the first transient run-in up above the 100^{th} pass. For the vertical force, the first values vary between F_v = 92 and 76N and gradually increase up to F_v = 98 N for the 800^{th} pass. The horizontal force follows the same trend, but the oscillations are between F_h = 33 and 40 N and then gradually increase to F_h = 40 N. The initial power was about P = 0.76 kW and decreased and stabilized at 0.57 until the 100^{th} pass. Following the 100^{th} pass the power gradually increases reaching P = 0.65 kW by the end of the tests. The results obtained contradict what was previous found. More investigation is needed to explain and understand this trend. The surface

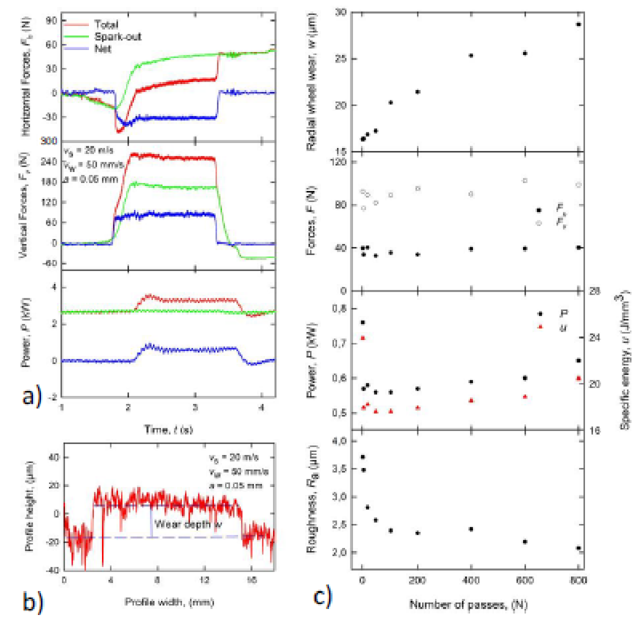

Figure 2. a. Measurements for the 100^{th} passes, b. Wheel wear profile at 400 passes, c. Wheel wear results

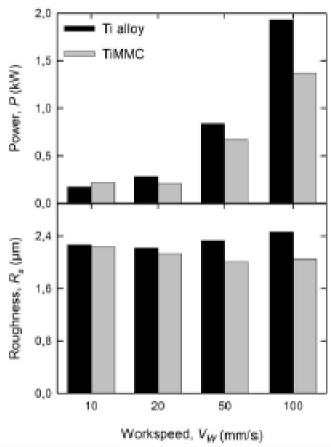

Figure 3. Workspeed effect on power and roughness

roughness decreases rapidly from R_a = 3.71 µm at the start of the grinding tests towards R_a = 2.39 µm for the 100th pass. After the 100th pass, the decrease in roughness is progressive and reaches R_a = 2.08 µm. The first transient run-ins up (100th pass) which induced a rapid increase in radial wheel wear from w = 17 to w = 20 µm, (i.e., the breaking of the protruded diamond grains), has a significant impact on the values of forces, power, and roughness.

Similar tests were carried out on a titanium alloy with an electroplated diamond wheel [17]. The roughness did not show a transient run-in up at the 100th pass, but horizontal and vertical forces, and power increase from the 100th pass. The roughness reached a steady state from the 100th pass. Even if the observed trends are not all similar, there seems to be a correlation for the evolution of the components from a radial wheel wear close to w = 20 µm. For the titanium alloy studied in the previous study, the power increases up to the 800th pass. While for the TiMMC the power drops dramatically and then increases gradually. The presence of TiC particles radically changes the tendency of power. Until the 100th pass, the power decreases because the protruded diamond grains of the grinding wheel break. The brittle fracture of diamond grains consumes less energy than the grinding of ductile material, reducing the power required. After the 100th pass, the power gradually increases because the protruded diamond grains have broken during the previous passes. The power required for grinding TiMMCs takes over as the grains break. The ductile behavior of TiMMCs matrix being more energy-intensive than the brittle fracture of diamond grains, the power required for grinding increases. It is important to note that the power required for grinding TiMMCs is less than that required for grinding titanium alloy. This difference is explained by the presence of TiC reinforcements which present a fragile type of rupture, reducing the power. The wear depth values from the 800th pass in Fig.2. c. were used to characterize the wheel wear resistance. The G-ratio value was calculated as 680. The value obtained for TiMMC was smaller than that obtained for titanium alloys under identical test conditions indicating that there is increased wheel wear and decreased wheel life for TiMMCs compared to titanium alloys [17]. It is important to note here that G-ratio was calculated from the total wear depth. If the initial wear of the wheel from the first pass is removed from the G-ratio calculation, its value reaches 1580. This shows the slow wear of the grinding wheel when grinding the TiMMC.

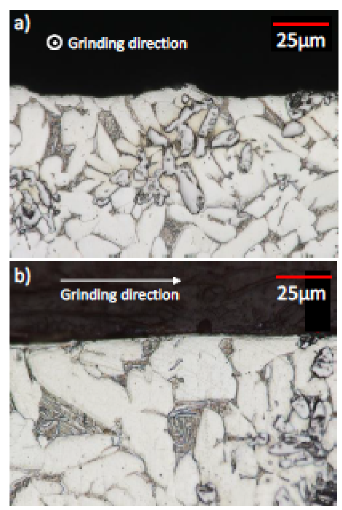

Figure 4. Microstructure at 400 passes on the YZ (a) XY and plane (b)

Fig.2. c. also shows specific energies. The initial value was u = 23.9 J/mm^3 and decreased until the 100th pass to 17.6 J/mm^3. More investigation is needed to explain this trend. Following the 100th pass, the specific energy increased progressively to u = 20.5 J/mm^3 which is lower than the final value obtained for titanium alloys (29 J/mm^3). This confirms that grinding TiMMCs is less energy intensive than grinding titanium alloys. The lower energy for

TiMMC is, as explained previously, due to the presence of TiC particles which, when they break, exhibit a brittle behavior, and actively participate in the reduction of energy consumption.

The results of the second set of tests are presented in Fig.3. The power P and the roughness R_a are presented according to the workspeed v_w for titanium alloy and TiMMC. The initial values of the power at v_w = 10 mm/s are P = 0.17 kW for the titanium alloy and 0.22 kW for the TiMMC. The power increases as the workspeed increases and reaches P = 1.93 kW and 1.37 kW for the titanium alloy and the TiMMC respectively. In general, the power required for grinding the titanium alloy is greater than that for grinding TiMMC. As the wheel surface conditions where equals for these experiments, the variations in power are due to the material. The brittle behavior of TiC particles can explain this trend. The initial value for the roughness is R_a = 2.27 µm for the titanium alloy at a workspeed of v_w = 10 mm/s and reaches 2.46 µm at 100 mm/s. The roughness increases with the workspeed. For the TiMMC, the initial value is R_a = 2.24 µm at v_w = 10 mm/s and 2.05 at 100 mm/s. The roughness trend for TiMMC is opposite to that observed for titanium alloy: it decreases as the workspeed increases. Grinding of titanium alloy leads to the formation of pile-ups and grooves owing to the side flow of the material. It might be due to the presence of TiC particles which seems to limit this phenomenon. The dislodgement and breakage of the particles lead to surface defects which are smaller, explaining the lower roughness.

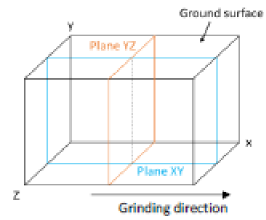

Figure 5. Cutting samples

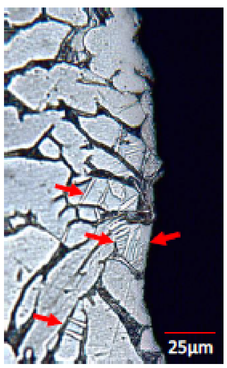

Figure 6. Twinning formations are shown by arrows under the ground surface at YZ plane

To study more closely the microstructure, samples were cut by EDM perpendicular (YZ plane) and parallel (XY plane) with the direction of cut, as shown in Fig. 5 It was seen that the sub-surface microstructure does not show any change for a 50 mm/s workspeed regardless of the number of passes. As an example, microstructure is presented at400 passes in Fig.4. The globular structure of the α phase and the Widmanstätten platelets do not seem to have undergone any major deformation either in the ZY and XY planes or even within a few microns of the ground surface. However, the plastic deformation occurred within 3 µm of the ground surface induces twins formation during the grinding (Fig.6). Since diamond is an excellent thermal conductor, it helps conduct the heat away from the grinding zone. Extreme temperature changes, particularly related to plastic deformation, are thus limited, and have only a minimal impact on the microstructure. However, the plastic deformation which takes place at the sub-surface of the ground surface is the seat of the presence of residual stress.

Conclusion

Grinding TiMMC with an electroplated diamond wheel results in lower forces, power, specific energy, and roughness than titanium alloy. Grinding wheel wear has a significant impact above 100th pass. G-ratios of about 680 was obtained for the specific removal rate of 2.5 mm^2/s. For similar conditions, the electroplated diamond wheel wear was higher for TiMMCs than titanium alloys. Specific energy on TiMMC slightly lower than titanium alloys. The presence of TiC particles considerably decreases the surface roughness when the workspeed increases. Twinning formation due to plastique deformation was observed after grinding.

References

[1] M. D. Hayat, H. Singh, Z. He, and P. Cao, "Titanium metal matrix composites: An overview,"

Composites Part A: Applied Science and Manufacturing, 2019.

[2] C. Escaich, Z. Shi, L. Baron, and M. Balazinski, "Machining of Titanium Metal Matrix Composites: Progress Overview," *Materials,* vol. 13, no. 21, p. 5011, 2020.

[3] Q. Miao, W. F. Ding, B. Zhao, J. H. Xu, Z. W. Liu, and J. He, "Grinding Experiments on PTMCs with Vitrified CBN Wheel," in *Key Engineering Materials*, 2014, vol. 579: Trans Tech Publ, pp. 163-166.

[4] T. Thepsonthi and T. Özel, "3-D finite element process simulation of micro-end milling Ti-6Al-4V titanium alloy: experimental validations on chip flow and tool wear," *Journal of Materials Processing Technology,* vol. 221, pp. 128-145, 2015.

[5] Z. Li, W. Ding, C. Liu, and H. Su, "Grinding performance and surface integrity of particulate-reinforced titanium matrix composites in creep-feed grinding," *The International Journal of Advanced Manufacturing Technology,* vol. 94, no. 9-12, pp. 3917-3928, 2018.

[6] X. Xi, W. Ding, Z. Li, and J. Xu, "High speed grinding of particulate reinforced titanium matrix composites using a monolayer brazed cubic boron nitride wheel," *The International Journal of Advanced Manufacturing Technology,* vol. 90, no. 5-8, pp. 1529-1538, 2017.

[7] Z. Li, W. Ding, L. Shen, X. Xi, and Y. Fu, "Comparative investigation on high-speed grinding of TiCp/Ti–6Al–4V particulate reinforced titanium matrix composites with single-layer electroplated and brazed CBN wheels," *Chinese Journal of Aeronautics,* vol. 29, no. 5, pp. 1414-1424, 2016.

[8] J. Monaghan and P. O'reilly, "The drilling of an Al/SiC metal-matrix composite," *Journal of materials processing technology,* vol. 33, no. 4, pp. 469-480, 1992.

[9] Z. Li, W. Ding, C. Liu, and H. Zhou, "Grinding performance of TiCp/Ti-6Al-4V composites with CBN wheels, part I: experimental investigation and surface features," *Procedia CIRP,* vol. 77, pp. 525-528, 2018.

[10] N. Hung, Z. Zhong, and C. Zhong, "Grinding of metal matrix composites reinforced with silicon-carbide particles," *MATERIAL AND MANUFACTURING PROCESS,* vol. 12, no. 6, pp. 1075-1091, 1997.

[11] H. Chandrasekaran and J. Johansson, "Role of material and grinding parameters in grinding of alumina fiber-reinforced aluminum alloys," *NIST Spec. Publ., 847 pp.,* vol. 55, 1993.

[12] M. Cook, "Diamond grinding and PCD machining of MMC engineering components," *Powder metallurgy,* vol. 41, no. 2, pp. 87-89, 1998.

[13] A. Di Ilio and A. Paoletti, "A comparison between conventional abrasives and superabrasives in grinding of SiC-aluminium composites," *International Journal of Machine Tools and Manufacture,* vol. 40, no. 2, pp. 173-184, 2000.

[14] Z. Zhong and N. P. Hung, "Grinding of alumina/aluminum composites," *Journal of materials processing technology,* vol. 123, no. 1, pp. 13-17, 2002.

[15] C. Guo, Z. Shi, H. Attia, and D. McIntosh, "Power and Wheel Wear for Grinding Nickel Alloy with Plated CBN Wheels," *CIRP Annals,* vol. 56, no. 1, pp. 343-346, 2007/01/01/ 2007, doi: https://doi.org/10.1016/j.cirp.2007.05.079.

[16] Z. Shi and H. Attia, "High removal rate grinding of titanium alloys with electroplated CBN wheels," *International Journal of Abrasive Technology 16,* vol. 6, no. 3, pp. 243-255, 2014.

[17] Z. Shi and H. Attia, "High performance of titanium alloys with electroplated diamond wheel," presented at the 9th CIRP Conference on High Performance Cutting, 2019.

APPENDIX C CONFERENCE PAPER AWARD

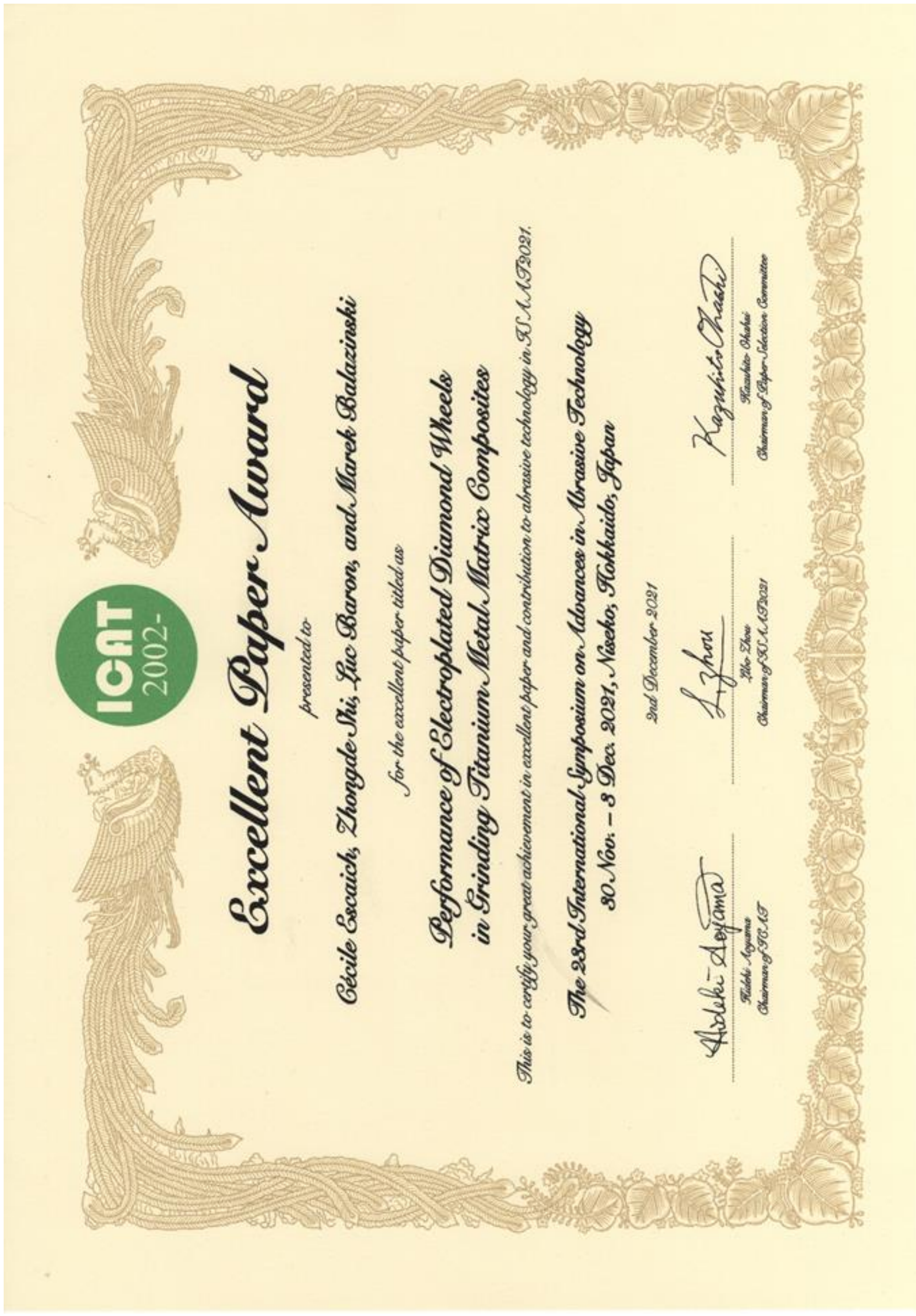

ICAT 2002-

Excellent Paper Award

presented to

Cécile Escaich, Zhongde Shi, Luc Baron, and Marek Balazinski

for the excellent paper titled as

Performance of Electroplated Diamond Wheels in Grinding Titanium Metal Matrix Composites

This is to certify your great achievement in excellent paper and contribution to abrasive technology in ISAAT2021.

The 23rd International Symposium on Advances in Abrasive Technology
30 Nov. – 3 Dec. 2021, Niseko, Hokkaido, Japan

2nd December 2021

Hideki Aoyama
Chairman of ICAT

Libo Zhou
Chairman of ISAAT2021

Kazuhito Ohashi
Chairman of Paper Selection Committee